2

SPECTROSCOPY AND NONTHERMAL PROCESSES

Monique Querci

PRELIMINARY REMARKS

This chapter presents observational data, mainly from spectral lines, which imply the existence of nonthermal phenomena—phenomena not expected to occur in hydrostatic thermal atmospheres under radiative equilibrium. Those sections of this chapter following this overview summarize spectroscopic data from the ultraviolet to the infrared; the chapter following covers spectral lines in the radio region. Sequentially, we survey:

1. The variability of those absorption lines whose excitation/ionization levels correspond to photospheric conditions. In some variable red stars, especially the Miras, such absorption lines are those whose velocity shifts are interpreted to be caused by subatmospheric pulsation driving outward compression waves: producing shocks by either wave-steepening or collision with infalling material from a preceding phase, or both. Such photospheres are already nonthermal.

2. The variability of the emission lines, interpreted as arising in higher atmospheric layers and whose diverse spectral characters imply a wide range of physical processes leading to their formation. Such processes that, in the Sun, are mainly interpreted in terms of thermal chromospheres, appear, in some pulsating stars, to reflect more dynamical circumstances such as shocks and extended atmospheres. So we try to survey these emission lines, of varying character, in terms of the different possibilities for their production, to try to infer the kinds of atmospheric regions existing in such stars. In this regard, we summarize recent suggestions offered by Willson and Bowen (1985).

3. The characteristics and variability of those absorption lines considered to be circumstellar because of their low excitation and because of certain characteristics of their profiles. We are particularly interested in the relation of the circumstellar observations, and regions, to mass-loss consequences.

This survey of the line spectrum, and the nonthermal extended structure that it implies for the atmospheres of many red giants and supergiants, leads naturally to asking about the relation between those outermost cool regions found and the source of that observed radiation diagnosed as coming from dust grains. So

C-3

we survey those observations, including data from the continuum as well as from the lines, and the inferences that have been drawn from them.

Finally, we summarize the attempts that have been made to measure directly angular diameters of these stars and to map the distribution of gas and dust in the most exterior atmospheric regions.

In both this chapter's survey of the line spectrum and the preceding chapter's survey of the continuum, variability of all features is stressed. From these discussions, we attempt to depict the dynamic motion of the atmospheric layers. But first, we must clarify certain ideas, as discussed by Wing (1979) in his review on Miras.

First, the radial velocity of the center of mass of the star must be determined. From among various velocities that might represent the motion of the center of mass (e.g., see Wallerstein, 1975), there appears to be a consensus of opinion in the literature (e.g., Hinkle et al., 1982, and references therein) for using the molecular emission of thermally excited SiO or CO. This idea has been stressed by Reid and Dickinson (1976) after the observations of SiO by Buhl et al. (1975) in some Mira stars, while Lambert and Vanden Bout (1978) and Dickinson et al. (1978) found further stars showing SiO and also CO thermal emission. As demonstrated by Morris and Alcock (1977), the thermal emission lines arise in the external layers of an extended low-density region. The velocity, inferred from the center of the emission profile, should then be considered as the velocity of the star center of mass (systemic velocity), because, paraphrasing a comment by Knapp et al. (1980), it is free of shifts caused by pulsation of the photosphere. Also, the stellar center-of-mass velocity may be obtained from the midpoint of the twin OH maser emission feature (see Rieu, this volume). The velocity of expansion of the emitting region is inferred from the width at the base of the SiO or CO line profile.

The second point to be decided is the spectral features indicative of the photospheric velocity. Until recently, the motion of the photosphere was supposed to be represented by an average radial velocity of the absorption lines, mainly those seen in the blue spectral region. Nevertheless, Wallerstein (1977) showed that a discrepancy exists between the changes in photospheric radius derived by means of photometric data and those deduced from the displacement of the line-forming region found from integrating the radial-velocity curve. It has now been proved that high-excitation-potential CO lines exist in the infrared region which unambiguously show the values and the amplitudes of radial velocity expected for the motion of the photosphere (see the sections *Changes in Absorption-Line Radial Velocities with Phase* and *Source of the Visible Spectrum*).

Finally, the measured radial velocities have to be further corrected for projection effects before deciding if the stellar layer is expanding or contracting relative to the center of mass. Although these correction factors for geometry and limb darkening are badly defined (Wallerstein, 1975, 1977), appropriate geometrical correction factors for Miras have been calculated (Willson et al., 1982).

We end these preliminaries with the following miscellaneous remarks:

1. The term "atmosphere" stands for all the stellar layers from the photosphere to the external envelopes.

2. The variability will be mainly dealt with from spectra of Miras, chiefly from some prototypes of M and S types for which the observational data are exhaustive. The phase coverage of C types is as yet too incomplete for detailed discussion.

3. We adopt the convention that "red" and "blue" shifts refer to shifts to longer and shorter wavelengths (or to lower and higher frequencies), respectively. We set the velocities as positive for infalling material relative to the center-of-mass velocity (red-shifted lines) and negative for rising material (blue-shifted lines).

4. The phase of events which occur in the preceding or following cycles is specified by substracting or adding 1.0 to the normal phase convention. When the observation time is given in days before or after the maximum light in the literature, the corresponding phases are calculated on the basis of the periods issued from Kukarkin et al. (1969, 1970).

5. To link radial velocities from optical features, generally given with respect to the Sun, to the center-of-mass velocity (a radio line velocity generally given with respect to the local standard of rest, V_{LSR}), we have to convert the latter to a heliocentric velocity (Lang, 1980).

PHOTOSPHERIC ABSORPTION LINES

Introduction

The spectra of the late-type stars are crowded with absorption lines. For the earlier of these, the atomic lines are quite strong in a relatively molecular-band free spectrum, while in the later types the molecular bands appear and the atomic line-strengths decrease.

Even at high dispersion, only a few regions are suitable for studying the atomic lines. One of these, nearly free of absorption by molecular bands, lies shortward of about 4400 Å; this blue region of the visual was extensively studied by the spectroscopists until the 1960s. Longward of this wavelength, interference by the TiO bands in M stars gradually increases, and the intensities and displacements of atomic lines become difficult to study. The spectra of S stars, in which the ZrO bands are less extended than the TiO bands of M stars, should be more favorable. Unfortunately, as there is little flux in the blue-violet region of these cool stars, only the phases near maximum light have been exploited. Moreover, the blue region contains circumstellar (CS) lines (excitation potential ≤ 0.5 eV) that may alter the conclusions on radial-velocity changes in papers written before these circumstellar components became well known. (See the section *Circumstellar Lines—Properties of Gaseous Shells.*)

Another region in which the depression due to molecular bands is not too strong is in the near-infrared (λλ 7900–8700). In recent years, high-resolution Fourier transform spectroscopy became available in the infrared region from 1.6 to 2.5 μm, making it possible to analyze the behavior of atomic and molecular lines there. The present advanced infrared spectroscopy is well suited to radial-velocity determinations: high resolution up to 0.07 cm^{-1} is practicable at all phases because Miras have relatively small light amplitudes in the infrared. We recall that red giants have their flux peak between 1 and 2 μm and that the 1.65-μm region corresponds to the minimum opacity due to H^-.

Survey of Changes in Absorption-Line Strengths with Phase

Blue-violet spectra of *Miras* extending over many light cycles indicate periodic changes in line intensities. Some examples come from the blue-violet region of *o* Cet, R Leo, R And; Buscombe and Merrill (1952) find that, although the majority of atomic absorption lines are much stronger at maximum light, not all elements show exactly the same variations in equivalent widths with phase. Also, the example of U Ori (Merrill, 1945) shows that changes in atomic-line intensities are not *a fortiori* correlated with great changes in the brightness of the star: while the magnitude of the star increases as much as 2.2 mag from phase -38 days to phase -4 days, changes in the atomic-line spectrum were minor. For molecular bands, numerous examples indicate that the molecular features strengthen with the (cooler) later types and within a type with the declining light phases (i.e., ultimately with a decrease in temperature). For M3–M6 Miras, the depth of the TiO bands at 4584 and 4955 Å becomes smaller near maximum light, and the earlier the type, the smaller the depth (Maehara and Yamashita, 1979). The TiO and VO bands at 1 μm, which appear in stars later than M6, strengthen toward minimum light (Lockwood, 1969). Sanford (1950)

reports on the appearance of strong CaCl bands in the orange and red regions of C stars, but only during minimum light. In the infrared, Hinkle (1978) indicates that the 4400- to 4800-cm^{-1} region in R Leo contains only weak molecular lines near maximum light (allowing for the identification of weak to moderate atomic lines). On the other hand, the strengthening of the water spectrum near minimum light is responsible for reducing the number of unblended lines by well over one half. Hinkle and Barnes (1979a) found that the H_2O column density in R Leo varies by about an order of magnitude with phase, while in χ Cygni (Hinkle et al., 1982), the CO column density strongly changes near maximum light and stays at a constant value from about phase 0.20 to 0.70. Incidentally, using the curve-of-growth/isointensity method (Hinkle et al., 1976), the excitation temperature is found as a function of phase for the various molecular bands; such a quantity is essential when discussing the structure of the atmosphere. (See the section *Photospheric Kinematics—The Shock-Wave Model.*)

Variations in Radial Velocities of Absorption Lines

Dependence of Absorption-Line Radial Velocities on the Excitation Potential. Line shifts of neutral atoms increase monotonically with the excitation potential of the lower atomic-energy level. Clearly deduced from the visual atomic lines in Miras (Merrill and Greenstein, 1956), it is now also shown for the IR atomic lines. As an example, in the blue spectrum of χ Cygni (Merrill, 1947b), Fe I lines with a lower state excitation potential of 1.0 eV, which is the value of most of the visual atomic lines measurable in Miras, are displaced toward longer wavelengths by 2 km/s with respect to the resonance lines; this is confirmed by Maehara (1968), who finds radial velocities from violet and IR absorption lines of Ti I and Fe I in χ Cygni decreasing with decreasing excitation potentials. The low excitation lines are shifted toward short wavelengths with respect to high excitation lines. Moreover, it has been noted from studies of both S Car in the infrared at high dispersion at all phases (Shinkawa, 1973) and χ Cygni (Hinkle et al., 1982) that the phase dependence of the relation between velocity and excitation potential relation varies with phase.

A similar dependence of radial velocity on the excitation potential is also found from molecular lines. Interesting examples are given by the irregular C star, TX Psc, in the visible range with AlH and SiH molecules (Peery, 1979) and in the 2.5-μm region with CO and HF molecules (Peery et al., 1977).

As discussed by Hinkle (1978), the excitation potential is one measure of the depth of formation of a line in the cool star photosphere: the higher the excitation potential, the deeper is the line-forming region (and also the weaker are the lines). The dependence of radial velocities on the excitation potential explains the strong dependence of the velocity of the absorption lines on the line intensity (Maehara, 1971) (i.e., our understanding of the temperature stratification and region of line formation leads directly to the phenomenon of a *velocity gradient* in the atmosphere). Finally, Pilachowski et al. (1979) note a strong correlation between the radial velocity and the ionization potential in several Mira variables.

Changes in Absorption-Line Radial Velocities with Phase

Blue Range in Miras. In his extensive study of the brightest phases over 16 cycles of o Cet's light variation (from 1935 to 1951), Joy (1954) proves that variations in the radial-velocity curves of atomic absorption lines, from λ3770 to λ4290, are evident from cycle to cycle; greater positive velocities correspond to the cycles with a greater brightness at maximum. This author also notes that in other Miras, at post- and pre-maximum, the atomic-line velocities do not repeat regularly from cycle to cycle. However, the typical general trend of the velocities in Miras shows that *the blue-violet atomic lines do not exhibit significant velocity changes with phase.* A striking example is given for R Leo by Hinkle and Barnes (1979b), who collected

data from Merrill (1946, 1952c) and Wallerstein (1975). The velocity is nearly constant at +12 ± 3 km/s from phase 0.8 to 0.3 and then decreases to about 7 km/s at minimum light.

Such a velocity trend of the photospheric absorption lines is inconsistent with the velocity behavior of the emission lines that support a pulsation interpretation, suggested by the periodic variations in brightness to be discussed in the sections *Changes in Emission-Line Radial Velocities with Phase* and *Atmospheric Kinematics* (part on *The Mira Stars): The Shock-Wave Model.* It confused the visual spectroscopists and prevented a deduction of an overall atmospheric structure of these stars until recently, when infrared techniques became available.

Infrared Range—An Example: the Mira χ Cygni. High-resolution Fourier transform IR observations by Hall et al. (1979), Hinkle (1978), Hinkle and Barnes (1979a, 1979b), and Hinkle et al. (1982) led to a real breakthrough in understanding *the Mira phenomenon.* These authors analyze molecular and atomic absorption lines of various excitation energies and strengths at several different phases and give a picture of how the velocity structure and, furthermore, the temperature structure and column densities change along the light cycle.

When summarizing the key observational results, a typical example used is a time-series spectra of χ Cygni (Hinkle et al., 1982). The authors rely on the CO bands from 1.5 to 5 μm in which the Δv = 3, 2, and 1 vibration/rotation bands are found. Figure 2-1, adapted from Hinkle et al. (1982), displays the changes in radial velocities with phase for groups of lines of low, high, or moderate excitation belonging to the second-overtone (Δv = 3) and the first-overtone (Δv = 2) bands. Obviously, χ Cygni has a composite absorption spectra with multiple velocity components.

The Second-Overtone Bands. Discontinuous S-shaped velocity curves with a *double-lined* spectrum for about one fourth of the light cycle, from before φ = 0.90 to about φ = 0.15, are the outstanding features in Figure 2-1 (upper panel). Additional evidence comes from Figure 2-2, which presents an average Δv = 3 line profile at representative phases. As summarized by Hinkle et al. (1982): (1) during the double-line phases, the line to the red (inward flow) fades as the line to the blue strengthens; (2) the absorption lines move to the red with phase; (3) a blue-shifted emission edge develops after phase 0.60 and emerges as a separate emission feature; and (4) the lines weaken during the emission-line and double-line phases.

Instances of absorption-line doubling in Miras near maximum light have been known earlier from near-infrared spectra. It has been reported for χ Cygni by Maehara (1971) from near-infrared atomic lines around 8000 Å. These lines reported on Figure 2-1 behave as the Δv = 3 lines. Not having a complete set of observations along the phase, Maehara could not deduce the discontinuous S-shaped curves. For the first time, Maehara showed that the blue components are formed in a much hotter gas (therefore in deeper layers) than the red ones. This result has been confirmed by Hinkle et al. (1982): given the stellar velocity of −7.5 km/s (Dickinson et al., 1978), the longward component corresponds to cool falling gas, and the shortward component to hot rising gas. We now understand why the blue region has never been detected for double lines: the opacity in the blue is too strong to let the deep layer be seen. Hinkle et al. further establish the run of the excitation temperature with phase; the temperature drops about 2000 K through the light cycle.

The First-Overtone Bands. In the Δv = 2 bands, absorption lines of low, high, or moderate excitation are distinguished. Generally speaking, lines with low rotational quantum numbers J″ are low-excitation lines (e.g., the (2–0) R8 or R10 lines (~0.02 to 0.03 eV)). A 2–0 high-excitation line is R92 (1.98 eV). Moderate-excitation lines are (3–1) R32 to R35 (~0.50 to 0.56 eV); higher excitation (3–1) lines such as R66 and R65 (~1.3 eV) are not shown

in Figure 2-1. The main results from the middle panel of Figure 2-1 devoted to the $\Delta v = 2$ bands follow:

1. The high-excitation (2–0) lines exhibit a large amplitude periodic change in velocity that mimics the second-overtone ($\Delta v = 3$) lines, but they double later in phase due to an assumed increase in continuous opacity from 1.6 μm ($\Delta v = 2$) to 2.3 μm ($\Delta v = 3$).

2. The low-excitation (2–0) lines do not have a periodic change in velocity; rather, they cluster around the center-of-mass velocity,

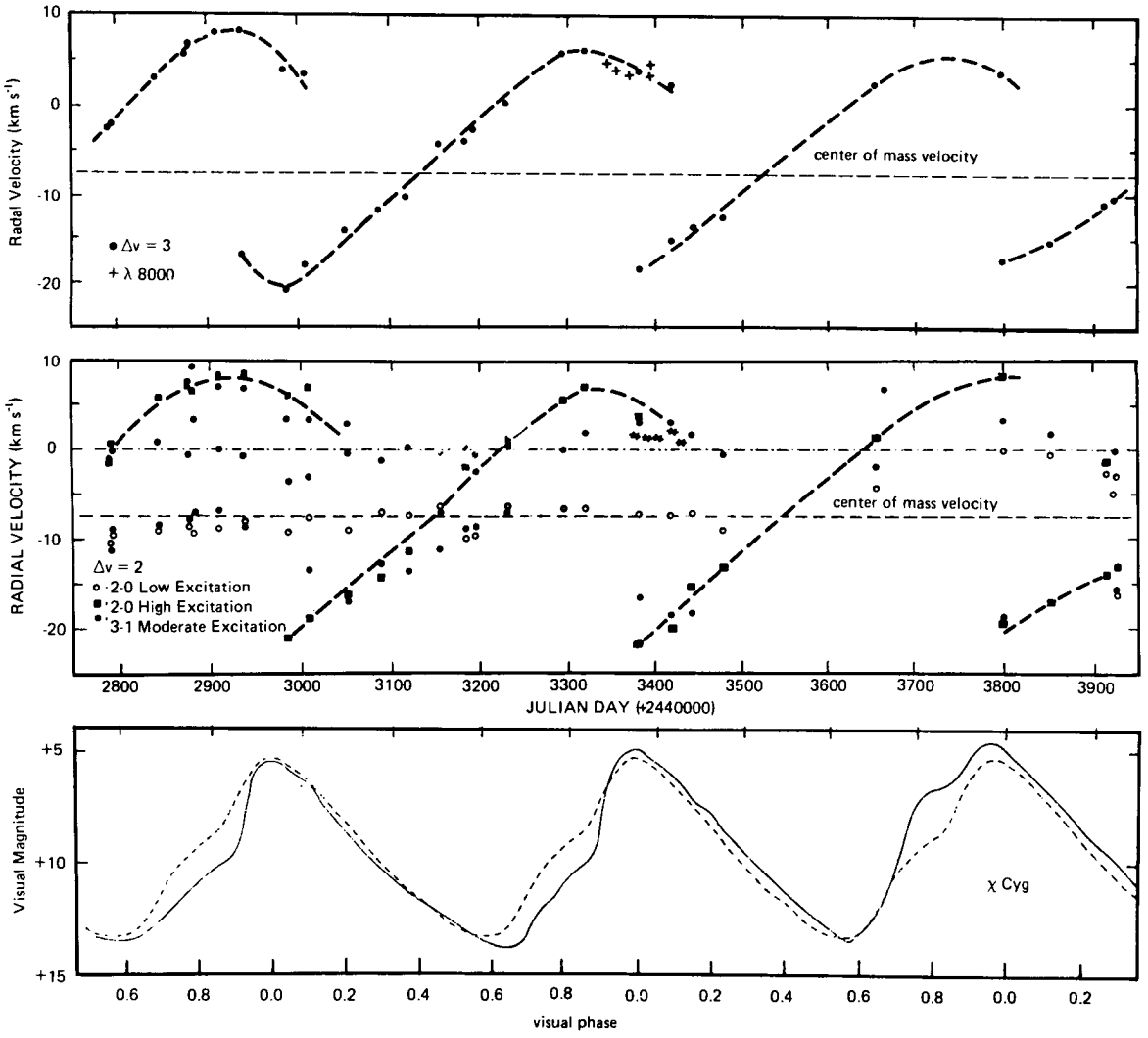

Figure 2-1. The S Mira, χ Cygni, in the infrared range. Upper panel: the mean CO second-overtone velocity as a function of Julian Day number (+ 2440000); crosses = the Maehara's (1971) atomic-line velocities from 8000 Å region. Middle panel: the CO first-overtone velocities for three different groups of lines as a function of Julian Day number; dot-dash line = mean absorption visual (4000 Å) velocity; stars = blue-violet region velocities measured during the same time interval as the CO (3, 1) moderate excitation lines. Lower panel: the visual light curve as a function of Julian Day number; dash line = average light curve; Solid line = actual light curve (adapted from Hinkle et al., 1982).

and one can infer an excitation temperature of the line-forming region of 800 K ± 100 K.

3. The moderate-excitation (3–1) lines exhibit line doubling, conspicuous at phases 0.01 and 0.24; however, extra components may be present (as at $\varphi = 0.04$). The general trend is as follows: one component always matches the (2–0) high-excitation velocity; the other component present is either at the velocity of the low-excitation (2–0) lines or at positively shifted (i.e., infalling) velocities relative to the center-of-mass velocity. Hinkle et al. (1982) add that considerable cycle-to-cycle variation is conspicuous: in some cycles, the infalling line is single; in others, multiple components are likely. The excitation temperature of the infalling lines is around 1500 K.

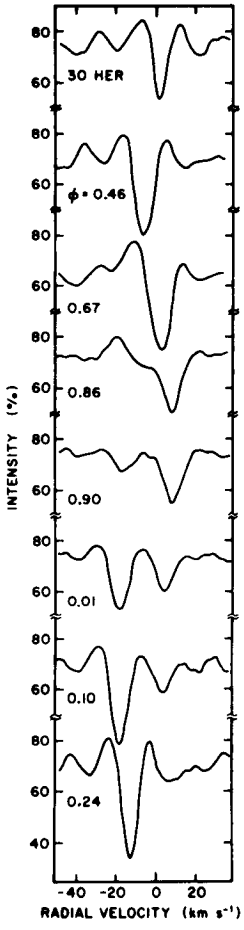

Figure 2-2. The S Mira, χ Cygni: Average CO second-overtone (Δv = 3) line profiles as a function of phase. The M6 III low amplitude variable 30 Her is shown for a comparison profile (from Hinkle et al., 1982).

To complete the description, we note the *fundamental bands* (Δv = 1) in the 4.6-μm region. The (1–0) band is indicative of a cool circumstellar shell. No velocity changes are noted. The excitation temperature is 300 ± 200 K. The circumstellar shells will be fully discussed in the section *Circumstellar Lines—Properties of Gaseous Shells.*

In short, four components have been identified in the spectra by Hinkle et al. (1982):

1. One component consists of second-overtone CO lines and the high-excitation component of the first-overtone lines, together with the atomic lines at 8000 Å. These lines share a discontinuous velocity curve of nearly 30 km s^{-1} amplitude and an excitation temperature change from 4000 to 2200 K. Both properties are indicative of lines formed in a pulsating region traversed by a shock front near maximum light. They are an indisputable indicator of the dynamics of the stellar photosphere.

2. One component deals with first-overtone lines with infall velocities. Hinkle et al. remark that this group of lines persists to at least minimum light and may well be present throughout the entire cycle. Their excitation temperature is about 1500 K.

3. Another component groups low-excitation first-overtone stationary lines (i.e., with the center-of-mass velocity) and with T ~ 800 K. This component is suggested to originate in the inner region of the circumstellar shell.

4. Finally, low-excitation fundamental lines with T ~ 300 K are formed in the expanding circumstellar shell.

The four components are the signatures of different regions in the atmosphere that will now be discussed.

Overall Picture of a Mira Atmosphere from the Absorption Lines (the example of χ Cygni)

Photospheric Kinematics—The Shock-Wave Model. The discontinuous S-shaped radial velocity curves were first observed for another class of pulsating variable stars, the W Virginis stars, for which the line doubling is explained by a shock wave model (e.g., Wallerstein, 1959). In the Mira χ Cygni, Maehara (1968), to account for the line doubling observed at 8000 Å around maximum light, put forward a two-layer model in which a layer of shock-heated gas is rising through a layer of cooler gas. The shape of the radial-velocity curve described by the first group of CO lines investigated by Hinkle et al. (1982) throughout three cycles fully supports the shock-wave model: radial stellar pulsation drives compression waves which develop into shocks *before emergence into the photosphere*. A first qualitative description of the model is given in Hinkle (1978) or Hinkle and Barnes (1979b) and is then updated in Hinkle et al. We rely on their various descriptions for a more comprehensive approach to the model.

> "By about minimum light, maximum radius has been reached and gas [from the outer layers] falls back [under a constant inward acceleration] while the deep layers become compressed and fall less rapidly...[A shock develops when] the photospheric gas moving inward can no longer decelerate smoothly into the underlying gas...that becomes nearly stationary at maximum compression.... [Otherwise], the shock region occurs where the falling photospheric gas of the last-cycle meets the photospheric gas of the present cycle at a velocity difference greater than that of sound... At this shock interface, the gas is heated from ~2000 K to > 4000 K [in χ Cygni] and molecular species are dissociated; atomic hydrogen is probably predominantly ionized.... The first indication of the emergence of the shock into the χ Cygni atmosphere is probably the brightening of the star after minimum light near phase -0.40. Between phases -0.40 and -0.30 the shock propagates through the infrared (1.6 μm) continuum. The infrared line-forming layers are first affected at phase -0.30 when the CO column density (Figure 6 [in Hinkle et al., 1982]) begins to decrease [due to the CO dissociation by the shock]. By about phase -0.10, the expanding gas behind the shock has cooled to the point where a detectable column density of CO can form. From phases -0.10 to 0.15, the CO continues to associate behind the shock zone while CO is simultaneously dissociated by the advancing shock.... The observations. . .[from phases -0.10 to 0.15] record (1) part of the previous photospheric gas falling inward and (2) gas for the next light cycle moving outward.... [Note that] the shock *has already passed through much of the photosphere* when the CO second-overtone spectrum becomes double lined.... By phase 0.15, the CO column density reaches its plateau value and from then until phase 0.7, it remains constant to within the accuracy of measurement. During this interval, the line forming layer expands, stops and falls back towards the stellar surface under a constant inwards acceleration of 0.098 ± 0.005 cm s^{-2}. The CO column density drops an order of magnitude by phase 0.85 and another by phase 1.1. The observed acceleration of the layer changes at phase 0.85 and it reaches an equilibrium infall value of 7.5 km/s which is maintained by a small amount of gas until at least minimum light."

Note that the weak CO emission lines of Figure 2-2 might result from the recombination of the CO behind the shock.

Some estimates of the physical parameters of the χ Cygni photosphere are available from

the foregoing model:

1. From $L \sim R^2 T^4$, where L is the luminosity ($L = 7000\, L_\odot$), T is the mean photospheric CO excitation temperature, and R is the photospheric radius (all quantities reduced to solar units), Hinkle et al. (1982) obtain: $R = 240\, R_\odot$ (i.e., 1.7×10^{13} cm). It is found that the stellar pulsation produces a variation in radius of $\pm 100\, R_\odot$.

2. The thickness of the CO line-forming region is the total thickness of the linearly accelerated part of the atmosphere, obtained from the time the rising shock takes to traverse the falling line-forming region. With some assumption on the shock velocity not directly measurable, Hinkle et al. find that, from phase -0.3 to -0.10, the outward-moving shock covers about 8×10^{12} cm. Concurrently, the infalling gas travels 1.2×10^{13} cm. Finally, the thickness of the CO line-forming region is 2×10^{13} cm, comparable to the radius.

3. The mass of the stellar atmosphere is $M \sim 2.5 \times 10^{31}$ gm (if one assumes $mL = 4200$ gm/cm^2 and an exponential distribution of the mass through the line-forming region).

Source of the Visible Spectrum. Besides the photospheric layers, we described another three atmospheric components seen by Hinkle et al. in χ Cygni from CO observations. These are: (1) a hot ($T \sim 1500$ K) gas infalling at about 8 km/s relative to the center of mass, (2) a cooler ($T \sim 800$ K) stationary shell, and (3) a still cooler ($T \sim 300$ K) gas expanding at 7.5 km/s. The last two components clearly correspond to extended atmospheric layers that will be detailed in the section *Circumstellar Lines—Properties of Gaseous Shells*. The infalling gas deserves further comment. From Figure 2-1 (middle panel, 3-1 CO lines), the infalling CO component velocity appears to be in agreement with the blue-violet absorption-line velocity, rendering plausible the idea of Hinkle et al. that the infalling region is the source of the visible spectrum. In fact, as the blue spectrum does not suffer the pronounced phase-dependent velocity change shown by the $\Delta v = 3$ photospheric lines, it can well be formed *above* this IR line-forming region (i.e., above the photosphere). Consequently, the fact that the visual (blue) atomic absorption lines do not arise in the photosphere removes the discrepancy in the determination of the sizes of the Miras that puzzled the astronomers (e.g., Wallerstein, 1977) when they used a photometric or a visual spectroscopic approach.

Hinkle and Barnes (1979b) explain that the continuum shortward of about 6000 Å, formed in the shock region near maximum phases, permits us to see only the component of the slightly doubled lines formed above the shock, producing illusion of infalling gas in the 4000 Å spectrum. Also, they explain the gross cycle-to-cycle variations of the blue visual velocities by suggesting that the infalling gas might be in clumps or in a layer of uneven thickness. In addition, Hinkle et al. (1982) present some evidence for this material falling back onto the photosphere from the 800 K quasi-stationary layer. Emission lines discussed in the next section will come back to this point.

Further Probes of the Pulsating Photosphere

The Mira M Star, R Leo. R Leo also provides evidence that a Mira variable is radially pulsating. It has been extensively studied in the infrared by Hinkle (1978) and Hinkle and Barnes (1979a, 1979b), as well as in the visual (Merrill, 1946, 1952c) and in the millimeter range (Wallerstein, 1975).

It is interesting to complete the results shown by χ Cygni with the analysis of molecular lines not only by CO, but also of OH and H_2O and of atomic lines in R Leo, by Hinkle (1978) and Hinkle and Barnes (1979a, 1979b).

Large amplitude radial-velocity variations with phase (S-shaped curves) are obtained for:

1. The low excitation OH first-overtone lines, the CO second-overtone lines together with the 2–0 high-excitation CO first-overtone lines and the atomic lines, all formed in the stellar photosphere: the excitation temperature ranges from 4500 to 3000 K. The velocity amplitude of the photospheric spectrum is around 25 km/s.

2. Some lines from the H_2O molecule. Their excitation temperature is about 1700 K, showing that they originate near the boundary layers of the photosphere, in cooler and outer layers. They are expected to move more slowly than the hotter CO and OH forming regions, due to a weaker mechanical coupling to the underlying pulsation.

In addition, still cooler overlying components that might be the inner portion of the circumstellar shell are distinguished, such as a H_2O layer at $\sim$1100 K, the velocity of which duplicates a CO plus OH region at $\sim$1000 K showing radial-velocity variations of $\sim$16 km/s amplitude; it is reasonably to be located at the inner boundary of the CS shell close to the star and still having a significant mechanical coupling with the photospheric layers.

Carbon Stars: Miras and Semiregular Variables. In the literature, a Mira carbon star, R Lep, is known for doubling the CN molecular lines in the 6100 to 6700 Å spectral range near maximum light (Phillips and Freedman, 1969). On the other hand, the radial-velocity curve drawn for R Lep as a function of phase from CN lines over the same spectral region by Sanford (1950; Figure 2-3) is illuminating. We now recognize that this curve has a distinct S-shape, which is also conspicuous in other Miras observed by Sanford (1950): V CrB, V Oph, and U Cyg. Unfortunately, the curves are average curves for several cycles, obliterating a possible line-doubling effect. Nevertheless, the Mira C stars probably behave in the same way that the Mira M stars behave, the pulsation being associated with the photometric variability. The amplitude of the shock is about 20 km/s in U Cyg and R Lep, but only about 15 km/s in V CrB and V Oph, thus lower than in the Mira M or S stars where it can reach up to $\sim$30 km/s.

For such semiregular C stars as RR Her, T Cnc, and V Hya, the characteristic radial-velocity S-curve is also noticeable in Figure 2-3, in particular for the SRb variable RR Her, but the amplitude is low ($\leq$10 km/s). However, such a low-amplitude shock seems able to ionize a sufficient quantity of hydrogen, since Sanford (1950) see Hα in emission in the quoted stars, except in T Cnc. We will return to hydrogen emission in SR variables in the section *Hydrogen Emission Lines*. We note that Hinkle et al. (1984), observing IR CO lines in M semiregular stars, noticed S-shaped radial-velocity curves, but *no* line doubling (e.g., X Oph). The M supergiant, α Ori, which will be fully discussed in the section *Atmospheric Kinematics*, part on *Other Giants and Supergiants*, is another example.

An interesting point to make from these radial-velocity curves is that they might be used to determine the stellar velocity, despite the restrictions noted by Hinkle (1978). This is important for the C stars, still hardly observed for the CO microwave thermal lines. (The SiO thermal lines might be observed only in stars with a high Si abundance.)

Analysis of Absorption-Line Velocity Histograms in Miras. Willson et al. (1982) plot histograms of the radial-velocity distribution of atomic absorption lines in some Mira variables at various phases. Furthermore, they investigate the dependence of velocity on excitation and ionization potential, wavelength, and line strength by a multiple regression technique (Pilachowski et al., 1979). From their analysis, they claim that the histogram of the visual spectra (4000 to 7000 Å), together with the IR molecular lines, is better understood physically

speaking *by assuming two shocks propagating in the atmosphere at any one time*, a large amplitude "lower" shock (at about 1 R_*), plus a smaller amplitude "upper" shock (1.5 to 2.5 R_*). The two-shock model is implied by the theory that one shock is formed per period and persists for more than one period in the atmosphere, becoming gradually weaker with time (Hill and Willson, 1979). Thus, the upper shock is the weakened relic of the lower shock from the previous cycle. Criteria for assigning spectral features to either the upper or lower shocks have been given (Hill and Willson, 1979; Willson et al., 1982). Linked to the lower shock are the visible continuum near maximum, the high-excitation components of the IR molecular lines, and more generally, absorption lines with higher excitation (T_{ex} > 3000 K) and ionization potentials than lines originating in the upper shock. The lines from the lower shock are expected to be weaker because they may be filled in by the continuum from overlying layers; they occur mainly in the red spectral range (≥ 7000 Å), where the strongly wavelength-dependent opacity (assumed due to the Rayleigh scattering) is much smaller. To the upper shock are linked the visible absorption-line spectrum (TiO included for the M Miras), the low-excitation component of the IR molecular lines, features from the blue spectral range, and generally speaking, features with low excitation (T_{ex} < 3000 K).

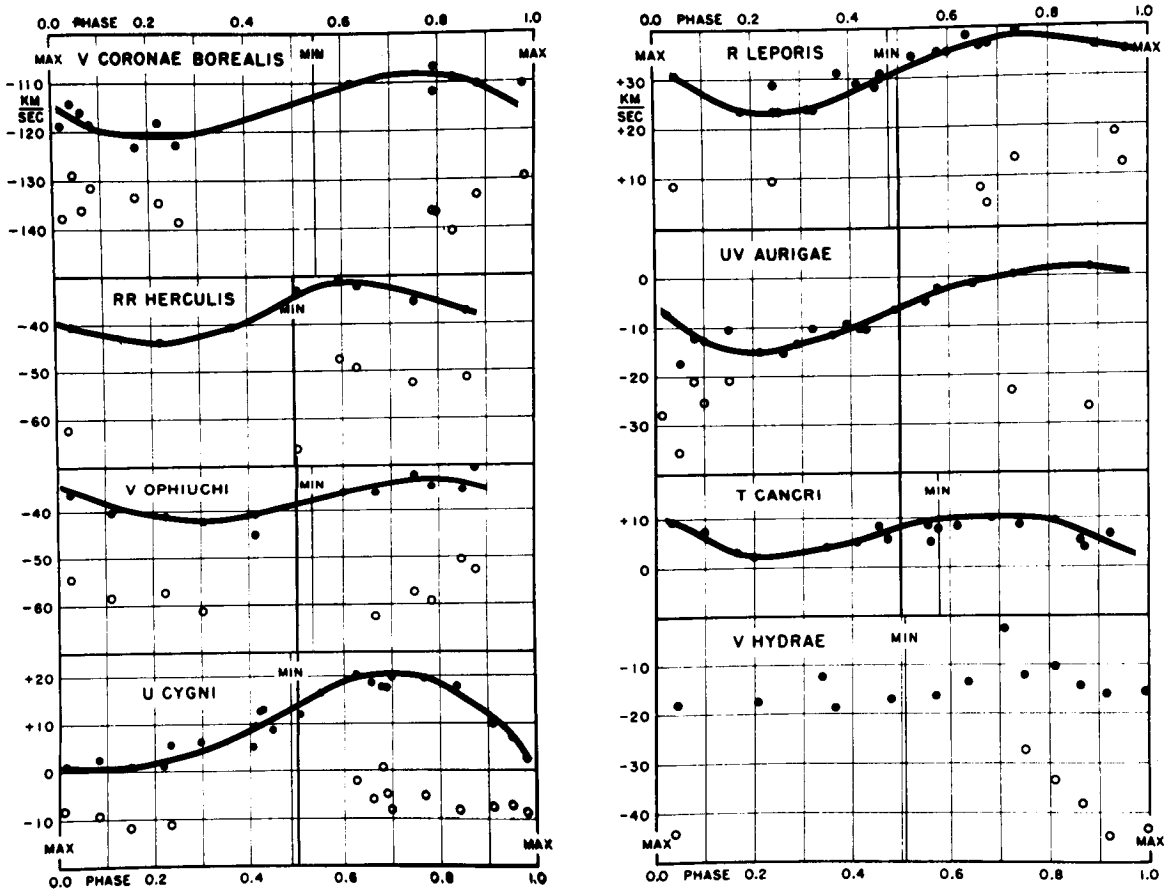

Figure 2-3. The radial velocities in carbon stars as a function of phase. Solid circles = CN absorption-line velocities; open circles = emission Hα velocities (adapted from Sanford, 1950).

Willson (1979) summarizes other criteria for the features assumed to form near the lower shock: (1) they are as regular as the light curve of the IR high-excitation line-velocity curves; (2) they show consistent phasing with the light curves; (3) they show overlying absorption; and (4) they are formed at large continuum optical depths (as are the IR lines). Two regions of line origin arise from each shock: postshocks A and C and preshocks B and D for the lower and upper shock, respectively, implying a four-component velocity (Figure 2-4a).

The main issue is whether there is an alternative interpretation of the observations *involving a single rising shock* (Figure 2-4b). As an example, we report RT Cygni as discussed by

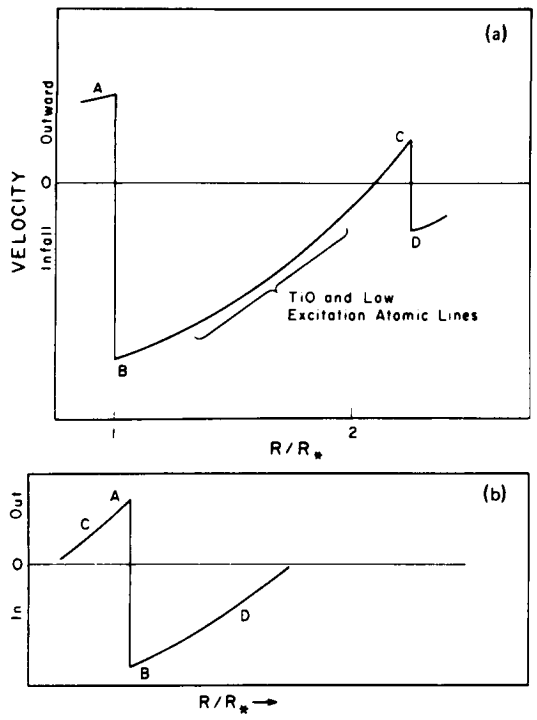

Figure 2-4. Schematic velocity structure in a Mira near maximum light: (a) if two shocks are assumed to propagate in the atmosphere at any one time; (b) if only one shock is assumed; (A) and (C) postshock line-forming regions; (B) and (D) preshock line-forming regions in lower and upper shock, respectively (from Willson et al., 1982).

Willson et al. (1982). On one hand, from their regression coefficients analysis, they conclude that the presence of at least one shock front in the reversing layer can explain the dependence of the velocity on the wavelength, line strength, ionization potential, and excitation potential with complete consistency. From the red and yellow spectral regions especially, it is seen that, as the shock rises through the atmosphere, first the low-lying higher excitation lines are affected, followed by the lower excitation lines that originate higher in the atmosphere. On the other hand, from the histogram analysis, near maximum light (φ = -0.02), the velocity structure might be consistent with a two-shock model (Figure 2-4a and Willson et al.'s Figure 5). For the lower shock, the postshock velocity at A is about +11 km/s, and the preshock velocity at B is about -20 km/s, while for the upper shock, C ~ +6 km/s and D ~ -8 km/s relative to a theoretical stellar velocity (Hill and Willson, 1979) at about -119 km/s. The velocities are corrected for geometrical effects. (See the section *Preliminary Remarks.*)

As emphasized by Willson et al. (1982), the A and C components are difficult to separate from each other (we will refer again to this point when discussing emission lines in the section *Atmospheric Kinematics*, part on *The Mira Stars: The Shock-Wave Model*) and very few lines are available to give the B component since they tend to be weak because of the filling in by the continuum from higher atmospheric layers. Willson et al. continue that, if the A and C lines are combined into a single region of origin and if the B component lines are ignored, using only the D component for the infall velocity, a single shock with a geometrically corrected amplitude of $\Delta v \equiv A - D \sim 19$ km/s is invoked to interpret the histograms. However, with such an amplitude, a shock in a Mira atmosphere is not likely to ionize sufficient hydrogen to produce the strong Balmer lines that are observed. (See the section *Hydrogen Emission Lines.*) An amplitude of at least Δv = 25 km/s seems to be required (Tsuji, 1971). However, as some B component lines are observed (at +8 and +25 days from maximum

in yellow and red ranges), it should be more plausible to consider a single shock, such as that in Figure 2-4b, with an amplitude $\Delta v \equiv A - B \sim 31$ km/s. Such a shock amplitude is inferred from the IR molecular absorption lines and the red atomic lines in χ Cygni (Figure 2-1, from Hinkle et al., 1982) or R Leo. In support of this single-shock model, one should recall (see the above section *Photospheric Kinematics—The Shock-Wave Model*) that the shock is first detected in the infrared (due to a lower opacity than in the blue region), early in phase, through the observed variation in the CO column density; it has passed through a large part of the atmosphere when the IR and red lines become double around maximum light. The D components, issuing mainly from the blue spectrum, appear to be formed well above the shock. This is in agreement with the idea (Hinkle et al., 1982) discussed in the above section *Source of the Visible Spectrum* that the blue absorption lines are no longer representative of the photosphere or the reversing layer of the star as previously thought; rather, they are related to an outer shell and formed relatively high in the atmosphere. Consequently, an upper shock appears to be no longer necessary to explain their nonperiodic fluctuations in velocity. Emission lines (see the section *Atmospheric Kinematics*, part on *The Mira Stars: The Shock-Wave Model*) will provide further arguments in favor of a single shock.

Summary: What information is obtained from the absorption lines?

They tell us that cooler circumstellar layers are present in Miras. In this framework, important results are: (1) the blue-violet absorption lines are linked to an outer layer rather than to the photosphere; and (2) a quasi-stationary shell exists in the Miras.

Infrared absorption lines, mainly molecular lines, prove that the photosphere of M, S, and C *Miras* undergo a shock-pulsation motion of the W Virginis-type linked to the radial global stellar pulsation driving acoustic waves. Generated by turbulence at the top of the hydrogen convective zone, these waves turn into shocks, dissipating energy and heating the stellar layers, as they propagate outward into layers of decreasing density (Stein and Leibacher, 1980). The characteristic of the Mira model is that *a shock is formed just below the visible photosphere*; this is essentially what we mean when speaking later about the photospheric Mira-like shock-wave model. The undisputable indicators of such a mechanism are the S-shaped large-amplitude radial-velocity curves with respect to the stellar phases and the line-doubling effect around maximum light.

For semiregular stars, data are still scarce. However, S-shaped curves from visible CN or IR CO lines are recognized in the few available examples, suggesting that the Mira-like pulsating mechanism might work in these stars. However, the curves have a much lower amplitude than in the Miras, indicating less available energy or larger damping. IR CO line doubling is also absent, meaning that the rising hot gas from deep layers cannot be seen at the same time as the cool infalling gas, but the cause is presently unclear. *Observations are urgently required on semiregular (SR) and irregular (L) stars.*

EMISSION LINES

We exclude here the radio emission lines (see Rieu, this volume) and emission in P Cygni line profiles, which are treated in the section *Circumstellar Lines—Properties of Gaseous Shells.*

In general, all the M, S, and C stars of Mira type show strong emission lines at some epoch, as do some semiregular stars. (See, for example, the compilations by Bidelman, 1954; Meinel et al., 1969; Yamashita, 1972; Stephenson, 1973; Keenan et al., 1974; and Catchpole et al., 1979.) Some additional semiregular variables show weak emission lines at some phases; others show emission lines at some phases in some cycles.

In what follows, the discussion on changes with phase will focus mainly on the Mira stars. Note that, among the 223 Miras reported by Catchpole et al. (1979), only some rare cases

are not mentioned as having emission lines (e.g., the M star, SU Pup, or the C star, RV Cen). However, these stars may not have been observed for a sufficient time.

General Behavior of Emission Lines with Phase

Optical Range of Mira Variables. Variability of the atomic emission lines in the visible spectral range has been known since the beginning of the century, whereas the UV range recently explored by satellites has seldom been used. In the following section, the discussion is based mainly on certain typical stars because the very similar behavior in various Mira spectra of many complicated details is remarkable (Merrill, 1952c).

The emission lines undergo striking modifications with phase. They can have a strong intensity and a broad profile and can appear as the most outstanding features in the spectrum, even at low resolution, or they may be radically altered and partly extinguished by the absorption lines above them or so weakened as to completely disappear. Moreover, this behavior is cyclic in the Mira stars, although some differences are noted in the pattern from cycle to cycle in a given Mira, and from star to star in the same spectral type (Merrill, 1952b). The emission lines are stronger and more numerous in cycles with a high maximum brightness (e.g., Hβ in o Cet is much more intense for the brighter maxima (Joy, 1954)).

Except for about one third of the period just after minimum, emission lines are usually present in the spectra. Roughly speaking, most of the lines are brightest just after maximum. The hydrogen Balmer lines, recognized up to H18 (Merrill, 1947a), characterize the spectra of Mira variables at maximum light when they are very bright, whereas at minimum light, they are weak or absent. With advancing phase, the Fe II(1) emission lines become outstanding features. For a given phase after maximum, the emission spectrum is completely different from the spectrum at the same phase before maximum. As an example, for o Cet, Joy (1954) in his Table 7 gives the phases in which the main lines of various elements in the optical range are just detectable, when they are at their maximum, and finally when they disappear. Some metallic lines appear early in the cycle on the blue part of the absorption lines. After the maximum, the number of emission lines of additional elements and their brightness rapidly increase, beginning with the lines from higher excitation potentials. Common are the main lines from the following neutral atoms: Fe I (in particular, the lines at λ4202 and λ4308 are abnormally strong in emission and indicative of a resonance mechanism), Mg I, Si I, Mn I, In I, and Co I; and from ionized atoms: Fe II, Ti II, Mn II, Ca II (H and K lines and the IR triplet lines), and Sr II. Some lines are so dominant that they obliterate the absorption lines.

An example depicting different behavior from most emission lines in various cycles is given by the S Mira star, R Cyg. In 1951, a large number of sharp metallic emission lines of certain multiplets were stronger a month before maximum light ($\varphi \sim 0.93$) than after it, with an abrupt decrease as maximum light was approached (Merrill, 1952a), contrasting with the classical behavior of the various metallic emission lines in Miras that become strongest after maximum. Further spectra were obtained at two successive maxima in 1957 and 1958 (Deutsch and Merrill, 1959). At the abnormally low maximum in 1957, the spectra show many more metallic emission lines than in 1951. They appear in absorption at the 1958 maximum, whereas in 1957, fewer absorption lines appeared and the resonance lines were much weaker than in 1958.

At minimum light, the striking feature is the high-excitation [Fe II] forbidden lines. Other lines such as [Mn I], [S II], and [O I] are also visible. Note that the forbidden lines are not mutilated by absorption lines (e.g., by the TiO lines which are strong in the M stars spectra); this should imply that they are formed above the TiO layer. Another particular feature of minimum light is the appearance of emission lines due to the AlH molecule identified in S-type spectra such as in χ Cyg (Herbig, 1956) and in U Ori (Wallerstein, 1975), a star which

does not show [Fe II]. Referring to the occurrence of molecular emission, Herbig (1956) also quotes AlO emission in the Mira M star, *o* Cet, at the abnormally low maximum in 1924 and emission by the violet CN molecule in R CrB near minimum light, which was also confirmed by Wing et al. (1972). A search for the AlO emission in spectra of several variables (Kipper and Kipper, 1979) indicates that this emission is an extremely rare event.

UV Range

Example of a Mira Variable, χ Cygni. Variation in emission-line strength with postmaximum phases has been observed for the S Mira star, χ Cyg (Cassatella et al., 1980), with the International Ultraviolet Explorer (IUE) satellite in the low- and high-resolution modes. At phase 0.04, at the limit of the optical spectrum near 3200 Å, the Fe II (V1) and (V6) lines are the only outstanding emission features. Two months later, at phase 0.18, the Mg II h and k doublet appears in emission, together with Fe II (UV 1, 32, 62, and 63) lines, whereas the Fe II (V6) lines are now almost unidentifiable at low resolution and the Fe II (V1) lines are still strong.

Example of a Semiregular C Star, TW Hor. Nine spectra of TW Hor (Figure 2-5) were obtained with IUE in the low-resolution long-wavelength mode during an interval of 3 years (Querci and Querci, 1985a). The striking feature is the variation in intensity of all the emission lines. The most important variations are shown by the Mg II U1 doublet at 2800 Å and by the Fe II V1 lines and the V II V7 lines around 3280 Å. The Fe II V1 + V II V7 blend varies by at least a factor of 10. It is strongest on LWR 7774 on May 16, 1980 ($\varphi \sim 0.72$), and weakest on LWP 1852 on April 27, 1983 ($\varphi \sim 0.70$). This points out a different behavior of the blend for very similar phases in various periods, unlike what is observed in Miras. On the other hand, the Mg II h and k blend varies less strongly than the Fe II V1 blend for nearly similar phases in different periods (LWR 7774, LWR 9049, and LWP 1852 at $\varphi \sim 0.7$).

The other emission lines are mainly other Fe II lines. Lines from the U3, U4, and U5 multiplets around λ2250 are visible in May 1980, absent in December 1982, and again observable 1 month later. They are of similar strength to the Mg II U1 lines on March 23, 1982, but only just detectable a day before (LWR 12834 and 12835). Note that the Fe II V1 + V II V7 blend does not change on such a short time scale. It should be concluded either that the various Fe II lines do not originate from the same chromospheric layers (as it is observed in α Ori by Carpenter, 1984, for example) or that the λ2250 Fe II lines are blended with another element (C II U43, for example).

The Fe II U3 + C II U0.01 blend at λ2325 exhibits a different behavior. It is broader on March 23, 1982, similar on March 22, 1982, and January 1983, and fainter on May 1980, demonstrating the variable contribution of the C II and/or Fe II lines. The Fe II U62 and Fe II U63 lines around λ2750 are sometimes detectable, mainly during March 1982. The Al II U1 lines at λ2670 are not visible on the image LWR 12834, but are suspected 1 hour later on LWR 12835 and, being much stronger 1 day later, on March 23, 1982. Presently, Al II U1 lines are the only lines through which such a short time-scale variation might be inferred; because they are very near the noise level (about 3σ), further observations are needed to confirm this variation.

Variations in Radial Velocities of Emission Lines

Changes in Emission-Line Radial Velocities with Phase—An Example: the Mira Star, *o* Ceti. The variation of radial velocities with phase is obtained from the sharp emission lines of metals in the visible region. In their initial stages, many of the emission lines appear as bright edges on the shortward sides of absorption lines (Merrill, 1940). We shall come back to such profiles in the section *Selected Emission-Line Profiles.* As the phase advances, they

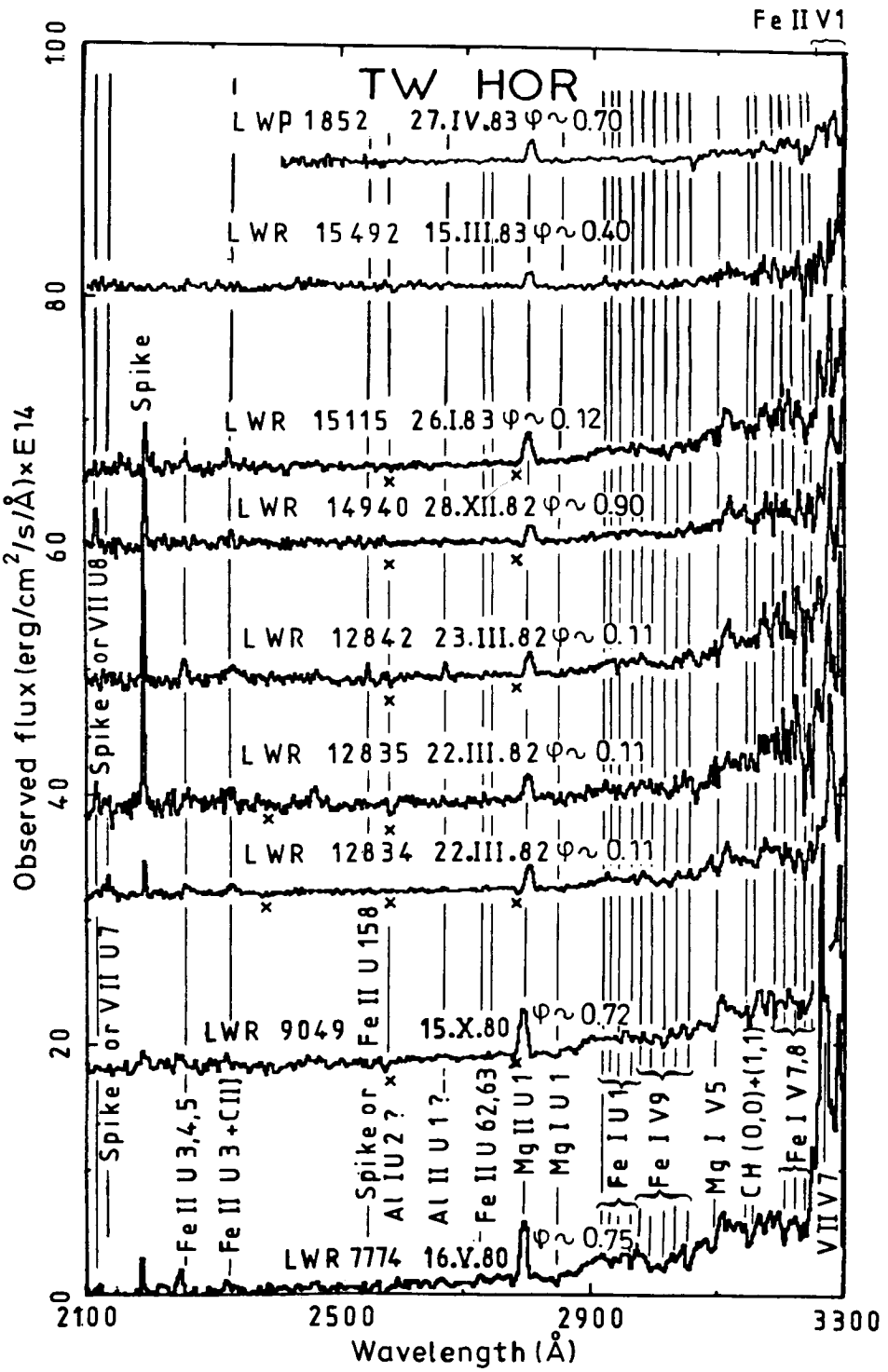

Figure 2-5. IUE spectra of the semiregular carbon star, TW Hor (N0; C7, 2; P ~ 157 days) taken on various dates from 1980 to 1983, illustrating emission-line variations with time. Note the particularly high emission in the Fe II V1 + V II V7 lines around 3250 Å on May 16, 1980, compared to its low level on April 27, 1983. The LWR 12834 and LWR 12835 images are two successive exposures about 1 hour each. The crosses indicate reseau marks (from Querci and Querci, 1985a).

increase in strength, shifting longward and encroaching on the absorption line that is apparently displaced longward. Velocity measurements of the hydrogen lines are possible at all phases if the lines are strongly overexposed. The most complete set of radial-velocity curves over many cycles is given for *o* Cet, from spectra in the region 3770 to 4290 Å obtained over a period of 16 years (Joy, 1954).

Because of differing processes leading to their formation, different spectral lines require particular physical conditions. For instance, the pumped emission lines (in other words, the fluorescent lines) arise in cool tenuous gas, whereas emission lines of singly ionized elements are formed in the hottest regions. Consequently, reliable radial-velocity curves cannot be drawn from emission lines belonging to different classes, as has sometimes been done in the past. Furthermore, it is now known that absorption lines with a low-excitation potential are circumstellar lines; they are blue-shifted and generally present a P Cygni profile. (See the section *Circumstellar Lines—Properties of Gaseous Shells.*) Finally, we discuss Joy's (1954) curves reproduced in Figure 2-6a, b. Also reported in this figure is the center-of-mass velocity of *o* Cet of 56 km/s (heliocentric; Engels, 1979; Knapp et al., 1982), enabling us to update Joy's discussion: *all the lines*, from their appearance to their disappearance around minimum light, *are seen to be formed in rising layers*.

While the ionized metals (Ti II, Sr II, and Fe II) have rather small velocity variations with phase, the neutral metal lines (Si I) show a large amplitude variation (Figure 2-6b). As for the hydrogen lines, Joy measures Hγ and Hδ because, in his spectra, they are visible over the longest time interval and are disturbed less by the overlying absorption than other hydrogen lines. Figure 2-6b shows the course of the velocity variations of the Hγ and Hδ lines in *o* Ceti and, for comparison, Figure 2-6d (i.e., Joy's Figure 4f) reproduces the R Leo, R Hya, and χ Cyg curves from numerous hydrogen lines up to H18. For R Leo, Hinkle (1978) plots the hydrogen velocity curve and a part of the IR CO and OH photospheric S-shaped velocity curves together (Figure 2-6c). The shape of the curves is similar, supporting the idea of a shock wave propagating in the photosphere (as discussed in the section *Photospheric Kinematics—The Shock-Wave Model*) which also excites the hydrogen emission. Moreover, the hydrogen emission-line curve lags in phase by 0.2; this is a further argument for a running wave through the photosphere, as discussed below. (See the section *Atmospheric Kinematics.*)

The shapes of the hydrogen curves of R Hya and *o* Cet might support the radial-velocity behavior with phase in Miras, in spite of the lack of measurements from $\varphi = 0.2$ to 0.4 in *o* Cet and of unpublished data of IR lines for these stars. The χ Cyg hydrogen curve is not representative because one lacks data at maximum light and it has an erratic behavior with phase, perhaps due to some difficulties in the measurements.

Figure 2-6a reports on pumped Fe I emission lines: the 4307.9 line is pumped by Mg II (2795.5 Å), together with the 4202 line, and the 4063 line is excited by Hϵ. The Fe I pumped lines are present at the same phase as the ionized metal lines, Sr II and Ti II. As for Fe II, the lines from multiplets (27) and (28) surprisingly cover all the star's period except for a few weeks after minimum, whereas multiplet (3) lines at 3914 and 3938 Å behave as the other ionized metals. (Note that all the Fe II lines are blended in the velocity curve of Joy, 1954.).

Dependence of Emission-Line Radial Velocities on Excitation Potential. The dependence of the radial velocities on the excitation potential of the upper level appears clearly in the emission lines of the ionized and neutral metals. The high-excitation Fe I lines yield algebraically greater velocities than the low-excitation lines (Merrill, 1952b). An illustration is provided by the Fe I lines in χ Cygni (Maehara, 1971), in which large velocity gradients occur in the emitting layer. In *o* Ceti, Joy (1954) also notes that the Fe I lines with a mean excitation potential of 5.3 volts, such as $\lambda\lambda$ 3852.6 (73), 3949.9 (72),

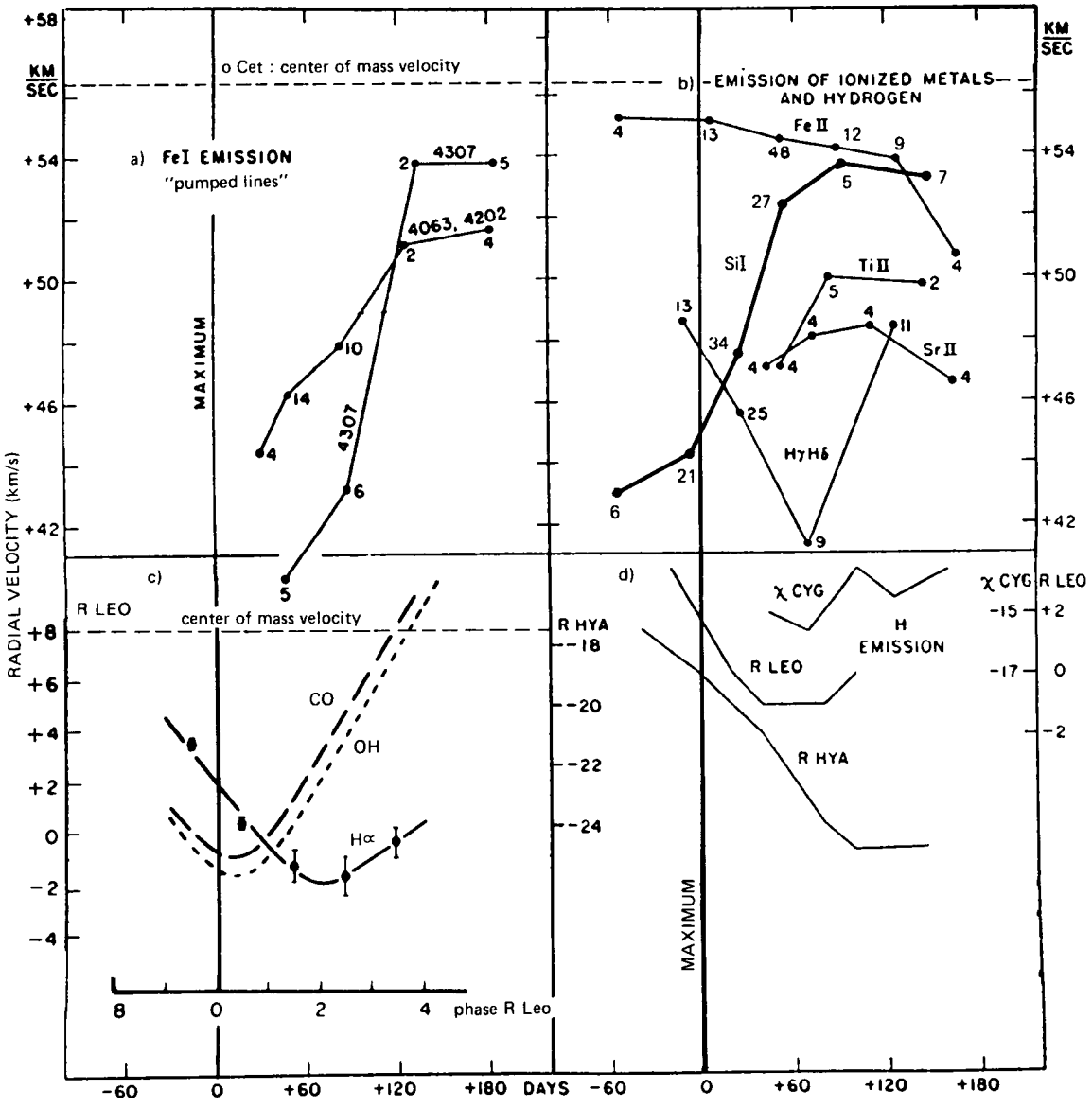

Figure 2-6. Mean radial velocities in M Miras plotted according to phase from maximum light: (a) pumped Fe I emission lines (λ4307 and λλ 4063, 4202) in o Cet (the numerals represent the number of measures included in the means and defined in Joy's (1954) Table 8); (b) emission lines from ionized metals (λλ 3759, 3761 Ti II, λ4077 Sr II, λλ 3938, 4233, 4178 Fe II), from the hydrogen-like neutral metal λλ 3905, 4102 Si I, and from Hγ and Hδ, in o Cet; (c) Balmer emission (solid line) and photospheric components of CO (long dashes) and OH (short dashes) in R Leo; (d) hydrogen emission lines in χ Cyg, R Leo, and R Hya. (a, b, d: adapted from Joy, 1954; c: from Hinkle, 1978).

and 3977.7 (72), give higher velocities than lines with a mean excitation potential of 4.5 volts, such as lines at 4063.6, 4202 (42), or 4307.9 (42) Å. Following the phase, the mean difference between high- and low-excitation lines is 2.5 km/s from +40 to +110 days (φ = 0.12 to 0.33) after maximum and 13.3 km/s from +110 to +170 days (φ = 0.33 to 0.51).

Using the data published by Joy (1954) for the metal lines in *o* Ceti, over eight cycles from -20 to +120 days around the maximum in each cycle (i.e., from φ = 0.06 to φ = 0.36 with a mean period of 331.65 days (Kukarkin et al. (1969)), Maehara (1971) finds the variation of the acceleration (the time derivative of velocity) with the visual magnitude at maximum, assuming a linear relationship between the radial velocity and the phase. From this, the smaller decelerations tend to occur in the brighter cycle.

Selected Emission-Line Profiles—Temporal Changes, Particular Shapes

Hydrogen Emission Lines. Very intense Balmer emission lines are observed in the spectra of the *Mira variables*. At the premaximum phase or shortly after maximum light, the lines appear to be much broader and severely mutilated by several superposed sharp absorption lines. Since the absorbents vary from one type of star to another, this explains the variation in line intensity with stellar type: Hβ is stronger in C stars than in M stars where it is affected by the heavy bands of the TiO molecule. Hα emission is usually disturbed by an absorption band in the M Miras and is absent in other types (Wallerstein, 1975). Examples showing Balmer line profiles in M Miras are given by Joy (1947) and Fox et al. (1984). With advancing phase, the absorptions disappear and the lines become intense and narrow, suggesting that the hydrogen-forming layers have progressed above the absorbing layers.

In the infrared, Paschen γ and Paschen δ are detected (Spinrad and Wing, 1969). A strong emission Paschen β line at 7802 cm^{-1} is found in *o* Ceti with the equivalent width of the line changing by a factor 2 on *a time scale of about 2 days* (Kovar et al., 1972). Because Pβ is not affected by molecular absorption, this might be an intrinsic variation in the strength of the hydrogen line. Kovar et al. confirm these variations in time when quoting the short variations observed in Hγ and Hδ by Odell et al. (1970) in *o* Ceti. Several Miras show a variation in the intensity of the Hδ emission, which also appears relatively free of overlying absorption, over 1 or 2 days, while the brightening of the stars remains constant to within 0.1 magnitude (Keenan, 1966).

Brackett γ is present in emission in *o* Ceti 40 days after maximum and also in R Leo (Johnson and Mendez, 1970). In the latter star, it is strongest at phase 0.94 and also broad (90 km/s across the base) (Hinkle and Barnes, 1979b). Bγ is already undetectable when the Balmer lines first appear at about phase 0.9 and reach their maximum intensity at phase 0.16. The differing lifetimes of the hydrogen lines in the visible and the infrared regions is explained by a continuum intensity in the visible which decreases with phase faster than the line intensity, which keeps the Balmer lines relatively stronger. This effect is reversed in the infrared. A depression of the continuum in R Leo around the Hγ emission is noted by Maehara (1971).

Jennings and Dyck (1972) summarize Balmer emission data for stars of *semiregular and irregular M types*, specifically excluding the Miras. Only five M giants and supergiants are quoted in the literature consulted from 1893 up to 1971 as showing or having shown Balmer emission. The most interesting data (originally from McLaughin, 1946) concern the supergiant, μ Cep, in which Hβ, Hγ, and Hδ emissions appear strongest just before the maximum light and then disappear as the star fades; the hydrogen lines become visible in absorption at minimum light. This is a Mira-like phase behavior. Such a behavior is also observed in the semiregular C stars, RR Her and V Hya (Sanford, 1950), in which Hα is present in emission from 0.25 period before to 0.25 period after maximum light. It is not observed at all in the semiregular C star, T Cnc.

Another different example is given by the semiregular C star, WZ Cas. Bidelman (1950) observes the hydrogen lines in emission on January 2, 1949, and recalls that the only available previous observations showing emission in Hγ goes back to 1903. Yamashita (1972) notes the absence of Hα and Hβ on his spectra taken in January 2–10, 1967. Examination of spectra on file at the Haute-Provence Observatory showed that the best covered year is 1978: hydrogen emission was visible on September 13–16, but no emission was detected on September 17 or on January 1, August 9, October 16–23, and December 16–17. Unfortunately, the available photometric data are too scattered over these periods to determine the corresponding light phase.

Generally speaking, the presence of hydrogen lines in emission, if any, in the SR variables is not likely to be regular from cycle to cycle or within a cycle, as in the Miras. Is it due to some fundamental differences in chemical composition or physical properties or to observational problems? In fact, the SR light-amplitude variations are smaller (see F. Querci, this volume), so that we can expect that the causes of the SR variations (e.g., in the shock-wave mechanism) are weaker than those producing the large-amplitude Mira variations and the emission lines around the Mira maxima. On the other hand, knowing that the cycle of an SRa variable is shorter than the Mira period, the duration of the emission lines may also be shorter. Much more closely spaced observations are needed.

Finally, we note that no emission has ever been observed in the hydrogen lines in the M supergiant, α Ori; they are asymmetric absorption lines (Goldberg, 1979; Dupree et al., 1984).

Violet Fe II Emission Lines. The Fe II lines from multiplets 1, 6, and 7 around 3200 Å were observed as early as 1947 by Merrill in postmaximum spectra of Mira variables (e.g., Merrill 1947b). The upper excitation potential is from 4.8 to 5.6 eV, adding up to a total ionization excitation energy of 13.5 eV from the ground state of Fe I. Multiplet (1) was noted as being remarkably intense. In R And during the postmaximum observed interval (+40 to +103 days (i.e., $\varphi \sim 0.10$ to 0.25)), several lines appear to change in relative intensity, while the radial velocities derived from several multiplets do not vary with phase or with excitation potential (Merrill, 1947a); this behavior also occurs in o Cet (Figure 2-6b).

Strong lines of multiplets (1), (6), and (7) were first seen in the spectra of the two M supergiants, α Herculis and α Scorpii (Herzberg, 1948) and were later detected in many other M stars (Bidelman, 1954; Boesgaard and Boesgaard, 1976) and certain carbon stars, such as the irregular variable, TX Psc (Bidelman and Pyper, 1963), and the semiregulars, TW Hor (Bouchet et al., 1983) and T Ind (Bouchet, 1984, private communication). In fact, Fe II emission is virtually always present in giants and supergiants cooler than M0 (Boesgaard and Boesgaard, 1976).

Fe II line profiles have been best studied in the M supergiant, α Ori (Weymann, 1962; Boesgaard and Magnan, 1975; Boesgaard, 1979). The profiles are broad (20 to 80 km/s). Some appear to be mutilated by overlying absorptions: Boesgaard and Magnan identify most of the absorbers with low-excitation lines of circumstellar origin. Many of the moderate and strong lines show steep-sided emission with a central reversal and are asymmetric (Boesgaard, 1973). The degree of asymmetry changes little with time, but the shortward peak is always stronger (Boesgaard and Magnan). The relative intensities of the lines and the intensity of the central reversal are apparently constant. On the plates taken by Boesgaard and Magnan (1975) and Boesgaard (1979) covering a 5-year period from 1970 to 1975, variations in the velocities of the Fe II emission lines follow the same pattern as those of the absorption atomic lines measured in the same spectral region (see Figure 1 in Boesgaard, 1979), implying that they follow the motions of the absorption-line-forming layer. Furthermore, the Fe II emission lines are red-shifted relative to these absorption

atomic lines. Adopting a center-of-mass heliocentric velocity, $V_* = 19.1 \pm 1$ km/s, for α Ori (Huggins, 1984, improving the Knapp et al. (1980) value of 18.8 ± 2.5 km/s), it appears that in the observing period: (1) the considered absorption atomic-line velocities in the blue-violet region are infalling with extreme red shifts of 6.0 ± 1.5 and 1.7 ± 1.8 km/s, (2) the Fe II emission lines also form in infalling layers with extreme velocities being $+12.5 \pm 2$ and $+6.5 \pm 1.8$ km/s relative to V_*. Boesgaard (1979) notes that the reversals in the Fe II emission lines measured in 1974 and 1975 are redshifted relative to the atomic absorption lines. Thus, the Fe self-reversals are also formed in infalling layers with velocities included between $+23.2 \pm 1.6$ and $+7.3 \pm 1.9$ km/s relative to V_*; they are probably the same layers in which the Fe emission is produced.

However, Van der Hucht et al. (1979) found that all the UV Fe emission lines observed in α Ori on September 16, 1976, with the balloon-borne Ultraviolet Stellar Spectrograph (and in particular, three lines from multiplets 6 and 7 also observed by Boesgaard and Magnan (1975)), are *blue-shifted* by -14 (± 9) km/s with respect to the Adams (1956) adopted "photospheric" radial velocity of $+21$ (± 4) km/s (i.e., $\sim -12 \pm 10$ km/s with respect to the systemic velocity). We conclude that in 1976 the Fe emission lines were correlated to an outflow of material and to an infall during the period 1970 through 1975.

Carpenter (1984) studies Fe II emission lines in the 2300 to 3000 Å region of four high-resolution IUE spectra of α Ori obtained from April 1978 to November 1982. Unfortunately, these line radial velocities are not absolute due to a lack of absolute wavelength calibration during the IUE exposures. It may be possible to correlate the photospheric radial velocities by Goldberg (1984) to the ones drawn by Carpenter from the studied spectra at the dates of the observations. Nevertheless, the average photospheric velocity is defined by Goldberg from IR and near-IR absorption lines, whereas it is measured by Carpenter from UV Fe I lines. Recalling the results from Miras that the IR and blue atomic lines are formed in very different layers (see the section *Source of the Visible Spectrum*), it might be hazardous to combine the two average "photospheric" velocities in α Ori. Rather, adopting a probable radial velocity of 21 km/s for the blue lines (as done by Van der Hucht et al., 1979), it appears that the Fe II emission-line centroids are in infalling layers during the observational period. A correlation of Fe II line asymmetry with intrinsic line strength, indicating velocity gradients inside the line-forming region, is also found (Carpenter, 1984).

The semiregular carbon star, TW Hor, deserves special mention. The Fe II emission lines can appear during only 2 consecutive days as in July 1979 ($\varphi \sim 0.75$) (Figure 2-7) or can last at least 4 consecutive days as in August 1981 ($\varphi \sim 0.7$; Bouchet et al., 1983). In addition, they can vary strongly in intensity over a few days; for example, they were observed on October 15, 1980 (IUE observation), then they nearly disappeared on October 17 and 18, and on October 19, they again became as strong as on October 15. Unfortunately, no radial-velocity data are yet available.

Ca II H and K Lines. The Ca II lines (3933 and 3968 Å) show a complex profile in the late-type stars (Deutsch, 1960), giving information on the atmospheric stratification and on the motion of the layers as a function of the geometric depth. The H line is less well studied than the K line due to a weaker oscillator strength and a possible contamination by the Hϵ hydrogen line. The various components that can be found in a Ca II K (or H) line profile are: the K_1 wings that refer to the broad absorption formed in the "photosphere," the K_2 chromospheric emission core onto which is superimposed a K_3 self-reversed absorption core of chromospheric (non-LTE radiative-transfer) origin, and a K_4 deep and sharp CS component. Moreover, faint emission lines of other elements may appear in the K_1-H_1 wings (Stencel, 1977; Linsky et al., 1979). The profile varies with spectral type, showing either a K_3 component inseparable

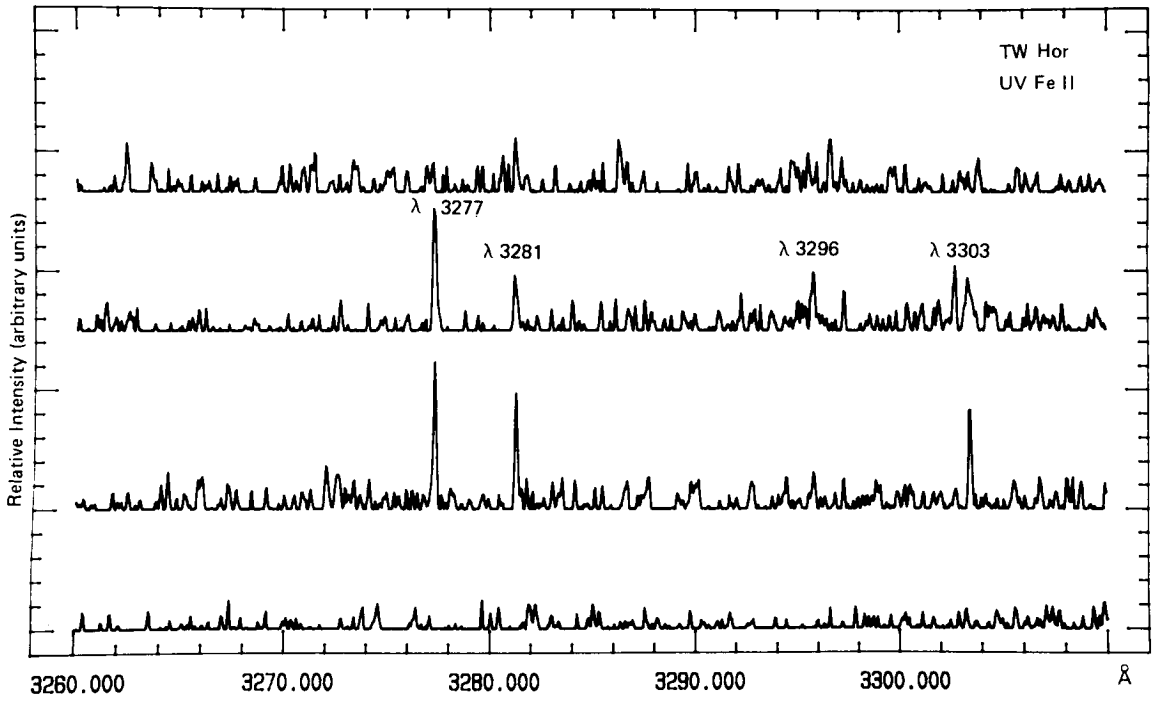

Figure 2-7. Violet Fe II line region in the semiregular carbon star, TW Hor, on four consecutive dates in July 1979 (bottom to top: July 13, 14, 15, and 16, respectively). The ordinates are in arbitrary units (from Bouchet et al., 1983).

from a dominating K_4 component or noticeable asymmetries, as described below. The CS component is discussed in the section devoted to the *Circumstellar Lines*.

The Ca II H and K lines in the *Miras* mimic the metallic emission lines in appearing only on the shortward edge of the H and K absorption cores. Merrill (1960) describes the phase behavior of the Ca II lines in the Mira variables (also see Figure 2 in Merrill, 1952c, which illustrates the line variation with phase in R Leo). In brief, as noted by Hagen et al. (1983), a single blue-shifted feature is seen, rather than the self-reversed absorption core observed in the semiregular and irregular giants (see below and Figure 2-8). These authors also remark that strong and phase-variable emission lines are found in the K_1-H_1 wings at 3938, 3945, and 3969 Å and that they are collisionally excited Fe II (V3) lines. Analogous to R Leo (Merrill, 1952c), o Cet shows pronounced wing emission lines at 3936 and 3938 Å at certain phases; there is a strong contrast variation with phase for the

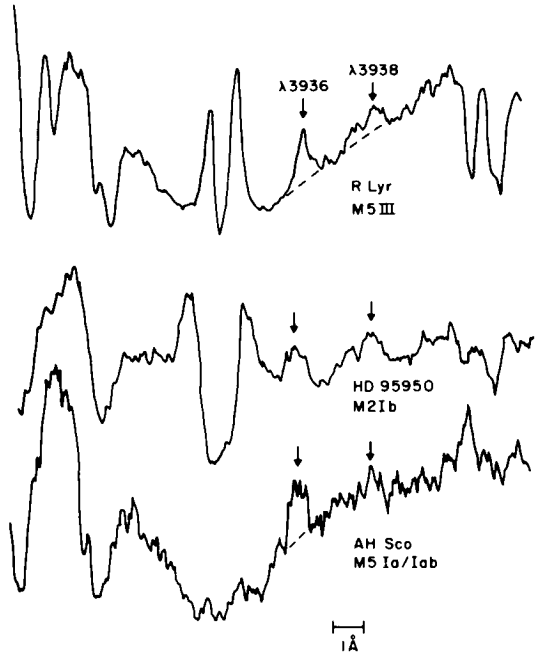

Figure 2-8. Representative Ca II K line profiles in various luminosity class M stars. K_1 wing emission lines are marked by arrows (from Hagen et al., 1983).

3938 Å line, while 3936 Å line maintains an almost unvarying contrast (Stencel, 1977).

A large sample of M *semiregular and irregular giants and supergiants* are observed by Hagen et al. (1983). In all the stars, the K_3 self-reversal component is completely dominated by the deeper CS K_4 component, which is generally blue-shifted relative to the line center. Representative profiles are differentiated (Figure 2-8): (1) the stars of luminosity class III show nearly identical profiles—the long-wavelength emission peak, K_2R, is stronger than the K_2 emission feature on the violet side, K_2V, due to the blue-shift of the narrow K_4 absorption; and (2) the latest giants and most of the supergiants show much broader K_4 features and reduced or no emission: the stars with reduced emission have either $K_2V \sim K_2R$ or $K_2V > K_2R$, depending on the slightly blue-shifted CS component (Stencel, 1978).

Figure 2-8 also mentions emission lines identified in the K_1 wings. All the stars of the sample show one or more of the H–K wing emission lines, even the stars which lack Ca II H_2–K_2 emission. Hϵ in emission is noted in some stars.

The supergiant, α Ori, was observed in the Ca II H and K region in 1974 and 1975 by Boesgaard (1979) with a concentration of six spectra over a 64-day interval. The Ca II K_1 feature is broad, and a deep central absorption reversal is present. The six close spectra show only small changes in the Ca II line profiles due to the position of the deep central absorption minimum. This is in contrast with the high time variation of the Ca II profile shown by Boesgaard (1973) from spectra taken in November 1970 and in December 1971, in which the brightness ratio K_2V/K_2R decreases from 1 to less than 1, and by Kondo (1973) from an undated spectrum in which $K_2V/K_2R > 1$ (compare Figure II-42 from Boesgaard, 1973, and Figure II-18 from Kondo, 1973). Changes in the V/R intensity ratio are common in late-type giants (see discussions in Mullan, 1984; Drake and Linsky, 1983). The measured radial velocities on the 2-year spectra give the following results, obtained by setting the α Ori systemic velocity at 19.1 ± 1 km/s (Huggins, 1984): (1) the absorption-line velocity in the Ca II region fluctuates between +26.0 ± 0.4 and 19.5 ± 0.3, evidencing infalling material (as already found for the absorption lines in the Fe II region); (2) the Ca II emission lines follow the same pattern as the blue-violet absorption lines and are red-shifted relative to the latter (as already noted in the foregoing section for the violet Fe II lines in α Ori during the same observational period) by a mean red shift of +5.9 ± 1.3 km/s; that is more precisely from +14.3 ± 3.9 to +5.1 ± 1.9 km/s with respect to the center-of-mass velocity, depicting *infalling* gas; (3) the position of the central reversals fluctuates around the systemic velocity from +1.4 ± 1.1 to −1.7 ± 1.1 km/s; we are likely dealing with the H_4–K_4 CS component (while the reversals for the Fe II lines are red-shifted, implying that they are formed in the same region as the Fe II emission).

On the other hand, from a series of observations of Ca II H and K lines in α Ori, Linsky et al. (1977) claim that the emission-line velocity with respect to the "photosphere" ranges from −12 to +10 km/s. If we adopt the averaged absorption-line velocity over the Ca II region of 23.8 km/s from Boesgaard (1979) since the authors do not give one, these measurements allow one to interpret the Ca II emission lines as *either infalling or rising material.* (The Fe II measurements in September 1976 by Van der Hucht et al. (1979) put the Fe II lines in rising layers.) If the period of observation of Linsky et al. is supposed to straddle the observations by Boesgaard and by Van der Hucht et al., a change in the dynamical structure of the star is to be taken into account.

Ca II Infrared Triplet Emission Lines. The Ca II infrared lines at 8497.7, 8541.7, and 8661.7 Å have been reported as being strong in emission in Mira stars at maximum and post-maximum phases. All lines are mutilated by TiO absorption in M stars and by CN features in carbon stars, except for the line at 8662 Å. In R Cyg, Tsuji (1971) notes that, for each emission

of the Ca II triplet, there is a shallow absorption feature toward the red that is a leftover part of the wing of the broad Ca II absorption; it is also clearly visible at 8662 Å in χ Cygni (for example, Maehara, 1968). For S Car, Shinkawa (1973) remarks that asymmetries in the absorption-line profiles are present, sometimes when emission is not, and that, in some cases, emission is only observed in one of the three lines of the multiplet, with asymmetries occurring in the other lines. (Her Figure 10 shows how, in S Car near maximum, the Ca II triplet line profiles, with their deep absorption core, differ from the profiles in χ Cygni.) An unidentified emission is also seen in the red wing of the 8662 Å Ca II line (reminiscent of the H-K wing emission lines) in nearly all of the spectra of S Car that exhibit the blue-shifted Ca II emission. However, this never happens in the larger wings of the other Ca II triplet lines (Shinkawa, 1973).

Emission in the Ca II triplet has been observed in the Mira C stars, U Cyg and RZ Peg, just after maximum light (Richer, 1971). Note that the Ca II infrared lines are in emission at maximum light, while the Ca II H and K lines are still in absorption, becoming later in emission (Contadakis and Solf, 1981). This recalls the differing lifetimes of the hydrogen lines in the visible and the infrared regions: the continuum intensity would decrease with phase in the visible faster than the line intensity.

In the supergiant, α Ori, Goldberg (1979) observed no emission in the Ca II triplet lines; rather, a strongly asymmetric absorption core was detected (see Figure 2-17).

Mg II h and k Emission Lines. In M semiregular giants and supergiants, the Mg II resonance doublet lines with the k component at 2795.5 Å and the h component at 2802.7 Å are observed at high resolution as two strong emission lines with a deep central self-reversal (e.g., Wing, 1978; Basri and Linsky, 1979). The reversals are displaced slightly shortward from the centers of the emission components; they are circumstellar absorption features, indicating a cool outer shell expanding at a moderate rate. All the observations of several stars—the M giants such as β And, γ Eri, μ Gem, and γ Cru and the M supergiants such as α Sco and α Her—particularly the numerous observations of the supergiant, α Ori (Kondo et al., 1972; Kondo et al., 1975; Modisette et al., 1973; Bernat and Lambert, 1976a; Wing, 1978; Carpenter and Wing, 1979; Basri and Linsky, 1979; Weiler and Oegerle, 1979; Van der Hucht et al., 1979; Dupree et al., 1984), display k line asymmetries, always observed on the shortward wavelength side of the intrinsic emission, whereas the h line is reasonably symmetric. Theoretically, the k line is expected to be twice as strong as the h line (Modisette et al., 1973). The k line asymmetry has been attributed to a selective absorption by Fe I UV3 (2795.006 Å) resonance transition, occurring in the cool shell surrounding the M star (de Jager et al., 1979, and references therein; also Kondo et al., 1977; Figure 2-9).

The M supergiants have much broader Mg II emission profiles than the M giants. From the survey of Weiler and Oegerle (1979), it appears that the Mg II k line shapes are not unique to a given spectral class. The width-luminosity correlation (the famous Wilson-Bappu effect) analogous to the Ca II one is seen in the Mg II h and k emission cores (e.g., Ayres, 1979).

A comparison of IUE flux obtained in August 1978 for α Ori with previous measurements obtained with the OAO-2 (Orbiting Astronomical Observatory; Doherty, 1972), BUSS (Balloon-borne Ultraviolet Stellar Spectrometer; Kondo et al., 1976), and Copernicus (Bernat and Lambert, 1976; Weiler and Oegerle, 1979) satellites shows that the Mg II flux in α Ori is fairly variable with time (Basri and Linsky, 1979), as also noted by Dupree et al. (1984) from Mg II fluxes measured from 1978 to 1984. Van der Hucht et al. (1979) find the Mg II h emission line (observed on September 16, 1976) to be indicative of an *outflow* velocity ($\sim$-3 km/s with respect to the systemic velocity), as also indicated by the violet Fe II lines they observe at the same epoch. Apparently, a special event occurred in α Ori about 1976, as already mentioned from the Ca II H and K and UV Fe II lines.

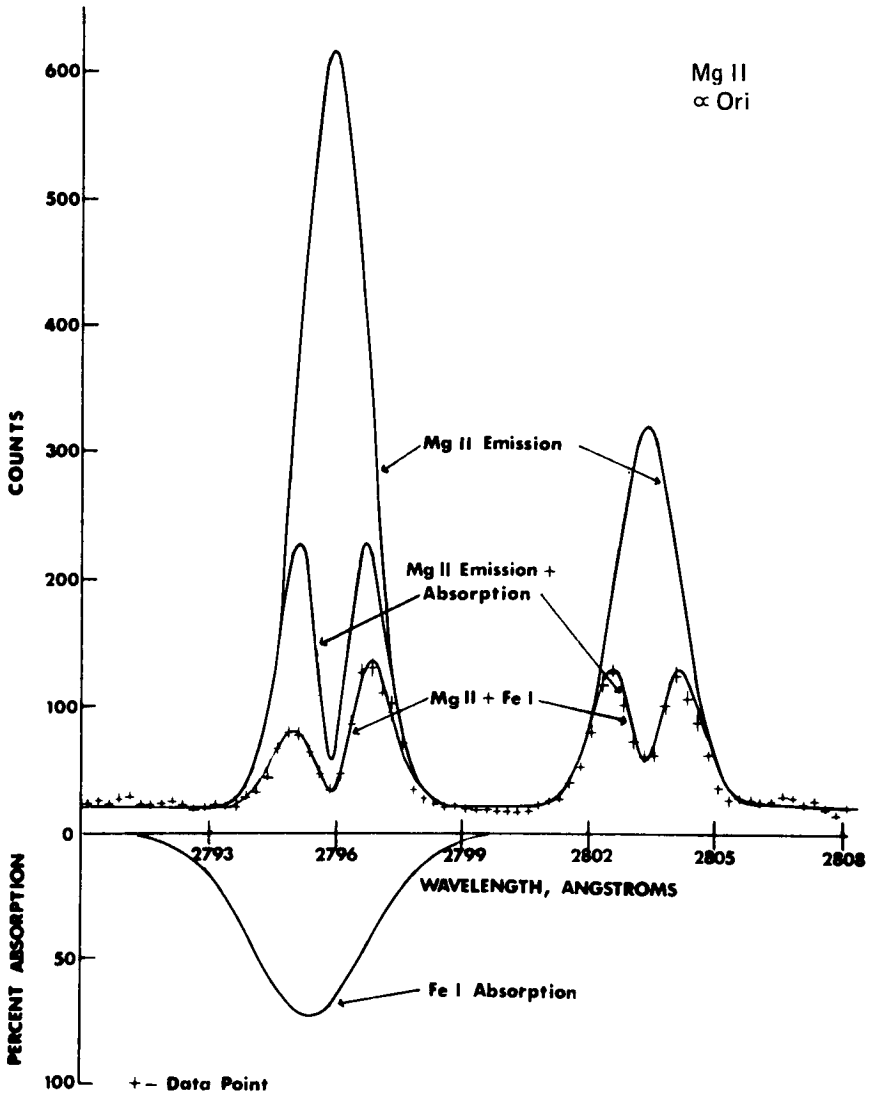

Figure 2-9. Synthetic spectra of the M supergiant, α Ori, in the vicinity of the Mg II h and k lines. The crosses represent the observations of Kondo et al. (1972) (from Modisette et al., 1973).

Figure 2-10 presents Mg II h and k lines from an IUE high-resolution spectrum of the S Mira, χ Cygni, at $\varphi = 0.22$ (Cassatella et al., 1980). The h and k lines are asymmetric with a sharp red edge. The profiles recall the Ca II H and K profiles from the Miras; the red part of the lines is hidden by the overlying circumstellar absorption, giving apparent blue-shifted emission lines. The k line is more blue-shifted than the h line due to the further mutilation on the red edge by the circumstellar Fe I resonance line at 2795 Å. As a result, only the h line is saturated. As noted by Stencel et al. (1980), the wings of the Mg II lines are frequently underexposed because of the limited dynamic range of the IUE detectors. In fact, the absorption core is not recorded in χ Cygni as it is for the Ca II H and K lines.

In addition, for the first time, Mg II h and k high-resolution profiles have been observed

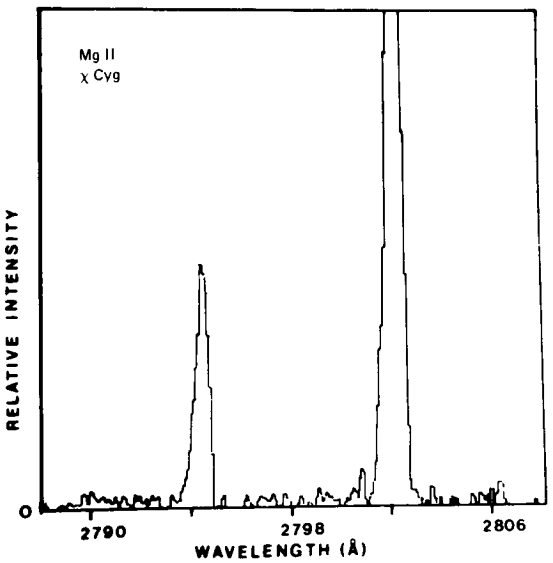

Figure 2-10. Mg II h and k lines from an IUE high-resolution spectrum of the S Mira, χ Cygni, at phase 0.22 (from Cassatella et al., 1980).

for the bright irregular N-type carbon star, TX Psc, suggesting an expanding chromosphere (Eriksson et al., 1985). Let us note that low-resolution profiles for N, R, and S stars have been published (Johnson and O'Brien, 1983; Eaton et al., 1985; Johnson and Ake, 1984; Johnson et al., 1985a; Johnson et al., 1985b; Querci and Querci, 1985a).

Other Emission Lines. Besides the classical emission lines just reviewed, other lines are valuable as additional indicators of the atmospheric structure.

The C II (UV 0.01) intercombination lines near 2325 Å have been observed with the IUE satellite at high resolution in several red giants and supergiants. Stencel et al. (1981) and Stencel and Carpenter (1982) showed that the relative intensities of emission lines within the multiplet are sensitive to electron density in the 10^7 to 10^9 cm^{-3} range, which is appropriate for measuring densities in the low-gravity cool stars. Carpenter (1984) applies the method to α Ori. He finds a mean density of 3.2×10^7 electrons cm^{-3}. A rough estimate of the geometric extent of the C II line-forming region may be predicted on the basis of the electron density, the total multiplet flux, and the temperature in the C II emitting region (Carpenter et al., 1985). So, with a temperature of the C II region set at 8300 K (obtained independently from the ratio of the total flux in the 2325 Å multiplet to that in the 1335 Å resonance-line multiplet by Brown and Carpenter, 1984), the thickness of the C II layer—perhaps close to α Ori chromospheric extent (see the section *Atmospheric Kinematics—Other Giants and Supergiants*)—is estimated to be 7.4×10^{13} cm (i.e., 1.5 R_*). Higher quality spectra and atomic data are needed to improve this conclusion (Carpenter, 1984; Carpenter et al., 1985).

The He I 10830 Å line has been observed in a sample of M, S, and C stars by Zirin (1976, 1982). The line is found in emission in Mira stars. In R Hya, the emission is seen at maximum ($\varphi = 0.93$), but not on the rise at $\varphi = 0.77$; in R And, it is a strong emission feature at $\varphi = 0.77$. However, in χ Cyg, no feature is detected either at a premaximum at $\varphi = 0.8$ or at the postmaximum at $\varphi = 0.16$ of the same cycle, or on the rise to the next maximum at $\varphi = 0.6$. Surprisingly, in R Gem, the emission is observed at minimum light. The He I emission is always accompanied by Pγ in emission, even in R Gem.

The helium line has also been detected in a few supergiants. The 10830 Å emission was observed in α^1 Her (on October 29, 1978) by O'Brien and Lambert (1979); its strength does not appear to vary over 8-month observations. The He I absorption line was detected in α Ori by Zirin (1982) in September 1965 and February 1973, but no detection is reported in February 1966 and December 1979 by this author, nor in November 1978 by O'Brien and Lambert (1979), nor in December 1974 by Sherbakov (1979). In the supergiant, μ Cep, He I absorption is seen in August 1965 (Zirin, 1982). Let us add the observation of a P Cygni profile in the helium line in the RCB carbon-rich star, R CrB, on January 18, 1978, on rise to maximum (Querci and Querci, 1978).

The He I 10830 Å emission demands densities of about 10^{12} electrons cm^{-3}. If the density is less, an absorption line may appear. However, an emission, as well as an absorption, He I line is excited only for temperatures of at least 20000 K (Vaughan and Zirin, 1968). In the solar-type stars, the He I line is excited by coronal X rays. Such an explanation is not valid in the cool stars, where there is an apparent lack of plasma hotter than, say, 20000 K and therefore no corona. Simon et al. (1982) suggest that the line in giants and supergiants is formed in the extended cool chromosphere at low densities by a scattering process. In the Miras, λ10830 emission is probably excited in the shock front progressing in the photosphere. We exclude the term *chromosphere* in discussing Miras; cf. the discussion in the section *Atmospheric Kinematics*, explaining the exclusion.

The emission lines from neutral atoms shortward of 4000 Å must be mentioned. In the M supergiant, RW Cep, numerous narrow emission lines, mainly from Fe I + Ti I, are superposed on the weak continuous spectrum (Merrill and Willson, 1956). Such emission lines from Ti I, V I, and Zr I in the 3900 Å region are also reported for the irregular carbon stars, UU Aur and Y CVn (Gilra, 1976). They are primarily zero-volt lines, assumed to be formed in an extended outer circumstellar shell, where the gas is neutral because the far-UV radiation is insufficient to ionize it (Querci et al., 1982). Similar emission from an extended region may also be responsible for filling in the Mg I absorption line in carbon stars (Johnson and O'Brien, 1983).

Finally, we noted in the section *Changes in Emission-Line Radial Velocities with Phase* that in the Miras some visual (blue) atomic lines first appear with blue-shifted emission (i.e., with inverse P Cygni profiles (P Cygni type profiles are defined in the section *Circumstellar Lines*)). A good example is *o* Cet (Joy, 1954). Also, Hinkle and Barnes (1979b) observe such Ti I, Sc I, V I line profiles in the 2-μm region of R Leo at premaximum phases, which they explain in the following way. The atomic absorption cores come from lower excitation levels of between 1.5 and 2.5 eV and behave with phase as the $\Delta v = 3$ infrared CO lines (as in Figure 2-1), showing an S-shaped curve. They are formed over an extended region of the atmosphere (in comparison to weak atomic lines coming from excitation levels of 4 eV or greater, such as Fe I lines and being therefore excited only in the deepest, hottest photospheric layers). At the phase at which the P Cygni type profiles appear (~0.6 to 0.8), the absorption cores are in infalling cool layers (Figure 2-1, upper panel), in agreement with their red shift with respect to the center-of-mass velocity. Like the IR CO absorption lines observed at such phases, they are produced by the inward-moving gas left over by the preceding rising shock wave. As for the excitation of the emission peak, we are dealing with an extended outer region, all the more as the phase is nearest to the minimum light where the photosphere is at its highest extension. Moreover, Hinkle and Barnes note that there is a large apparent velocity difference between the "stellar" disk (this part limited by the continuum optical depth unity) and off the edge of the disk; such conditions favor emission by scattered light from the stellar radiation field, giving its full meaning to the observed P Cygni type profile.

Ti I inverse P Cygni profiles at 1 μm have also been observed in *o* Cet (Ferlet and Gillet, 1984). The lower excitation level of the lines is 1.9 to 2.1 eV, which is roughly in the same range as the 2-μm metallic lines previously discussed. The difference with R Leo comes from the phase of observation which is just after the maximum ($\varphi = +0.04$). At maximum light, there corresponds a minimum radius of the pulsating photosphere. Consequently, the Ti I line-forming region above the continuum optical depth unity (in other words, the Ti I emitting region) is still sufficiently extended at maximum light in *o* Cet so that scattering effects are still possible. Ferlet and Gillet claim that the Ti I emission might be formed through the ballistic motion of the infalling material.

However, this seems unlikely because the emission peak is at the *o* Cet center-of-mass velocity, which is quite normal when dealing with scattered emission in an extended zone.

In conclusion, it can be found for atomic lines of similar strength from the blue to the IR range, which are formed throughout an extended atmospheric layer.

Atmospheric Kinematics

The Mira Stars: The Shock-Wave Model Resulting from Pulsation Plus Matter Infall. From the above survey of observations of emission-line variability, we are now able to complete the qualitative description of the shock-wave model developed earlier (mainly from the behavior of the infrared molecular lines in the Mira, χ Cygni, following Hinkle et al., 1982). We assume that the emission lines arise as a consequence of the formation of an upward-moving shock by the collision of the outward-moving pulsation wave and the infalling matter from the preceding pulsation cycle, and are thus formed under post-shock conditions (Willson, 1976). The observations of Figure 2-6 place the emission-lines in rising matter. But we consider that the fluorescent lines require different physical conditions for their formation.

Unfortunately, there is not yet a set of data that covers all the spectral range from the UV to the IR wavelengths for a given star. Let us summarize the main data at hand on temporal changes in the emission lines as well as in the absorption lines:

1. We know the behavior of the CO infrared absorption lines and of the blue-violet atomic absorption lines (Figure 2-1) from χ Cygni and that of the CO (and OH) infrared lines and of the hydrogen emission lines from R Leo (Figure 2-6c). The behavior of the hydrogen emission lines, neutral and ionized metallic emission lines, and fluorescent lines from *o* Ceti (Figure 2-6a, b) is also known. Furthermore, data from other stars give additional information (e.g., that from S Car, Figure 2-11).

2. Comparisons between radial-velocity curves give meaningful information on the relative location of the absorption and emission lines. As discussed in the section *Changes in Emission-Line Radial Velocities with Phase* and displayed in Figure 2-6c, the hydrogen radial-velocity curve for R Leo has a shape similar to the IR CO and OH rising component curves, but particularly near maximum light, it lags in phase by 0.2. A wave moving outward from the deepest layers of the star will first disturb the spectral features arising at great optical depths, and their radial velocity will be ahead in phase compared with the radial velocity of features situated at smaller optical depths. Near maximum, the hydrogen emission line-forming region is situated higher in the atmosphere than the CO and OH absorption line layers.

Let us assume a hypothetical Mira star for which all the previous observational information is available, with the radial velocities from the hydrogen and IR lines behaving with phase in *o* Ceti as in R Leo. First, the observations at maximum light could be interpreted in the

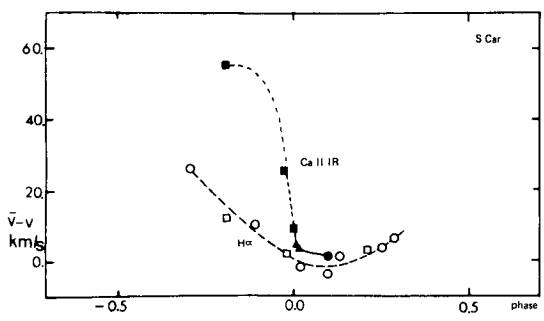

Figure 2-11. Velocities of Ca II infrared triplet emission lines and Hα emission as a function of phase in the M Mira, S Car (adapted from Shinkawa, 1973).

following manner. Hydrogen emission originates in a shock which precedes the layers (kept moving outward due to the outward momentum given by the shock wave), giving rise to the shortward component of the CO (and OH) line-doubling. The Si I emission-line velocity is similar to the hydrogen velocity (i.e., about -10 km/s with respect to the stellar velocity in *o* Ceti), and thus one should expect that both Si I and H lines are excited by the same shock. Similarly, the Ca II IR emission lines which have nearly the same velocity as the Hα lines (from S Car, Figure 2-11; see also Contadakis and Solf, 1981) are also likely to originate from the same shock front. Secondly, the propagation of the shock with phase in such a model would be depicted as follows by implementing the emission-line information into the scheme that describes the absorption lines in the section *Photospheric Kinematics—The Shock-Wave Model*. From the IR absorption lines, the emergence of the shock into the photosphere is at phase -0.3 when the total CO ($\Delta v = 3$) column density begins to decrease. It progresses outward, and at phase -0.2, the emission in Hγ, Hδ, Si I, and Ca II lines is detectable. (Note that Hα emission is seen in S Car as soon as phase -0.3 in Figure 2-11.) From phase -0.10 to 0.15, the CO second overtone becomes double-lined, and the hydrogen emission is at its maximum strength. The shock must have traveled through most of the photosphere because, at phase -0.2, the hydrogen lines are strongly mutilated by overlying absorption (as Ti O in M Miras), while at maximum, they are quite sharp. By means of the emission lines, the rising shock can be followed until minimum light (Hγ, Hδ, and the Si I (2) line at 4102 Å are in emission in *o* Ceti up to $\varphi = 0.65$, 0.57, and 0.60, respectively, from Table 7 in Joy, 1954), and its passage must also account for the CO column density variation.

The ionic emission lines and the fluorescent lines fit the foregoing explanation. Among the first, in *o* Cet at maximum light, the Fe II lines, especially the chief line of multiplet 28 at 4178 Å (that appears in emission and lasts as the hydrogen lines do), have a mean velocity clearly lower by about -3 km/s than the H and Si I lines ($v \sim -10$ km/s; Figure 2-6b). We suggest two possible interpretations: a second shock located higher in the atmosphere and structure within the shock front itself.

The Two-Shock Model. As described in the section *Analysis of Absorption-Line Velocity Histograms in Miras*, Willson et al. (1982, and papers cited therein) favor the coexistence of two shocks, particularly at maximum light, at different altitudes in the stellar atmosphere. An example taken from these authors and involving emission lines is given by the histogram of the velocity distribution in the blue spectrum of RT Cygni 4 days before maximum ($\varphi = -0.02$; Figure 2-12). Emission lines of Si I ($v \sim -14.5$ km/s) and hydrogen ($v \sim -8.5$ km/s) are likely to be assigned to the lower shock (in A), while emission lines of Fe I, V I, and Cr I and of ionized metals ($v \sim -3.5$ km/s) are assigned to the upper shock (in C; see also Figure 2-4a).

Similarly, in *o* Cet, the hydrogen and Si I emission lines, together with the blue-shifted IR molecular absorption lines, should again arise from the lower shock, while the Fe II emission lines, with $v = -3$ km/s at maximum light, would be produced by the upper shock. The aperiodic Fe II velocity curve with phase also supports the idea of an upper shock. The Ti II (13) and Sr II (1) lines (which appear in emission in *o* Cet at $\varphi = 0.03$ and $\varphi = 0.13$, are at their maximum strength at $\varphi = 0.24$, and last up to $\varphi \sim 0.5$ and 0.6, respectively) also show rather small aperiodic velocities and could be related to the upper shock, though their mean velocity ($v \sim -7$ km/s and -9 km/s, respectively) is larger than that inferred from Fe II ($v \sim -3$ km/s). The upper shock is "observationally" lost from phase 0.6 to phase 0.8. In fact, the Ti II and Sr II lines are reminiscent of the ionic emission lines that appear in the RT Cygni histogram (Figure 2-12) between the lower and upper postshock components (A and C) at $v \sim -6$ km/s). As noted by Willson et al. (1982), it is generally rather difficult to separate these postshock components.

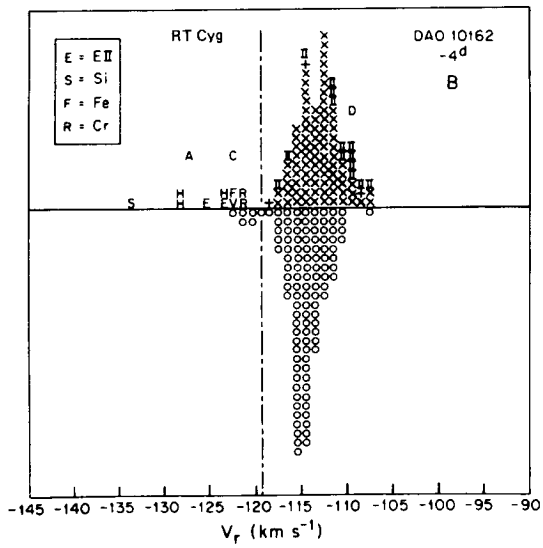

Figure 2-12. Histogram of velocity distribution in the blue spectrum of the M Mira, RT Cygni, just before maximum light (φ = -0.02). Lines of "high excitation" (arbitrarily chosen as χ_{ex} >1 eV) are plotted above the horizontal line; lines of low excitation (<1 eV) are plotted below. Emission lines are indicated by the symbol for the element above the line; ion lines are shown as "II," and emission from ions as "EII." Doubled lines are shown as a pair of dots at the appropriate velocities above or below the line, depending on their excitation class. A "+" sign indicates "very high excitation" (≥ 3 eV) lines (from Willson et al., 1982).

Structure of Shock-Front in Single-Shock Interpretation. When describing the absorption lines in the carbon star, RT Cygni (in the section *Further Probes of the Pulsating Photosphere*), we presented the two-shock model of Willson et al. (1982) and concluded that a single-shock model need not be ruled out. Arguments by Wood (1981, 1982) also sustain this conclusion. From the variations with phase of the Balmer emission-line profile and flux in a sample of nine M Miras, it appears that a simple shock model can account for the velocities and temperatures of the Balmer line-emitting region (Fox et al., 1984).

How can one account for the velocity variations in the various emission lines, such as those observed in *o* Cet, with a single rising shock? The velocity of the emission lines is an indicator of the postshock velocity, and their variability is related to changes in the postshock velocity with phase. Furthermore, the various emission lines might be indicative of the velocity gradient within the shock front.

In the front structure, ionization and excitation processes occur in the relaxation zone behind the outward propagating shock face (for example, Slutz, 1976; Whitney and Skalafuris, 1963), specifically in the zone called "internal" by Whitney and Skalafuris. While Slutz investigates the postshock propagation in the conditions prevailing in a Mira atmosphere, Whitney and Skalafuris detailed the shock-front structure in a long-period Cepheid, W Vir. Both authors recognize that their investigations of shock variation with temperature, density, and velocity as a function of the distance, x, to the shock face or as a function of the face velocity, V_s, is based on simplified assumptions. However, their results provide at least a guide for a qualitative interpretation of the observations. In Whitney and Skalafuris's cepheid "internal" relaxation zone, for a given temperature, density, and velocity at the shock face, and also in Slutz's Mira relaxation zone, the run of the temperature and velocity as a function of x shows that both variables decrease significantly in value as x grows, all the more so because V_s is higher. When traveling down density gradients as in a Mira atmosphere, the shock wave is expected to accelerate. Whitney and Skalafuris find that, for increasing V_s (ΔV_s = 40 km/s) in W Vir, the temperature increases very rapidly at the front of the "internal" zone called "1" ($\Delta T_1 \sim 92000$ K) and increases gradually at the rear of this zone, called "2" ($\Delta T_2 \sim 19000$ K). The velocity is rapidly increasing at "1" ($\Delta V_1 \sim 9$ km/s), while rather gradually increasing at "2" (ΔV_2 = 3.8 km/s); for the lowest V_s, it is nearly constant.

In *o* Ceti, as the shock propagates through the atmosphere (i.e., as it increases in velocity with phase), the Fe II lines are kept at a nearly

constant velocity, indicating that their region of formation might be in the relaxation zone near the rear of the "internal" zone (region "2"), whereas the hydrogen lines would be at the front of this zone (region "1"), in particular at $\varphi = 0$ and 0.2.

As stressed by Wood (1979), a direct interpretation of emission-line velocities in terms of postshock velocities are, in practice, subject to complicating factors because of the unknown optical thickness of the emitting region and geometric and limb-darkening effects. (See the section *Preliminary Remarks.*) Reliable velocities for the postshock region require a model that simulates the emission process, as well as information about the detailed thermal structure of the relaxation zone and the shock-wave kinematics in a Mira atmosphere that lies over several density-scale heights. An encouraging result is given by Wood (1979), who computes a long series of isothermal models covering 92 pulsation periods: the postshock velocity follows the same variation with phase as that of the observational hydrogen emission-line velocities, with a steep rise at maximum followed by a decline. A favorable feature of Wood's models is the inclusion of periodic shock injections into the Mira atmosphere rather than the propagation of an isolated large-amplitude shock, which neglects the periodic nature of the shock, as in Slutz's (1976) model. (See de la Reza, this volume, for details on shock-wave gas dynamics.)

Finally, we conclude by looking at the fluorescent lines. They are selectively excited; for example, the Fe I (42) line at 4307 Å is excited by the Mg II k line. Incidentally, as the Mg II lines are mutilated by overlying circumstellar absorption, they must arise at the upper shock in the two-shock model frame. In the single-shock model, it seems likely that the shock has to be high in the atmosphere when the Mg II lines first appear in emission ($\varphi = 0.18$ (i.e., at +73 days) in χ Cygni from the section *General Behavior of Emission Lines with Phase*). It would be interesting to know if the fluorescent lines are really in emission at the same phases as those of the exciter.

Clearly, the fluorescent lines are located in cool tenuous layers. Their velocities imply that they arise from outwardly moving matter and therefore considerably ahead of the shock itself. (Just above the shock, matter is infalling.) These lines must come from an expanding outer shell, in layers in which the expansion velocity is not yet constant. From the Fe I line at 4307 Å in o Ceti, the velocity changes by about 14 km/s from phase 0.14 to phase 0.40 and then stays constant up to phase 0.56 where no more velocity measurements are available, although the line is visible up to phase 0.78. The layers that produce such a line might be between the low-excitation 800 K CO first-overtone line shell with stationary velocity at the center of mass and the low-excitation 300 K CO fundamental line shell expanding at a constant velocity, as seen in χ Cygni. (See the section *Changes in Absorption Line Radial Velocities with Phase.*)

It is worth noting that the Mira shock-wave model described in this section is related to the most probable phase behavior of the features as generally observed in the life of a Mira. However, we noted on the o Cet example that cycle-to-cycle variations happen (e.g., more intense hydrogen emission is known to be linked to the brighter light maxima ($m_v \sim 2.5$)). This is indisputably confirmed by the absence of Hα emission at $\varphi = 0.04$, just after the June 1983 maximum of o Cet (Ferlet and Gillet, 1984) that appears to be a faint one ($m_v \sim 4$). A weak (i.e., a low shock amplitude) or an overdamped shock wave, preventing sufficient hydrogen to be ionized, could be the explanation. (Such shocks are discussed below in the C star, TW Hor.)

Atmospheric Kinematics—Other Giants and Supergiants. For illustration, we select the most thoroughly documented cases among the red stars: the M supergiants, μ Cep and α Ori, and the C giant, TW Hor, for which cross checks

between features in emission and/or in absorption might give an insight into their mechanism of origin.

Examples of a Mira-like shock wave progressing in the photosphere of irregular variables come from the H I Balmer emission in the supergiant, μ Cep, and in some C stars that show the same phase dependence seen for the Miras. (See the section *Selected Emission-Line Profiles*.) Also, S-shaped velocity curves typical to the presence of photospheric shock waves are observed from absorption lines in semiregulars. (See the section *Further Probes of the Pulsating Photosphere*.)

In μ Cep, a striking feature is the lack of detectable emission in the Ca II H and K lines, while the Fe II and Mg II lines appear strongly in emission. Hagen et al. (1983) assign Mg II emission to a Bowen fluorescence with Lyman β emission. Boesgaard and Boesgaard (1976) conclude that the Fe II emission in μ Cep comes from an outer region with respect to the photosphere, by analogy with α Ori (see below). Quite simply, from rough considerations on their ionization potential, their oscillator strengths, and the (supposed solar) atomic abundances, it may be expected that the Mg II and Fe II cores are formed above the Ca II ones (e.g., Basri et al., 1981). Therefore, they cannot be formed by the shock invoked for the Balmer emission because, if so, the Ca II H and K lines should have an emission component. We could imagine that some cycles see a Mira-like phenomenon, while in other cycles, a rising shock develops only in high layers of the atmosphere such as in TW Hor (discussed below) or in β Peg, in which the Fe II emission lines are seen to be blue-shifted with respect to the systemic velocities. Mira itself suffers exceptions such as at its June 1983 maximum (discussed in the previous section). However, whatever the mechanism, *it will stay speculative as long as temporal correlations between the various features, as well as their radial velocities with respect to the systemic velocity, are not known*. It is remarkable that the Mira-like shock-wave phenomenon can be detected in μ Cep thanks to a series of observations by McLaughin (1946). To our knowledge, no further observations over several other light phases have been done since then.

As for α Ori, the first observations to be regularly spread in time (from 1970 to 1975) concern the Fe II emission lines that are seen in infalling matter with respect to the systemic velocity over the observing period (Boesgaard and Magnan, 1975; Boesgaard, 1979). First, Boesgaard and Magnan show that a model with an extended envelope and a fluid velocity nearly equal to the Doppler velocity is well suited. Then, Boesgaard and Boesgaard (1976) confirm that the Fe II intensities are primary indicators of shell extent. Therefore, Boesgaard models the Fe II lines by adapting the method developed by Kunasz and Hummer (1974) for a spherical moving envelope in which the radial velocity is not more than a few times the Doppler velocity. However, Boesgaard does not specifically solve for the line source function, but parameterizes it to simulate a chromospheric rise in temperature, followed by a subsequent decline due to radiation losses in an extended envelope subject to velocity gradients. The best fit of the model parameters to the observed strong self-reversed Fe II line at 3228 Å in α Ori is obtained for the values shown in Table 2-1. Such values have been verified to fit profiles of other weak and strong Fe II emission lines in the star, with a change in the optical depth only. In brief, *Fe II emission lines are produced in an outer region relative to the α Ori photosphere, called the chromosphere, that is extended up to about 1.8 R_**. Let us recall that the UV C II line-forming region extends up to 1.5 R_* above the photosphere with a mean excitation temperature of 8300 K.

It appears that, to account for the large line breadths in Fe II (FWHM ~ 85 km/s for the 3228 Å line), high velocities are required; the Doppler velocity (microturbulence) is about 9 km/s throughout the Fe II shell, and the large-scale motions (macroturbulence) are about 8 km/s. These velocities are marginally subsonic as the sonic velocity is about 9 km/s at the surface of α Ori. Boesgaard (1979) also recalls how large the breadths are in the Ca II K_2 feature

Table 2-1
Shell Model Parameters* to Match the Fe II λ3228 Line in α Orionis (from Boesgaard, 1979)

Size of Fe II region	1.8 R_*
Optical depth T	500
Fluid velocity near star (km/s)	+60
Fluid velocity, outer edge (km/s)	+18
Doppler velocity near star (km/s)	9
Doppler velocity, outer edge (km/s)	9
Macroturbulence (km/s)	8
Core brightness	0.3
Density distribution exponent	2
S_1†	0.25

*The density distribution within the shell is $\varrho \sim r^{-2}$.
†S_1 is such that $S_1 T$ represents the optical depth at which the line source function reaches its maximum value.

(186 km/s) and in the Mg II k emission line (410 km/s at the base) in α Ori. Such broad features are suggested to reflect *high nonthermal random motions*. Note that no homogeneous chromosphere could reproduce the Mg II k line profile (Basri et al., 1981). Furthermore, to fit the red shifts in the emission and in the central reversal, a gradient in the fluid velocity is required; the material is accelerating inward from 15 to 20 km/s at 1.8 R_* (the outer shell edge) to 60 km/s at the stellar surface. Because the free-fall velocity is 61 km/s, the matter is accelerated by the gravitational field. In addition, the material is *infalling at supersonic speeds and would produce a shock front*. In fact, such a shock front would have the conditions necessary to excite the emission lines. Let us recall that infalling gas in α Ori is also seen from Ca II H and K and UV Fe II emission cores.

On the other hand, *outfalling* material from the Fe II, as well as from the other chromospheric indicators, Mg II, and Ca II H and K emission lines (particularly in September 1976) is observed in α Ori. Another example of fluid velocities indicative of expanding matter from the Fe II emission comes from available data on the giant, β Peg (Boesgaard, 1981). There the material expands from 0 to 25 km/s within the Fe II region, which is 2.0 R_* in size. The Fe II line widths are also very broad, implying a microturbulence of 10 km/s within the Fe II region. However, from the Ca II K_4 circumstellar absorption feature observed in β Peg, also formed over a velocity gradient of 0 to 25 km/s, the turbulence beyond about 2 R_* averages ≤4 km/s.

The extreme broadness of the features and the corresponding high Doppler velocities probably caused by nonthermal motions are explained by Boesgaard (1981) by a turbulent exchange of material between the photosphere and the chromosphere. This author presumes that the chaotic mass motions are attributed to large-scale convective cells which Schwarzschild (1975) assumed to arise in the photosphere of red giants and supergiants.

In this view, how should the emission lines be excited? Boesgaard (1979) stipulates that the matter might be driven upward by photospheric convective overshoot into the chromosphere from the large-scale convective cells, and some of it may then return toward the star at high velocity. These convective cells are often put forward in the literature to explain unexpected observations (for example, Hayes, 1982; Goldberg et al., 1981; Goldberg, 1984; Antia et al., 1984). However, we do not really understand how they could be responsible for driving mass up to 2 R_*. Also, arguments by Karovska (1984) about polarization observations, which will be presented in the section *Interpretations of the Polarization Observations*, question the suggestion by Goldberg et al. that these authors might have observed such a structure in α Ori.

To clarify the atmospheric dynamics of this star, let us highlight the striking features among the relevant available observations from 1970 to 1978—a period during which α Ori has been rather well monitored.

The data on absorption lines are displayed in Goldberg's (1984) Figure 5. First, let us recall

that in the Miras the radial velocities permit one to distinguish beyond objection the phase behavior of the low-excitation-potential absorption lines ($\chi \leq 1$ eV) with no CS component (see the section *Circumstellar Lines*) from that of the high-excitation-potential absorption lines ($\chi \geq 2.5$ eV; e.g., Figure 2-1, middle panel). The low-excitation lines (from the 4000 Å region) which are observed in infalling matter (an artificial effect as explained in the section *Source of the Visible Spectrum*) do not present a significant change in radial velocities with the light cycle, in any case not so striking that the changes shown by the high-excitation lines with their S-shaped discontinuous radial-velocity curve (consequence of the run of a shock wave). Noting that, in the cool star photosphere, the higher the excitation potential of a line, the deeper its layer of formation (see the section *Dependence of Absorption-Line Radial Velocities on the Excitation Potential*), there are the deep photospheric layers which are therefore the most disturbed by the radial pulsation of the star. We propose *to define the stellar "photosphere" as the part of the extended atmosphere in which the high-excitation absorption lines form (i.e., the fully pulsating part)*. The lines of weak or moderate potentials belong to layers just above the photosphere (i.e., layers not as much mechanically coupled with the deep pulsation), we call intermediate layers to chromospheric layers. By analogy with the Miras, let us adopt this picture for the supergiant, α Ori. In fact, IR atomic absorption lines of excitation potentials about 2 eV (Goldberg, 1979), reported from October 1975 to 1981 on Figure 5 in Goldberg (1984), clearly show a pulsational motion around the systemic velocity of 19.1 ± 1 km/s (also see Figure 12 in Goldberg, 1979); they define what we call the photosphere of α Ori. On the other hand, the absorption lines from the blue (Fe II and Ca II H and K) spectral region reported on the Figure from November 1970 to October 1975 (seen infalling over the observational period; see discussion in the sections *Violet Fe II Emission Lines* and *Ca II H and K Lines*) apparently designate the intermediate layers to the chromosphere.

Now, let us add that the fully pulsational atmospheric part may not be as easy to distinguish in the semiregulars for which the total pulsation amplitude is around 10 km/s, as noted in the section *Further Probe of the Pulsating Photosphere*—it is about 6 km/s in α Ori—as in the Miras for which the pulsation is about 20 to 30 km/s amplitude. Accurate Fourier transform spectroscopy measurements in IR are desirable, as is the case for the IR atomic lines quoted above for α Ori.

Rather suddenly, between October 1975 and September 1976, the α Ori chromosphere stopped its infall revealed by observations of Fe II and Ca II H and K emission lines since November 1970, and matter outfalls (from the observations by Van der Hucht et al. (1979) of the Fe II and Mg II h and k cores). This outfalling motion apparently lasts to at least March 25, 1978, when we note the absorption Hα core (Goldberg's (1979) observation), which is also a chromospheric indicator, blue-shifted with respect to the systemic velocity (see discussion in the section *Examples of Time Variation in Various CS Line Profiles*). Finally, on April 22, 1978, the Fe II emission cores are seen again infalling, as well as on August 16, 1978, when the Mg II h and k cores are also in infall (Carpenter's (1984) observations).

In consequence, it might be that an event has perturbed the chromosphere at the end of 1975 or in 1976. Specifically, the Fe II and Mg II h and k emission core-forming regions, as well as the Hα absorption core region, are changing their motion with respect to the center-of-mass velocity, while the "blue" absorption lines and the Hα wings remain infalling, suggesting that they are formed in lower chromospheric layers that are not affected by the event. On the other hand, the self-reversed Mg II h and k lines (Van der Hucht et al. (1979) and Carpenter's (1984) observations), together with the λλ 8542 and 8662 Ca II IR cores (Goldberg, 1979, and discussion again in the section *Examples of Time Variations in Various CS Line Profiles*), are always seen to be outfalling, suggesting that their formation in outer atmospheric layers is also undisturbed. Finally, the self-reversed Ca

II H and K lines (observed only from September 1974 to October 1975) distribute around the center-of-mass velocity, perhaps illustrating a quasi-stationary shell. (A complete diagram of the available observations extended to other periods is in preparation by Querci and Querci (1985b).)

What we have just described might be caused by the tidal effect of the close binary companion discovered by Karovska (1984), located specifically at 2.5 R_* (i.e., at 0.″05) from the α Ori center in Welter and Worden's reconstructed image observed in January 1976. (See the section *Geometrical Shell Expansion*.) In fact, recent characteristics of the companion orbit give $T = 1980.4 \pm 0.1$ and $P = 2.08 \pm 0.05$ years (see Figure 2-35); this means that the presence of the companion might be observed, in 1976, from January or from April or from June, considering the error bars in the T and P data. Once the companion has no more effect on the observed part of the chromosphere, the matter would stop and fall down toward the star as described above through the Fe II lines; it would recover a uniform motion as observed from the Fe II high layers and the "blue" absorption region, which share a common motion (Boesgaard and Magnan, 1975) in the 1970 to 1975 period. Also, at the time when the chromosphere might undergo the influence of the companion, no special effect is detected in the photospheric radial-velocity curve.

Finally, we discuss the C star, TW Hor, which might give a clue to the questions raised above. In this star, no hydrogen is detected either in emission or in absorption, nor Ca II H and K reemission in spectra with 12 Å/mm dispersion covering about 3 years (1979–1981; Bouchet et al., 1983). However, violet Fe II lines around 3200 Å are seen in emission at times by spectroscopic observations over this period and by the IUE satellite up to 1983, together with the Mg II h and k emission. (See Figure 2-5 and the section *UV Range* in *Emission Lines*.) Photospheric Mira-like shock waves (as defined in the *Summary* on *Photospheric Absorption Lines*) seem unlikely in such a star because the shock appears to have a velocity amplitude in the photosphere too low to ionize a significant fraction of hydrogen and to give Balmer emission. (Incidentally, hydrogen absorption lines might be not seen because the H^- continuum opacity is larger than the hydrogen line center opacity (Avrett and Johnson, 1984).) On the other hand, a "chromosphere" that excites the emission lines is more plausible. Such a chromosphere needs a heating mechanism that is inefficient in the Ca II and hydrogen line-forming regions; in other words, the temperature minimum would be so flat that the chromospheric flux would be too small for exciting an identifiable Ca II or H emission, but the heating must be sufficient in higher layers to excite the Mg II and Fe II lines. This could agree with the model chromosphere by Schmitz and Ulmschneider (1981) of low-gravity stars, linked to the short-period acoustic heating theory (see also Bohn, 1984). In short, acoustic waves are generated by turbulence at the top of the hydrogen convective zone, and they propagate outward into the photospheric layers of decreasing density, becoming shock waves around the temperature minimum where they dissipate their energy and heat the chromospheric layers. In some cooler stars, the radiative damping is so extensive that the position of the temperature minimum is shifted to a greater height compared to the shock formation; the models show a flat temperature minimum and a gradual chromospheric temperature rise. Querci and Querci (1985a) attempted to test such a heating theory for TW Hor in estimating the acoustic flux and the chromospheric radiative losses. The total integrated emission-line flux at the Earth from image LWR 7774 in Figure 2-5 (where emission lines Fe II, Mg II, C II, and V II are at their maximum intensity), normalized to the total radiative flux of the star measured at the Earth, is $f(\text{lines})/f(\text{bol}) = 48 \times 10^{-7}$. The main contributor lines to the radiative cooling are the Fe II V1 + V II V7 lines with a flux of 36×10^{-7}, while the Mg II flux is 45×10^{-8}. Table 2-2 gives Mg II emission-line fluxes in several N and M stars. However, from a single high-resolution long-wavelength IUE spectrum of

Table 2-2
Magnesium II Emission-Line Fluxes*

Star	Spectral Type	10^8 f(Mg)/ f(bol)
TW Hor†	N	45
TX Psc	N	10
T Ind	N	22
BL Ori	N	5
HD 37212	R8	<140
HD 52432	R5	<210
α Her	M5 II	130
72 Leo	M3 III	670
β Peg	M2 II–III	360
α Ori	M2 Iab	320

*From O'Brien and Johnson (1982), except TW Hor from Querci and Querci (1985a).
†From image LWR 7774 in Figure 2-5.

the N star, TX Psc, recently obtained (Eriksson et al., 1985), it appears that the Mg II are heavily absorbed by overlying matter and the low values of Table 2-2 may not give a true picture of the strength of the chromosphere in these objects. In spite of uncertainties in the radiative damping rate supported by the waves as they travel through the photospheric layers (up to 99 percent of energy lost by radiative damping (Leibacher and Stein, 1981)) and in the H^- radiative loss rate (no direct measure available), the heating acoustic waves, which are in fact shock waves dissipating their energy high in the outer atmosphere, may account for the emission lines in the cool low-gravity semiregular carbon star. In fact, equivalent acoustic slow magnetic waves should be better suited because they should account for the time variability in the lines in TW Hor, thanks to a variable magnetic field creating plages in the outer chromospheric layers, particularly influencing the Fe II lines. It remains to be verified whether such a mechanism is able to support the full chromosphere of supergiants that might be rather extended, as suspected from the observation of the λ10830 He line in absorption. As suggested by Hartmann and Avrett (1984), Alfven waves might be called for (see de la Reza, this volume).

Atmospheric Kinematics—Summary. What do we learn from the emission lines in addition to the absorption lines?

For the Miras, we were able to give further arguments in favor of a photospheric shock-wave model, previously revealed from the IR absorption lines. We fully discuss it by following the shock progression in the photosphere thanks to the appearence and disappearance of the various emission lines and their radial-velocity variations with phase. The single-shock interpretation (only one shock propagating in the photosphere at any time in the period) is strengthened.

Unlike SR or L giants and supergiants, we never mention the notion of chromosphere when discussing Miras. Naively, as the emission lines can be excited in shock fronts as well when the waves cross through the photosphere as when they reach higher atmospheric layers, the term "chromosphere" appears here questionable in its "solar" meaning. For theoretical grounds, we refer the reader to a recent paper by Willson and Bowen (1985) that explains why these authors entirely avoid using the term "chromosphere" and that defines the convenient zones to distinguish in pulsating stars such as the large amplitude Mira variables. These zones are determined primarily by the dynamics behavior of the star and its atmosphere; in fact, the extent of the atmosphere is linked to its dynamics, not to its temperature structure.

The fluorescent emission lines depict the presence of an outer layer in Miras, as already noted from a few absorption lines. Further data summarized in the next paragraph on circumstellar lines will help to clarify the shell structure finally discussed in the section *Summary: Structure of Expanding Gaseous Envelope.*

For the semiregular giants and supergiants, we attempt to draw general conclusions from the selected cases we have discussed. On one hand, the supergiant, α Ori, shows evidence of an extended chromosphere up to 1.8 R_* (i.e., up to 10^{14} cm, with R_* = 900 $R_\odot$ from Weymann, 1962) clearly depicted by the classical chromospheric indicators such as the Fe II, Ca II, Mg II, and C II emission lines. There,

the temperature is about 8300 K from the C II emission lines and even to 20000 K where the λ10830 He I absorption line is seen. The mean electron density is 3.2×10^7 cm^{-3}, as measured through the UV C II lines. The star is a very attractive object because it might allow us to observe the influence of a binary companion on its high chromospheric layers, mainly through the emission lines. Also, the few observational data we have in hand let us begin to guess how the structure of such an extended atmosphere (the photosphere as defined above, the intermediate layers, and the low and high chromosphere) might be, without speaking of the outer circumstellar shells.

The other supergiant, μ Cep, might be a more "classical" star (not a priori suspected to be a binary). From the behavior of the Balmer emission lines, it teaches us that shock fronts can indeed form in the stellar photosphere in the same manner as in the photospheres of Miras. Inversely, TW Hor might prove that shock waves are really able to dissipate their energy only at the chromospheric level. Depending on the physical parameters (mainly temperature and gravity) introduced in the modeling, a more or less flat temperature minimum followed by a more or less gradual temperature rise is obtained. Such shocks, issuing from short-period acoustic waves, are drastically damped in the photospheric layers. Note that the longer the wave period, the higher in the atmosphere the waves dissipate.

As a general synoptic conclusion, the observational results hint to us that a basic common heating mechanism might be at work in the atmosphere (at this step we do not look after the CS shells) of the various "red giants," Miras, or semiregular giants and supergiants. In fact, it appears that the efficiency in the line excitation is a question of the ability of the shock acoustic waves to heat the layers through which they propagate; high efficiency occurs at a different atmospheric level from one star to another and changes with time in a given star. In the Miras, the waves turn into shocks generally before emerging in the photosphere. However, it may happen, as in the Mira prototype, *o* Cet, that the wave crosses over the photosphere without dissipating energy. In the semiregulars, the waves may also turn into shocks in the photosphere as in the carbon stars, RR Her and V Hya, or in the M supergiant, μ Cep (from Hα emission-line behavior). However, there are several examples in which the waves dissipate high in the atmosphere of the semiregular giants or supergiants, creating a stellar chromosphere (e.g., μ Cep at times, β Peg where outfalling Fe II emission lines are observed, and TW Hor). We put the supergiant, α Ori, in this category. However, it is a case in which emission lines are seen not only in outfalling matter, but also in infalling matter. This star is not the prototype we took because it is a star with companions. It might be that, because of suffering the influence of a close companion, the matter is able to fall down with supersonic velocities.

Finally, we reemphasize the importance of *simultaneously monitoring temporal variations* in selected lines, such as Fe II and λ2335 C II violet lines, Mg II h and k, Balmer, Ca II H and K, λ10830 He lines, Ca II IR triplet lines, and molecular IR absorption lines, along the stellar period to progress in understanding the dynamical structure of a particular star and in atmospheric/chromospheric modeling. Until now, the interpretations are by far intuitive and qualitative.

Editorial Comment: In discussing the He I λ10830 line, as well as in the above summary on *Atmospheric Kinematics*, the author remarks that she does not use the term *chromosphere* in Miras, deferring to the suggestions by Willson and Bowen (1985) that, for pulsating stars, other atmospheric regions than those used for quasi-thermal stars are more appropriate. It is useful to abstract their suggestions, detailed in the cited references, here. The first reference discusses a number of regions; the second amalgamates them to four. The lower two focus on what replace photosphere and subphotosphere; the outer two, the exophotosphere. The lowest region, termed *undulosphere*, represents the locus of quasi-standing pulsation waves becoming progressive waves and steepening into

shocks. Its upper boundary is where the shock amplitude takes a value (assumed to be) fixed by the condition of periodicity. In the *agitosphere*, an (assumed) isothermal and radiative-equilibrium shock, with an amplitude limited and decreasing outward, still distends the atmosphere over any hydrostatic-equilibrium value. Emission coming from mechanical dissipation may vary, but its emission-measure $\ll$ volume of the region. Phenomena of a nonradiative energy dissipation significantly perturbing its thermal state lie in the *calorisphere*, which embraces the solar-type chromosphere-corona, they not being strictly applicable here. The densities are too low to permit rapid cooling. This region ends at the (conventional) *sonic* point. All the atmosphere above the thermal point is simply called *wind*. The authors emphasize that any given star may have all or only some of these regions, depending on the particular circumstances. The wind may be hot or cold. They suggest that, for rapidly rotating stars such as the Be, there may be a hot polar wind and a cool equatorial one. They stress the need for many more detailed observations to test their suggestions, which are based on their long-time efforts on numerical modeling. Certainly, these suggestions go beyond a preoccupation with solar-type, and even broader quasi-thermal, variable-mass-loss, stars. One continues to be impressed by the need for—or depressed by the lack of—far-ultraviolet data on the higher energy-shock phenomena and far-infrared and radio data on the coolest outer atmosphere. One also remains bemused by the search for hot polar and cold equatorial regions in rapidly rotating stars in the face of little evidence for their existence—which lack, of course, may again simply reflect insufficient observations.

CIRCUMSTELLAR LINES—PROPERTIES OF GASEOUS SHELLS

Appearance of Circumstellar Lines and Their Implication

The circumstellar (CS) absorption lines are characterized either by a P Cygni line profile defined as a line with a deep absorption core displaced toward the violet and bordered on its red wing by an emission component, or by a simple blue-shifted absorption line with one or more components. In the main, CS lines have excitation potentials less than 1 volt—often resonance lines—implying a shell excitation temperature of less than 1000 K (Goldberg, 1979). Known for some years in the blue spectral region, P Cygni lines have been detected in recent years in UV spectra through satellite observations (Van der Hucht et al., 1979) and in the infrared by Fourier transform spectroscopy at high resolution (Bernat et al., 1979; Bernat, 1981). Figure 2-13 gives examples of such line profiles.

Certain CS profiles, such as the CS H and K components of Ca II, can be seen in the spectra of all giants and supergiants later than M0 (Deutsch, 1960). Other lines, such as Na D, Sr II 4078, Ca I 4226, etc. appear in the M5 giants and are easily seen in all supergiants (Reimers, 1975). The best-studied star is the supergiant, α Ori, observed since about 1935 to the present with increasingly higher resolution; we will refer constantly to this star in the following paragraphs. For example, striking CS features, mainly in the blue range, are noted by Adams (1956) and Weymann (1962). Note that today, the interpretation of Adams' observations is in the recognition of P Cygni line profiles, whereas Adams himself mentioned line doubling, seeing violet and red-shifted absorption features. This comment pertains to all papers on CS lines before, say, 1960. Because dispersions of at least 10 A/mm are required to detect the CS components, prohibitively long exposures have been necessary for most red-giant stars. Only one C star, TX Psc, is reported to show such absorption cores in the blue atomic resonance lines (Deutsch, 1956). However, astronomical sites with good violet transparency and large telescopes raise hopes for obtaining sufficiently exposed spectra for these stars with reasonable exposures.

As early as 1935, Adams and McCormack (1935)—the first to discover absorption-line

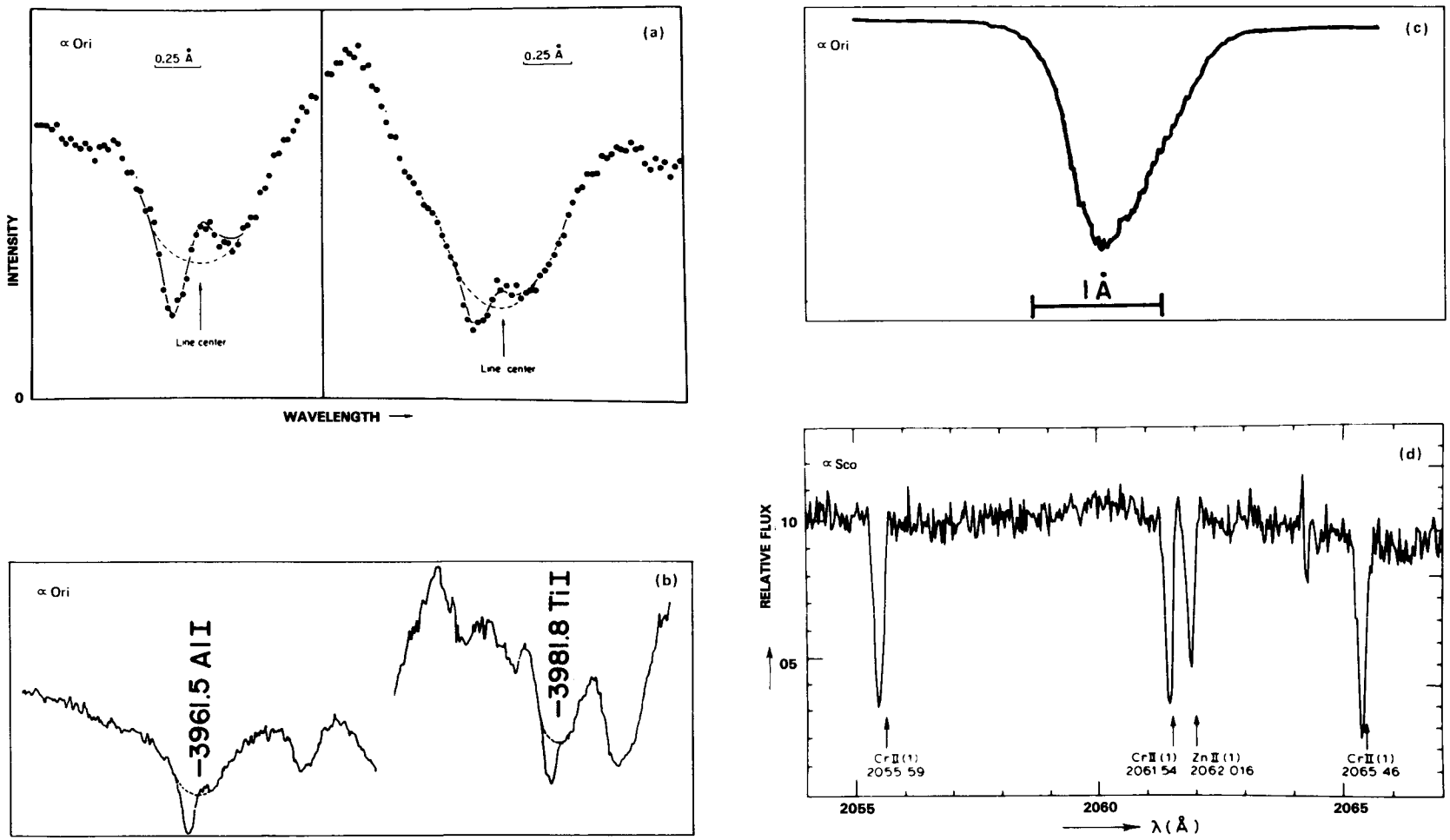

Figure 2-13. Selected circumstellar lines in the M supergiant, α Ori: (a) Mn I resonance lines at λ4030.8 (left) and λ4033.1 (right), showing a P Cygni type profile. The interpolated core of the photospheric line is shown by the dashed line, while the predicted shell absorption core with redward emission is shown by the solid line (from Bernat and Lambert, 1976a); (b) λ3961.5 Al I and λ3981.8 Ti I CS lines (from Weymann, 1962); (c) asymmetric core in Hα (from Weymann, 1962); (d) CS absorption lines of Cr II near λ2060 in the M supergiant, α Sco (from de Jager et al., 1979).

cores from atoms and ions in zero-volt levels invariably displaced blueward from the lines of the photosphere in the spectrum of M stars (α Ori, α Sco, α^1 Her, and o Cet)—attributed them to an extended expanding atmosphere. Today, it is well known (Rottenberg, 1952; Mihalas, 1978, p. 472) that a blue-shifted absorption line originating in an idealized spherical symmetric expanding envelope will be bordered on the red by an emission component, representing scattered radiation reemitted by the shell. In fact, as Reimers (1978) remarks: (a) owing to a sufficiently low density in the envelope, line scattering dominates over true absorption, and (b) because the scattering shells are dimensionally large in relation to the star, the P Cygni profiles end up being superimposed on the photospheric absorption lines.

Figure 2-13a shows clearly that the emission component is a blend of shell emission and the broad underlying photospheric absorption line (Bernat and Lambert, 1976a). Moreover, Sanner (1977) found that the circumstellar emission component in the Miras, χ Cyg and R Leo, is shifted longward of the "stellar" emission lines, thereby denying any common origin with these lines. The strongest CS features take the form of a "pure" P Cygni profile, especially when they lie in the cores of relatively narrow photospheric lines (Sanner, 1976).

The envelopes extend several stellar radii above the region in which the local continuum (and usually the photospheric absorption lines as well) is formed. We shall return to this topic later. Here, we simply note that the extent of the circumstellar shells was first suspected around 1956. Deutsch (1956, 1960) reported on the α Herculis system, a visual binary composed of an M supergiant star and of a giant G star which is a spectroscopic binary. He found that the strongest of the shifted absorption CS lines in α^1 Her were also present in the spectrum of its companion, α^2 Her. Because a G-type star never shows such zero-volt lines, he concluded that the extended envelope of the M star incorporates the G star. Furthermore, the deep absorption CS component Ca II K_4 visible in the spectrum of the companion is the only motionless feature, while all other components of the Ca II K line display normal orbital Doppler shifts. The Ca II K_4 line does not share the orbital motion and therefore obviously originates in the CS gas that extends outside the orbit of the G star. The angular separation of the visual pair is 4".7, about 360 times the radius of the M star (Reimers, 1975). Similar observations of CS absorption lines in the spectra of other visual near companions and stationary CS lines in spectroscopic binaries among red giants, implying that the shell is decoupled from the photosphere, prove that the CS gas is in fact lost to the interstellar medium. The CS lines are the spectroscopic signature of mass loss. The mass loss itself—its rate and its mechanisms—is reviewed by Goldberg (this volume).

Temporal Changes in CS Line Profiles

General Behavior. Generally speaking, these variations must be discussed in relation to the photospheric radial velocity. As an example, the general behavior of CS features in optical spectra of α Ori shows (Adams, 1956) that: (1) numerous lines have a variable violet asymmetry, (2) well-marked emission in the P Cygni profiles becomes ill-defined with time, and (3) a wing may emerge on the violet edge of the blue-shifted strong absorption lines and disappear in about 2 years. Its appearance and its behavior are associated with that of the red-emission peaks; when the latter is faintest, it is strongest and widest. Clearly, it appears that the intensity of the emission component is correlated to the photospheric velocity (Bernat and Lambert, 1976a). When the photosphere-envelope velocity difference is at its greatest, the emission component is at its strongest.

Sanner (1976) indicates from a sample of 11 M late giants and supergiants that several P Cygni profiles vary on a time scale of a few months or less. In Mira stars, P Cygni profiles are pointed out in the K I and Na D resonance lines at maximum and postmaximum phases (χ Cygni: Bretz, 1966; Sanner, 1977—R Leo: Lambert and Vanden Bout, 1978). Nevertheless, the strong variations in radial velocity with

phase for the circumstellar optical lines as shown for o Ceti in Figure 5 of Joy (1954), which are normally expected to be found at a constant velocity (see the section *Physical Conditions in Gaseous Shells*), are caused by the relatively strong variations in radial velocities of the photospheric spectrum during a cycle.

Circumstellar line-strength variations may have causes other than the photospheric variations—perhaps a time-dependent ionizing UV radiation field, which, one suspects, could explain the variations of the Ca II H and K lines in early M giants (Figure 2-14) or discrete shell ejections, giving rise to multiple shell components.

Examples of Temporal Variations in Various CS Line Profiles. Goldberg et al. (1975) and Goldberg (1976, 1979) observed the *K I resonance line at 7699 Å* in α Ori at high resolution, as shown in Figure 2-15. The component labeled "λ_{ph}" that denotes the position of the photospheric line center is determined relative to the position of photospheric lines with excitation potential ≥ 2 eV. It is clear that the smaller the radial velocity of the photosphere (V), the deeper the absorption profile and the fainter the red emission. These effects are correlated to the photospheric line, which is strongly displaced to the violet at low radial velocity. Sanner (1977) notes also that the emission component was absent on April 9, 1976, corresponding to a low value of V. Besides α Ori, the emission component in the CS K I line is also variable in the supergiants 119 Tau and α^1 Her (Sanner, 1976). Figure 2-15 also shows that two absorption components are present in the K I profile. We shall report on such line-profile features in the section *Evidence of Multiple Absorption Components in CS Lines.*

Sanner (1976) emphasizes the variability of the *Ca II infrared line profile at 8542 Å* in spectra observed with a resolution of 4 km/s. In α Ori, the line profile over 3 years shows net blueward absorption of up to 70 mÅ and, for several scans, a net redward absorption. Once again, these variations, occurring over a time scale of several months or less, might be caused by variations in the radial velocity of the underlying photospheric line. Sanner notes

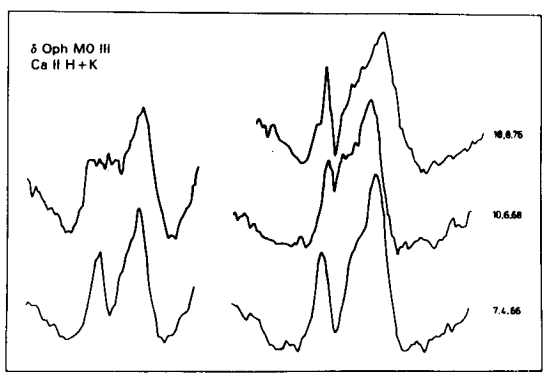

Figure 2-14. Variable circumstellar Ca II H and K lines in the early M giant, δ Oph (from Reimers, 1981).

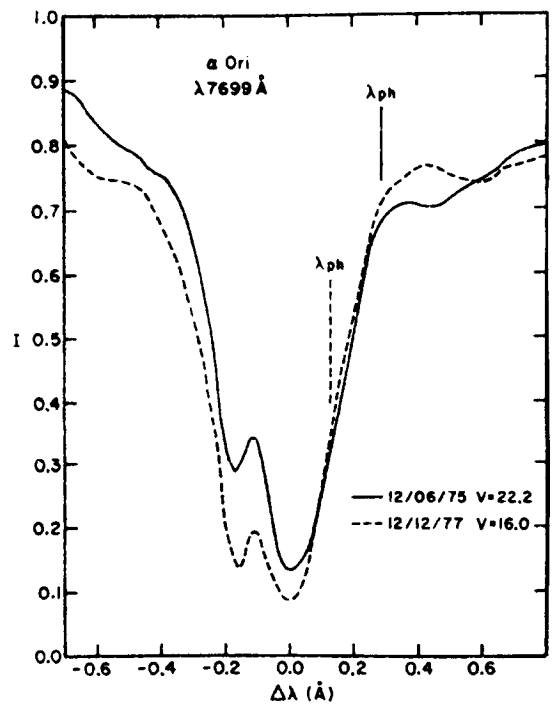

Figure 2-15. K I line profiles in the M supergiant, α Ori, on two different dates when the photospheric radial velocity was V = 16.0 and 22.2 km/s, respectively. λ_{ph} denotes the position of the photospheric line center (from Goldberg, 1979).

similar variations for the semiregular giant stars, R Lyr and β Peg. The Ca II line profile is also given for a few supergiants by Bernat (1977): the line appears to be definitely asymmetric in α Sco at 0.12 Å resolution (Figure 2-16).

In α Ori, Goldberg (1979) recorded the three IR triplet lines simultaneously (for example, Figure 2-17) from October 1975 to February 1979. The radial velocities averaged for the 8542 and 8662 Å cores are outfalling relative to the α Ori systemic velocity of 19.1 $\pm$ 1 km/s (Huggins, 1984). As for the line wings, the bulk of the data suggests that they belong to infalling matter because their radial velocity remains above 19.1 km/s. However, the red shifts are scattered from 0 ($\sim$5 values over 20) to +3 km/s. Is the infall artificial, due to difficulties in the measurements (though the observations are accurate Fourier transform spectrometer ones)? Is the forming layer to be considered rather stationary at the center-of-mass velocity, as claimed by Goldberg (1979)? (In fact, this author presumes the systemic velocity to be at 21 to 22 km/s.) More data are necessary to judge.

Goldberg (1976, 1979) reports observations of the *Na D lines* in α Ori, using the same techniques as for the K I line at 7699 Å. These lines are heavily saturated. In Figure 2-18, showing the Na D profiles on different dates, it appears that about the top third of each profile follows the motion of the photosphere, whereas the lower portion is static. From observations of the Mira, χ Cygni, on July 10, 1976, Sanner (1977) remarks that the emission feature is more pronounced in the D_1 line at 5896 Å than in the D_2 line at 5890 Å, while the photospheric absorption D_2 line is known to be deeper than the D_1 line; he explains this inversion in line strength by the fact that the amount of radiation scattered by the envelope depends partly on the intensity of the underlying photospheric line.

Finally, concerning the *Balmer lines*, we hesitated to range them in a section dealing with

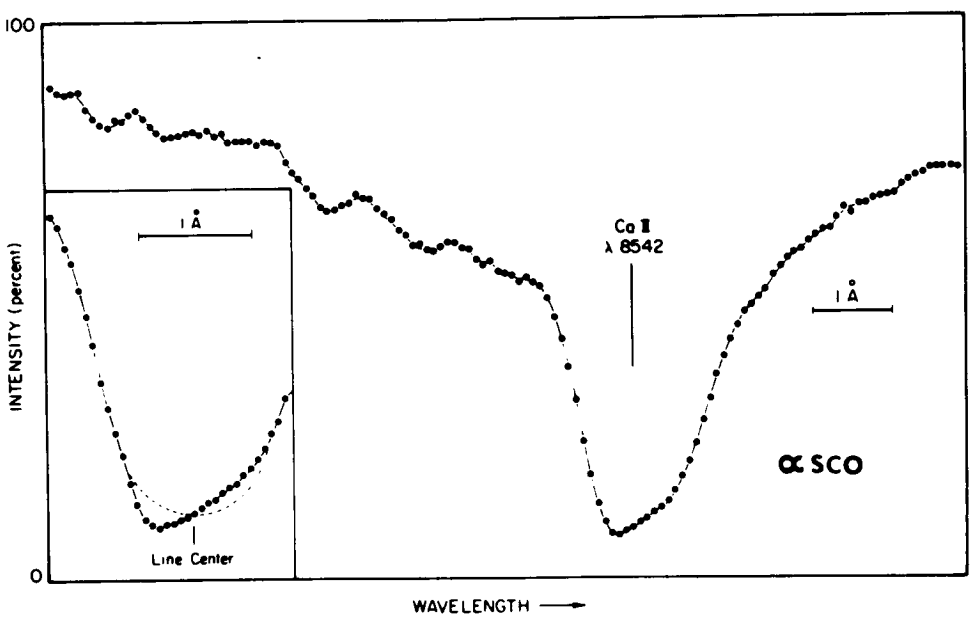

Figure 2-16. Ca II λ8542 line profile in the M supergiant, α Sco, illustrating the asymmetry of the core (better displayed in the inset). Broken line shows estimated photospheric line profile by a reflection about the line center (from Bernat, 1977).

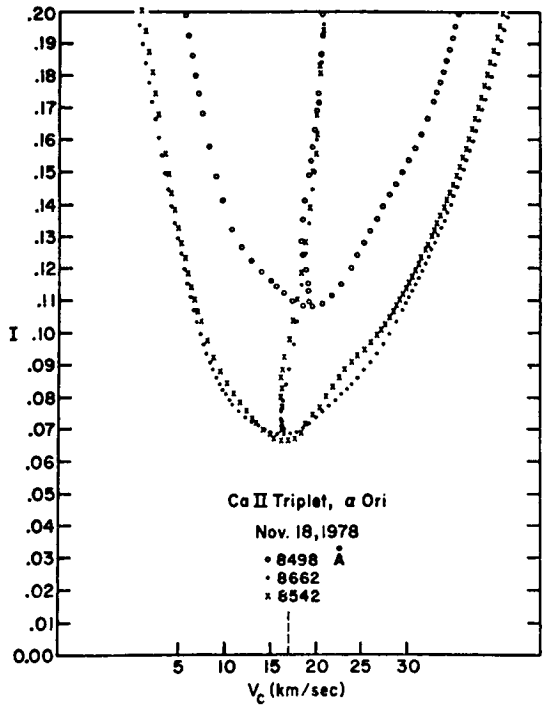

Figure 2-17. Ca II triplet line profiles in the M supergiant, α Ori. The loci of the bisectors are plotted. The vertical dashed line marks the phototospheric radial velocity (from Goldberg, 1979).

CS lines. In fact, because of the excitation conditions they need, these lines are rather chromospheric indicators. However, because they are asymmetric absorption lines in numerous giants and supergiants, we present them in this section. In α Ori, the core in the Balmer line Hα and/or Hβ (e.g., Figure 2-13c) appears to be asymmetric (Weymann, 1962; Goldberg, 1979, 1981; Dupree et al., 1984). We note that they may be either blue- or red-shifted relative to the systemic velocity. For example, Goldberg's Hα core velocities recorded on March 25, October 23, and December 15, 1978, give a blue shift of -3.7 ± 1.1 km/s and then no shift at all, respectively. On the other hand, we find the following red shifts: +1.5, +8.9, and +10.2 km/s from the three measurements of Dupree et al. on August 26, 1983, and January 23 and February 26, 1984, respectively. It is obvious that the Hα core region changed velocity relative to the center-of-mass velocity between 1978 and 1984. The same sources of data provide evidence of an infalling forming region from the Hα wings.

Asymmetric Hα lines and violet-displaced or, in some cases, red-displaced emission components have been observed in 16 red supergiants of the I Per association, some of which show time variations in the Hα line (Gahm and Hultquist, 1971). For example, on August 19, 1969, the Hα line in the supergiant, BD + 56°595, is broad with a central reversal (Figure 2-19), and the violet absorption component is displaced by about 20 km/s. On September 24, 1969, the Hα line is narrower; a reverse P Cygni profile with a strong violet-shifted emission is observed, but no obvious change is seen on the red side of the absorption line. The authors note that the mean radial velocity of the photospheric lines is similar during both observations. The light curve of the star for the period of observation is not known.

Variation of CS Lines with Spectral Types and Luminosity Classes

Particularly well studied in M stars are the CS components of the *Ca II* resonance lines at 3934 and 3968 Å—henceforth called K_4 and H_4 (Boesgaard and Hagen, 1979). The appellation H_3 and K_3 is reserved for the chromospheric absorption, particularly important in the G and K giants. (See the section *Selected Emisson-Line Profiles.*) In the M giant stars, the K_4 component superimposed on the chromospheric K_2 emission dominates K_3 completely. In early M giants, it is narrow and deep with very steep sides, reaching zero at the blue-shifted central intensity (see Figure 1 in Vaughan and Skumanich, 1970). In fact, the contribution of the H_3-K_3 components might not be significant because it appears to be very weak in those M0 giants in which no CS component is to be seen. (Note that only certain M0 III stars, such as β And, show a CS component.) In the coolest giants and most of the supergiants, the K_4 absorption is much broader (see Figure 2-8). The H and K lines are the most

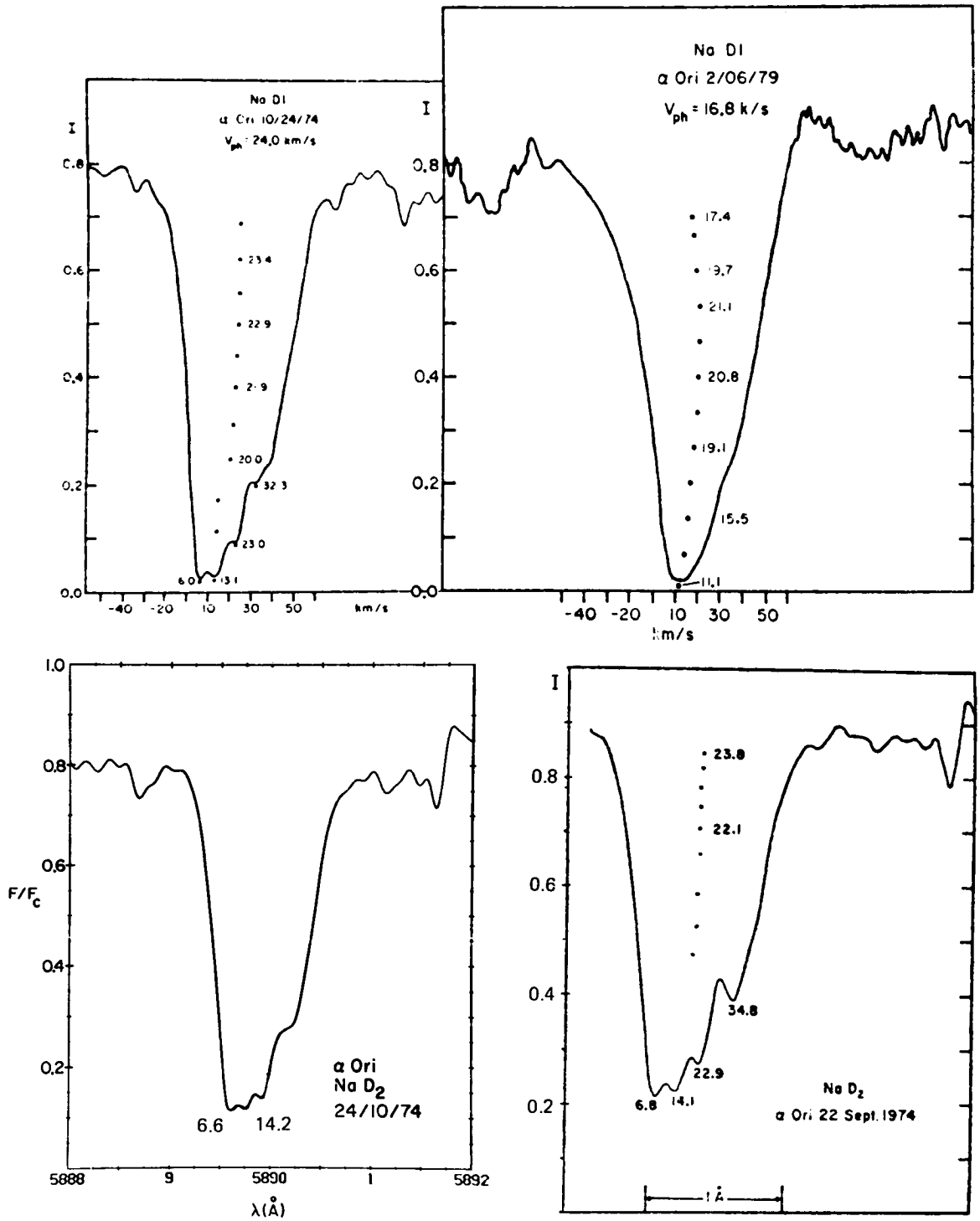

Figure 2-18. Na D line profiles in the M supergiant, α Ori, on different dates: Top: Na D_1 profile when the photospheric radial velocity was 16.8 and 24.0 km/s, respectively (from Goldberg, 1979). Bottom: Na D_2 profile when the photospheric radial velocity was 24 km/s (right, from Goldberg, 1979; left, from Goldberg, 1976, and private communication, 1980, for the noted values of velocities).

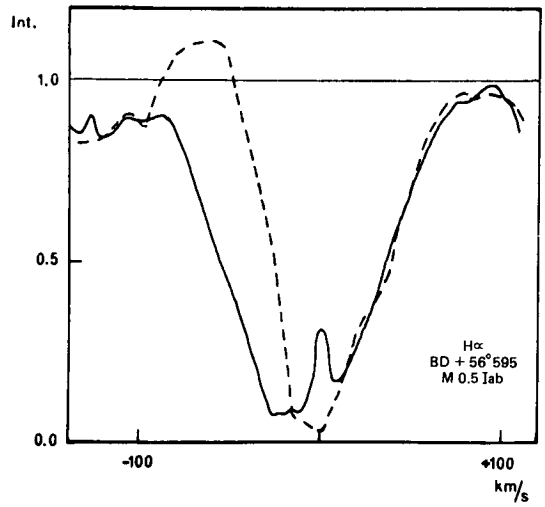

Figure 2-19. Hα *profile in the M supergiant, BD + 56°595 (M0.5 Iab) on August 19 (solid line) and September 24 (dashed line), 1969. The radial velocity in abscissa is given with respect to the mean velocity of the photospheric lines (from Gahm and Hulquist, 1971).*

obvious CS feature in giants and supergiants (Deutsch, 1960; Reimers, 1975; Boesgaard and Hagen, 1979; Hagen et al., 1983). At dispersion of 4.5 Å/mm, the CS H and K lines can be seen in the spectra of all giants of types later than M0.

In spite of their diversity, the CS H and K line profiles correlate with spectral type. The following correlations have been established in the M giants by Boesgaard and Hagen (1979) through about 60 spectrograms intentionally heavily exposed to reveal the deep CS cores:

1. A correlation exists between the spectral type and line strength. The Ca II K_4 feature shows a marked regular increase in strength toward late spectral type due to a widening of the feature. (The violet edge of the profiles remains fairly stationary, while the red edge moves redward toward later spectral types.) The average line width of the K_4 line (a good indicator of the line strength) varies from about 120 ± 70 mÅ at M1 to 600 mÅ at M7. Modeled K_4 line profiles in M giants reveal that the changes in width of the profiles are produced by an increase in the turbulence velocity and/or line formation over a velocity gradient (Boesgaard and Hagen, 1979; see also the section *Physical Conditions in Gaseous Shells*). In the supergiants, the strength of the CS H and K lines also increases with advancing spectral type and augments rapidly with greater luminosity (Reimers, 1975). The width of the absorption H and K cores in later giants and in supergiants might be caused by large velocity gradients combined with a double ionization of Ca in the inner parts of the shell.

2. A correlation exists between the expansion velocity (given by the displacement from line center in km/s) and the spectral type (or line strength). The later the spectral class, the lower the velocity. The average K_4 line displacement varies from about -20 km/s at early M to about -10 km/s by M6. Moreover, there is considerable scatter in the velocities for a given spectral type, perhaps revealing intrinsic variations in the CS shells from star to star (Boesgaard and Hagen, 1979).

The correlation between the spectral type and the expansion velocity shows much more scatter for the supergiants than for the giants (Reimers, 1975). The CS Ca II H and K cores, strong in supergiants and late M giants, do not show reemission (Reimers, 1978). The scattered photons are captured by CS dust at these short wavelengths and at these great line optical depths.

Sanner (1976) shows the behavior of the strong resonance lines of *Na I* at 5890 and 5896 Å for four early M giants and five supergiants (M2–M5) at resolutions of 2 and 4 km/s. From this sample, he notes the strengthening of the CS asymmetry with later spectral type and increasing luminosity, and the marked breadth of the lines in the supergiants. Boesgaard and

Hagen (1979) study a sample of 61 M giant stars (M0–M7) with a dispersion of 8 or 6.7 Å/mm. They confirm that the asymmetry becomes more apparent toward later types (Figure 2-20, left). None of their M0–M1 giants shows CS cores, but the M0-type supergiant, σ CMa, does (complementing the sample of Sanner for supergiants of early types). The increase in strength and velocity is minimal toward cooler M giant stars (i.e., the core displacement from the photospheric line center varies around –7 km/s at M2 to –11 km/s at M6). Boesgaard and Hagen (1979) also indicate an average equivalent width of 230 ± 75 mÅ for the CS Na I components. They propose that the low velocities could result from the formation of these lines of moderate optical depth in an envelope involving a gradient velocity.

The *Hα* line appears to be asymmetric in about one-half the stars of the sample of Boesgaard and Hagen (1979; Figure 2-20, right), including stars of all M subtypes. Their cores are blue-shifted with respect to the photospheric velocity determined from a sample of photospheric lines. In no way does this allow one to speak of a shell expansion beginning within the chromosphere of these stars because the radial velocities are not related to the systemic velocity. The equivalent width of the Hα core and its displacement from line center does not vary much with spectral type. The authors note an average equivalent width of the CS component of 27 ± 10 mÅ and an average displacement of –3.8 ± 1.6 km/s. The average concerns the stars of the same spectral type. From a larger sample of M0–M4 stars, including some supergiants listed by Merchant (1967), Boesgaard and Hagen (1979) point out that Hα is asymmetric whenever CS cores are visible in the Na D line. On the spectrum of α Ori, Weymann (1962) notes that the hydrogen lines are abnormally strong with equivalent widths of about 1 Å for Hα and Hβ. Hα shows a marked asymmetry (Figure 2-13c).

Besides the Na I D lines already mentioned, Sanner (1976) studies several atomic lines (i.e., Sr II λλ 4078 and 4216, Ba II λλ 4554 and 4934, K I λ7699, and the lines of the Ca II infrared

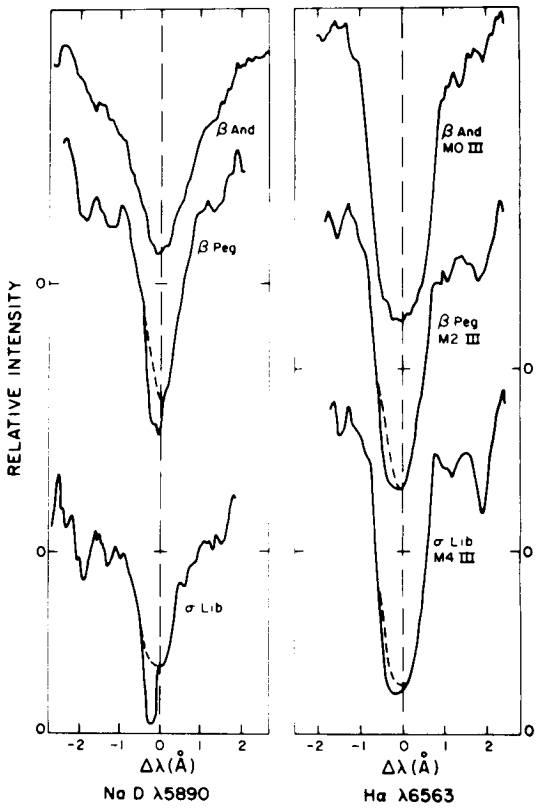

Figure 2-20. Line profile variations in representative M giants, Na I λ5890 line (left), Hα line (right). The dotted lines outline the "effective continuum" (from Boesgaard and Hagen, 1979).

triplet (λλ 8498, 8542, and 8662) in about 10 giant and supergiant stars. The line K I λ7665 was observed exclusively in the supergiant, μ Cep, because of severe O_2 telluric interference there. We quote Sanner:

- *Sr II lines*: "The strengthening of the CS asymmetry with later spectral type and increasing luminosity can be seen in both lines, in spite of severe blending in λ4078." (See Figure 1 in Sanner, 1976.)

- *Ba II, K I lines*: "The lines of both Ba II and K I are symmetric in the giants, CS components not appearing in stars with M_v fainter than about –2."

- *Ca II lines*: "The CS Ca II triplet features are generally comparable in strength to those in the Ba II line. In the giants, the asymmetries in these lines weaken progressively along the sequence λλ 8542, 8662, 8498; λ8498 is generally symmetric. In the supergiants, the asymmetries in λ8542 and 8662 are comparable, while that in λ8498 is weaker.... The triplet lines do not show marked CS emission, in contrast to the profiles of the metal [Sr II and Ba II] and trace [Na I D and K I] lines."

Evidence of Multiple Absorption Components in CS Lines

At high resolution (≥2 km/s), the CS cores of some lines are resolved into multiple components. As noted by Sanner (1976), in the Na and K lines, these components appear either as fine structure in the absorption lobe of the P Cygni profile or as sharp isolated lines blueward of it. The optical components are named by velocities obtained by simple measurements of the absorption minima with respect to the photospheric velocity generally known from lines with no shell contribution (e.g., from lines with excitation potentials of 2 eV or more (Goldberg, 1976)). For the lines of the fundamental (1–0) vibration/rotation band of CO around 4.6 μm, note that Bernat (1981) gives minima relative to the center-of-mass velocity, which he assumes to be equal to the time average of the photospheric radial velocities as taken from Abt and Biggs (1972). The determination of the expansion velocities of the shells will be discussed in the following paragraph. Temperatures are sometimes assigned to the components; these will be explained in more detail below.

Figure 2-15 shows the presence of two absorption components in the K I λ7699 line profile of α Ori. Goldberg (1979) plots the heliocentric velocities of the deeper component recorded from about 1974 to 1979, which are remarkably constant around a mean value of 10.9 ± 0.3 km/s. The blue component of the K I line, likewise plotted on Figure 2-15, shows an apparent increase from 4.2 ± 0.2 to 5.0 ± 0.2 km/s, beginning in March 1977. The author wonders if this increase is real or not. The K I line observations of Sanner (1976) emphasize the importance of a sufficiently high resolution for the detection of the components; the blue component is not seen at low resolution (4 km/s) in Sanner's Figure 11i, while a strong and wide component, together with a weak and narrow one, is clearly identified at 2 km/s resolution (cf. same figure).

Another example of double components is given by the Na D lines at λ5890 and λ5896 in α Sco, where they are at the same heliocentric velocities (Table 3 in Sanner, 1976).

The fine structure of the Na D lines in α Ori observed by Goldberg (1976, 1979) shows four absorption features (Figure 2-18). Multiple components are striking in the λ7699 K I line in α Sco (Figure 2-21) and also in μ Cep, an extreme case in which up to six components are detected (Sanner, 1976; see also Figure 1 in Bernat, 1981).

High-resolution spectra in the infrared also show multiple components in the low-excitation lines of the fundamental CO band near 4.6 μm. For example, line profiles in *o* Cet (Hall, 1980) display a complex structure (Figure 2-22) with three clearly resolved circumstellar components: one, the reddest, at a heliocentric velocity of 62.7 km/s, possibly similar to the center-of-mass velocity, and two others expanding at 7.5 km/s, corresponding to the velocities of the OH, H_2O, and SiO masers. The rotational temperatures are 200 and 70 K, respectively. The number of components in a CO line of the fundamental band depends on the luminosity; the most luminous star (μ Cep) has five components, intermediate stars such as α Ori or α Her show two, and class III stars show only one (Bernat, 1981). Note that objects such as IRC + 10216 show two components in the CO fundamental lines (Ridgway and Hall, 1980; Keady et al., 1984), components which are also recognized in the CO first overtone (2.3 μm), along with a further component at 2.5 km/s. In α Ori (Bernat et al., 1979), the two components are

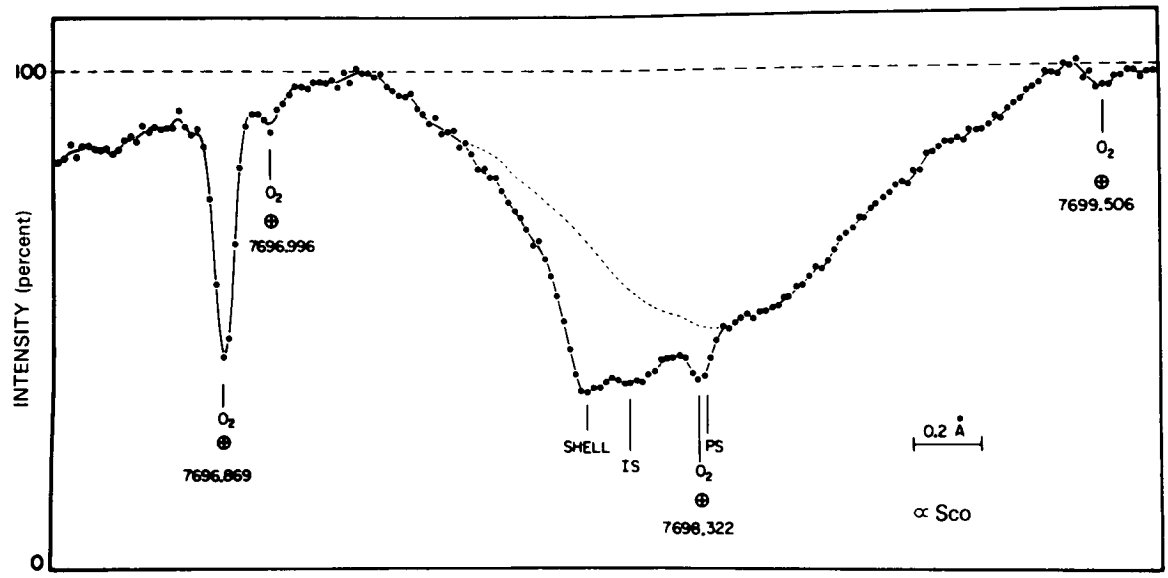

Figure 2-21. K I λ7699 profile in the M supergiant, α Sco (resolution 0.05 Å). Telluric O_2 lines, a possible interstellar component (IS) and the center of the photospheric line (PS) are shown. The broken line is a reflection of the observed line about the photospheric line center (from Bernat and Lambert, 1975).

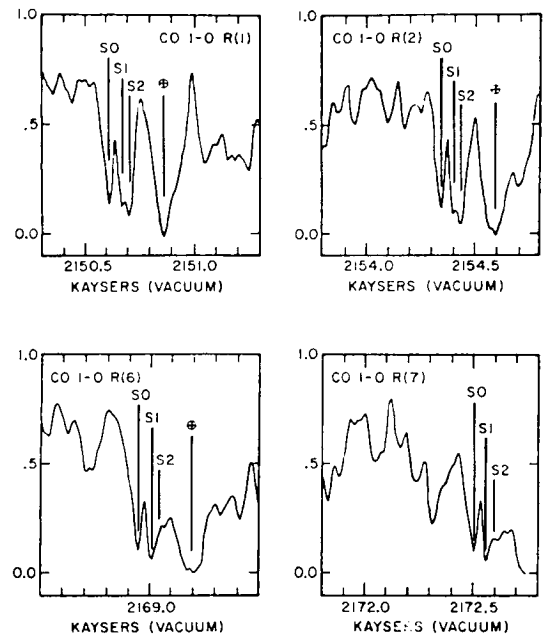

Figure 2-22. Selected CO (1–0) vibration/rotation lines from a 0.6-km/s resolution spectrum of the M Mira star, o Ceti. Components (S0, S1, S2) due to three CS shells and telluric absorption are noted (from Hall, 1980).

S_1 at ~11 km/s (T ~ 200 K +50, -10) and S_2 at ~4.8 km/s (T ~ 70 ± 10 K) relative to the center-of-mass velocity, assumed equal to a mean photospheric radial velocity from Abt and Biggs (1972). S_2 corresponds to the velocity of the blue component distinguished in the K I line (5.0 km/s; Goldberg, 1979) and also in the CO (2–1) radio emission line (Huggins, 1984).

Table 2-3 summarizes such multiple velocity structure from infrared CO lines in some typical stars. Goldberg (1976) and Hagen et al. (1983) note that, besides the K I line, doubling of the CS absorption features has been observed only in Na D, Ca II, and CO lines.

Concerning the origin of the components, the weak blue component in the K I λ7699 line in α Ori is unambiguously circumstellar since it is associated with the radio CO emission line. As for the Na D lines in the same star (Figure 2-18), the minima at 6 or 7 and 13 or 14 km/s might correspond to the two different shells expected for the K I line; they have higher values than the K I line because they are not as much affected by the redward emission. The origin

Table 2-3
Multiple Shell Components from Infrared Vibration/Rotation CO Observations in Selected Stars*

α Ori[a]			o Cet[b]		χ Cyg[c]			IRC + 10216[d]		
T (K)	v km/s	D R_*	T (K)	v km/s	T (K)	v km/s	D R_*	T (K)	v km/s	D R_*
70	4.8[e]	2000 (~55″)	70	12.2	60±20	10		450–200	14	15–30[f] (0″35–0″7)
200	11	150 (~4″)	200	7.5	300±200	7.8	100	1000–500	11	4–11 (0″09–0″3)
			(800)	0	800	0	10	1800–1200	2.5	1–3 (0″02–0″07)
					1500	Infall				

*All the velocities refer to outfalling matter, otherwise noted.

Notes:
[a]From Bernat et al (1979).
[b]From Hall (1980); components also detected in mm-wave CO spectra (Knapp et al., 1982).
[c]From Hinkle et al. (1982).
[d]From Keady et al. (1984).
[e]Also detected in K I λ7699 line and in mm-wave CO spectra (Knapp et al., 1980; Huggins, 1984).
[f]Also measured by Dyck et al. (1983); see Table 2-5.

of the apparent components at about 23 and 32 or 35 km/s is not fully understood. Goldberg (1979) suggests that they must be the emission counterpart of P Cygni profiles, having their absorption part at 6 or 7 and 13 or 14 km/s, respectively. On the other hand, Goldberg (1976) points out that "the structure could be accounted for if there were a single-peaked emission combined with interstellar absorption near the center of the photospheric component." Bernat and Lambert (1975) account for one of the multiple components in the scan of the K I line in α Sco (Figure 2-21) as having a possible interstellar origin. An irrefutable example of interstellar origin is given by one of the double components in the Na D lines in the carbon star, T Lyr (Utsumi, 1971).

As for the fundamental lines of CO in α Ori, Bernat et al. (1979) were able to detect lines arising from transitions of ^{13}CO. The $^{12}C/^{13}C$ ratios they derive prove that the two components observed in the CO lines arise in matter ejected from the photosphere and confirm their circumstellar origin, particularly for the cooler component (~70 K) that could be suspected to be interstellar. Bernat (1981) assumes that all absorption features seen in the fundamental CO lines in his sample of nine M giants and supergiants are CS, although ^{13}C lines are not technically observable. However, arguments described by Bernat (1981), such as the nondetection of 4.6-μm CO lines in the interstellar medium, the inconsistency of the CO velocities with velocities derived for nearby stars from optical lines, and the temperatures of some components which are too excessive to be alloted an interstellar origin, render the assumption justifiable.

Double absorption components are not seen exclusively in late giants and supergiants. In some early M giants, such as β And, the Ca II H and K lines show two distinct components. In other early giants such as α Vul and α Lyn, Reimers (1978) notes that the CS Ca II H and

K lines may consist of weak multiple velocity components.

Quantitative Analysis of CS Lines: Shell Characteristics

Methods. As Bernat (1977) successfully shows, difficulties for an accurate interpretation of the CS features come from unknown quantities, particularly the shell geometry and the velocity field. Some evidence that the flows in α Ori are not spherically symmetric is presented, and multiple absorption features in the line could be caused by episodic ejections that negate the steadiness of the flows. However, to make the transfer of radiation tractable, constant expansion velocity and spherical symmetry are assumed. A notable advance in the interpretation of CS line profiles for these highly idealized spherical atmospheres came with the application of the observer's frame method of Kunasz and Hummer (1974); that is, the formal solution of the transfer equation in an expanding extended spherical atmosphere in the low-velocity regime (comprehensively explained by Kunasz (1974) and Mihalas (1978, p. 459) as well). It was first adopted by Bernat (1977) and Hagen (1978) for the fitting of the theoretical line profiles to high-resolution data in M stars. Later, the method was often used in the various studies on the circumstellar envelopes (e.g., Boesgaard and Hagen, 1979; Boesgaard, 1979, 1981; Bernat, 1981). However, Keady et al. (1984) favor the comoving frame formalism of Mihalas et al. (1975; see also Mihalas, 1978, p. 503) to calculate the line radiative transfer in the flow, whereas Sahai and Wannier (1985) use the Sobolev escape probability method.

To determine the effect of shell parameters on the line profiles, Hagen (1978) calculated a series of line profiles, varying the optical depth (around unity), the expansion velocity (around 10 km/s), and the turbulent velocity (from 3 to 10 km/s; cf. her Figure 3), which are the only variables that significantly affect the resultant line profile. For this theoretical test, the author determines the underlying photospheric line by a gaussian fit to the Al I λ3944 line of μ Cep. As the optical depth increases, the P Cygni profile becomes progressively clearer: the absorption core becomes sharper and the red emission comes more into focus. The greater the value of the expansion velocity, the greater the violet shift of the CS absorption core. As the turbulent velocity mounts, the P Cygni profile disappears to give an asymmetric profile with a broader, shallower, and less blue-shifted absorption core. However, the turbulence has a negligible effect on the equivalent width of the absorption core and hence on the column densities. Hagen (1978) emphasizes that:

1. The profile is sensitive to the amount of matter in the shell rather than to its distribution within the shell.

2. The outer shell radius has no more influence on the emergent profiles than the inner radius, as long as both are significantly larger than the stellar radius.

3. The change of the power in the power-law density distribution has only a small effect on the emergent line profile.

Another difficulty in the analysis of line profiles comes from a lack of knowledge about the profile of the underlying photospheric line. A common method for inferring this profile (Weymann, 1962; Hagen, 1978; Bernat, 1977; Figure 2-23) assumes equal emission and absorption, so that a symmetric underlying profile can be hand-drawn. Bernat notes the uniqueness of this profile. Generally, the position of the line center of the photospheric component is inferred from nearby photospheric lines with high excitation potential. This empirical method gives the basic quantities for the absorption component of the CS line, displayed in the resultant shell line profile of Figure 2-23: the expansion velocity, v_e, the line center depth, and the width at half-maximium (WHM). The method is excellent for the strong lines. For the lines with a sharp CS core (i.e., lines with sufficient optical depths as shown by

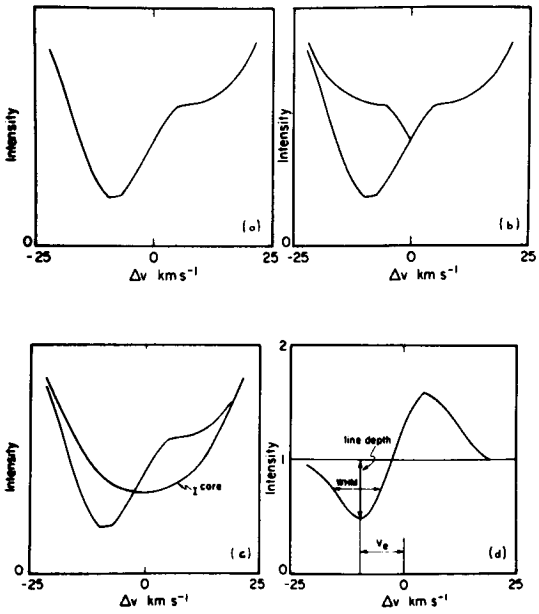

Figure 2-23. The determination of the shell line profile: (a) the original profile; (b) the flip assuming that both line wings are purely photospheric; (c) the drawn-in smooth photospheric profile; (d) the resultant shell line profile (from Bernat, 1977).

the theoretical line modeling), the radiative-transfer calculations show that the position of line minimum is determined by the expansion velocity, and vice versa. Note the remark made by Hagen (1978) and Bernat (1977) that the shell optical depths or the derived column densities are not very sensitive to the photospheric line profile. However insufficient knowledge of the photospheric radiation field lamentably prevents the modeling of the shell line profile (Bernat, 1981).

Another important quantity, in addition to the expansion velocities, is the gas-column density, which is related to the optical depth (Sanner, 1976; Hagen, 1978) and which influences the mass-loss rate (Goldberg, this volume). The method for obtaining them is clearly described by Hagen (1978). Briefly, the equivalent width of the absorption core in the resultant line profile of Figure 2-23 is measured. Then, given the expansion velocity (as easily determined from sharp CS cores), a series of theoretical line profiles are calculated with different shell optical depths. Theoretical equivalent widths are plotted against corresponding optical depths, and observed equivalent widths are converted to line-center optical depths. Finally, column densities along the line of sight are calculated. In order to relate them to the total abundances, the relative abundances in the different ionization stages must be determined. A linear fit in a plot of the derived column densities versus the excitation potential of the line level implies that the populations may be described by a single excitation temperature (Bernat, 1981).

Physical Conditions in Gaseous Shells. In what follows, we mainly refer to studies by Bernat (1977), Hagen (1978), or Sanner (1976), giving a summary of the results of the column densities, the shell temperatures, and the velocities. Other details can be found in Goldberg (this volume), in particular, a discussion on the shell inner radius which is so vital for determining the mass-loss rate. The section ends on shell distances inferred through the CS line profiles.

The observed *column densities* derived by Hagen (1978) from visual lines in some M giants, supergiants, and Miras are given in Table 2-4 as an example. In these gaseous envelopes, lying over warmer layers, the dominant ionization state of most metals is probably the singly ionized state. This is the case with Ca II, Sr II, and Ba II. However, most of the resonance lines arise from neutral metals (i.e., from a trace ionization state). As Bernat (1977) and Hagen (1978) show, the ionization balance within the CS shells is uncertain, and total abundances are better determined by using lines arising from the dominant stage of ionization. The Sr II resonance lines, unsaturated in these stars, are often chosen (Sanner, 1976; Hagen et al., 1983). The amount of CS matter in the line of sight assumes cosmic abundances, a point that could be open to criticism (Hagen et al., 1983). A scheme of determination of the hydrogen column density is given by Tanabé and Kamijo (1981). Inferred column densities of hydrogen atoms in the shell of some supergiants (in cm^{-2}) are: α Ori, 1.3×10^{22}; α

Table 2-4
Observed Gas Column Densities (cm^{-2})*

Ion	μ Cep	α Ori	α Sco	α Her	X Her	RX Boo	HD 207076	W Hya	R Leo
Fe I	1.3 (15)	9.1 (14)	7.5 (14)	4.9 (14)	2.5 (14)	2.2 (15)	1.0 (15)	6.6 (14)	<2.5 (14)
Al I	3.4 (13)	1.7 (13)	1.4 (13)	2.6 (13)	...	...	...	...	...
Mn I.....	1.5 (13)	1.3 (13)	3.2 (12)	1.0 (13)	1.8 (13)	1.3 (14)	4.0 (13)	2.8 (14)	1.8 (14)
Sr II.....	1.9 (12)	3.7 (12)	9.7 (11)	1.1 (12)	1.6 (11)	1.9 (11)	2.7 (11)	<1.6 (11)	3.4 (11)
Ba II	7.2 (11)	2.1 (11)	4.7 (11)	...	...	...	...	...	...
Sc II.....	2.3 (13)	1.9 (12)	9.7 (12)	4.4 (12)	...	...	...	...	...
Cr I	8.3 (12)	2.2 (13)	9.2 (12)	9.3 (12)	4.0 (12)	2.0 (13)	8.7 (12)	1.0 (12)	<1.0 (12)
Ti I	2.2 (13)	8.5 (14)	8.4 (12)	1.6 (13)	4.0 (13)	3.0 (13)	3.1 (13)	1.3 (13)	<8.4 (12)

*From Hagen (1978).

Sco, 1.9×10^{22}; α Her, 6.6×10^{21}; and μ Cep, 7.3×10^{21} (Bernat, 1977).

From observations of the fundamental 4.6-μm CO band in nine red giants and supergiants, Bernat (1981) derives column densities and demonstrates that there is no correlation of total CO column density with total gas (hydrogen) column density. We will discuss later what this result might imply for the shell structure.

Bernat (1977) indicates that radiative rates are orders of magnitude larger than collisional ones for the atomic species in the circumstellar envelope of α Ori. Consequently, the derived *excitation temperatures* do not give the kinetic temperatures in the shells. In the case of lines of the fundamental CO band, however, Bernat et al. (1979) show that collisional processes dominate and, therefore, the excitation temperatures are indeed electron temperatures, such as the temperatures of 200 and 70 K derived for the observed shells in α Ori (see also Ridgway, 1981a).

As shown earlier, *the expansion velocity of the shells* (otherwise known as the stellar wind velocity) is inferred from the blue shift of the CS lines, generally related in the literature to a mean photospheric velocity. Again, we emphasize that the expansion velocity must be finally related to the systemic velocity to be meaningful. In α Ori, through the Mn I and Cr I CS lines observed over 25 years, Weymann (1962) finds that the heliocentric radial velocity of the absorption-line cores varies over a range of only 2 km/s around an average value of +10.4 km/s. This near-perfect constant radial velocity is also confirmed by Goldberg (1979) from measurements of the K I deepest component at 7699 Å (see the section *Evidence of Multiple Absorption Components in CS Lines*) and by Linsky et al. (1977) on various optical CS lines. Hall (1980) reports that, at spectral resolutions of the order of 10 km/s, the observed 4.6-μm spectra of M supergiants and Miras show sharp CO lines with expansion velocities of about 10 km/s, which are totally consistent with the visible atomic resonance-line values. A constant expansion velocity is expected if the CS lines are produced in a quasi-steadily expanding envelope, many times larger than the star itself and well separated from it.

From a survey of the expansion velocities drawn from the core shift of metal lines, Reimers (1977) finds a continuous transition, on the average, of stellar wind velocities from luminous M supergiants (10 km/s), to late M giants (15 km/s), to medium M giants (20 km/s), and to early giants (25 km/s). As pointed out by Goldberg (1979), the direct measurement of the line shift gives a smaller velocity than the true velocity because the red side of the absorption profile is filled in with emission. Goldberg quotes the model calculations by Bernat (1977) and Sanner (1976) that predict errors of about 25 percent. For example, the corrected heliocentric velocity of the inner shell of α Ori (from

the K I deepest component) is 13.5 km/s (Goldberg, 1981) instead of the apparent value of about 10. Bernat (1977) remarks that the expansion velocities show no dependence on optical depth, excitation potential, or ionization state, further proof of a constant outflow velocity for the matter. (The Ca II H and K lines that show a variable expansion velocity are exceptional, coming from perturbations by chromospheric effects.)

The expansion velocities are always much lower than the surface escape velocity $v_{esc} = (2\ MG/R)^{1/2}$ (for example, Deutsch, 1960). Reimers (1977) notes that there seems to be a shaky correlation between stellar wind velocities and velocities of escape at the stellar surface. At any rate, the expansion velocity of the matter at several hundred stellar radii is greater than the escape velocity there, further demonstrating that the matter is really lost to the interstellar medium.

Shell expansion velocities are also inferred from the half-line width of thermal CS, SiO, or CO emission. A measurement such as this in CO J = 2–1 line in α Ori by Huggins (1984) gives a velocity of 14.1 ± 1 km/s. Is a previously detected shell implied? The question is open. For a sample of red giants, supergiants, and Miras, there is no relation between expansion velocity and radius (as measured by the temperature), such as larger radii correlated with higher expansion velocities (Bernat, 1981). The supergiant, α Ori, is another example (Table 2-3).

It could be expected that *velocity gradients* in the envelope produce a difference in radial velocity among the CS lines of the various neutral and ionized elements. Weymann (1962) emphasizes that, owing to the greater optical depth in H_4 and K_4 cores in relation to the other lines, velocity gradients could affect the CS H and K lines. In fact, these lines give convincing evidence for velocity gradients in the wind acceleration region (very inner shells) of M giants, depending on the stellar type, as we have discussed in the section *Variation of CS Lines with Spectral Types and Luminosity Classes*. According to Reimers (1975) and confirmed by Boesgaard and Hagen (1979), at spectral type M1, the expansion velocity given by the H_4 and K_4 lines is larger by 15 km/s than the velocity of the other line elements. This difference then decreases to zero at M5 and, with the later types, shows lower expansion velocities of about 5 km/s than the CS lines of other elements. This velocity gradient is the cause of the wider Ca II H and K lines and less blue-shifted core as the spectral type advances.

From modeling of the K_4 feature, Boesgaard and Hagen (1979) find that, in the earliest M giants, the narrow entirely blue-shifted core cannot have been formed over a great velocity gradient. Moreover, as these authors find no evidence for a Ca II K_4 feature at zero velocity (their Figure 4), they infer that the acceleration to a terminal velocity occurs very rapidly. They show that the broadening of the K_4 feature with the simultaneous advancement of the type is indicative of a large turbulence and/or velocity gradients in the shell. In fact, in modeling the K_4 profile, these authors find that a minimum velocity (inner shell velocity) affects the red edge of the profile only, whereas a maximum velocity (outer shell velocity) affects the blue edge. This confirms the conclusion of Reimers (1975, 1981) that the inner radius of the observed shell decreases with later types in the wind acceleration region. It is interesting to note Reimers' (1975) observations that some individual stars having CS Ca II lines which are variable in time (Figure 2-14) map the line-strength/velocity relation of Ca II K, intrinsically showing the various regimes of the wind acceleration. Reimers (1975) supports Deutsch's (1960) model in which the line-strength/velocity relation among the various classes of the M giants would be due to a Ca ionization structure.

As for the M supergiants, in α Ori, Weymann (1962) detects no significant velocity gradients among the CS lines over 25 years of observation, except for a small average deviation of about 1.7 km/s noted for the Ca II H and K lines; we recall that, from September 1974 to October 1975, these lines distribute around the systemic velocity (+2, −1

km/s). A general observation is that, in all M supergiants, only the CS Na D and the strong Ca II H and K cores (up to 1 Å) have very low expansion velocities (2 to 5 km/s). From IR CO observations in α Ori, α Her, and α Sco, Brooke et al. (1974) notice occasional large velocity gradients.

Finally, there is observational evidence of *shell turbulent velocities* (i.e., microturbulence defined as nonthermal velocities with an assumed gaussian distribution (Reimers, 1981)). From measurements quoted by Reimers (1981) for the supergiants α Her, α Sco, and α Ori, this author states that, on the average, the microturbulence is found to be one half the expansion velocity. Boesgaard and Hagen (1979) derive limits on the turbulent velocities in M giant stars; they increase from the order of 2 km/s or less for M0 giants to 4 km/s or more for M6 giants. Reimers (1981) notes that "if the microturbulence is caused mainly by wind velocity variations on a time scale short compared to typical flow times in the observed shell (10 to 10^3 years), the relative amplitudes of these variations are then similar to those in the solar wind."

A direct approach to the *shell extension* involves the detection of CS line emission off the star. We recall that the emission results from resonance-line scattering of photospheric radiation by neutral atoms in the shell. The λ7699 K I line is most often used for this purpose, with α Ori as the favorite star once again. However, let us mention an attempt on the supergiant, μ Cep, by Munch et al. (1979), using the Na I D_2 line.

The first such direct mapping of the α Ori shell was obtained by detecting the presence of K I emission out to 4–8" from the disk center by Bernat and Lambert (1975). In further series of observations, Bernat and Lambert (1976b) and Lynds et al. (1977) observe the K I emission out to 5" (i.e., 200 R_*) at numerous position angles around the star. The northwest quadrant shows more intense K I emission. Bernat et al. (1978) spatially extended the observations up to 30" (600 R_*) by using a two-dimension television detector, which was adequate to explore regions of the shell at large radius which were too faint to be detected by the single-channel scanner of the previous experiments. Honeycutt et al. (1980), using the same system with a narrowband filter, detected the gas shell surrounding α Ori out to a radius of 50". They confirm that the northwest quadrant is brighter by a factor of about 2. They suggest that this might be due either to an asymmetrical mass ejection giving a denser shell or to an asymmetrical stellar surface intensity giving more K I photons to be scattered. The authors state that the 50" radius corresponds to 9500 AU or 55 light days, if a distance of 190 pc is accepted for α Ori (Weymann, 1962). With a constant expansion velocity of 10 km/s, the outermost potassium would have been ejected 4500 years ago. In March 1981, Mauron et al. (1984) mapped the α Ori shell at the K I line up to 63", using a Fabry-Pérot etalon and a CCD camera. They found a slight asymmetry of the brightness distribution but not in the same direction as Honeycutt et al. (1980), who observed in March 1977: it is the southwest quadrant that appears to be brighter, while the southeast quadrant is fainter than the average.

Usually, the physical mean distances of the various shells to the photosphere are determined on the assumption that the dust and the gas are in equilibrium in the shell. The relation between the excitation temperature and the radius for the gas is directly obtained from a dust-shell model (for example, Tsuji's (1979) α Ori dust model; also see Lefèvre, this volume). Such distances are shown in Table 2-3. The equilibrium hypothesis appears to be badly in error. Bernat (1981) comments on the microwave CO emission from α Ori observed by Knapp et al. (1980), which leads to the cooler (70 K) shell detected through the CO fundamental; the mm-wave spectra give a shell distance five times smaller than the classical equilibrium assumption applied to the fundamental CO lines (see also a discussion by Goldreich, 1980). We shall not elaborate further on this highly difficult question: the correct interpretation of excitation temperatures in terms of physical distances needs detailed

theoretical models, themselves linked to a better understanding of the mass-loss mechanism, as Bernat (1981) emphasizes. This author also hints that CO may certainly be present in the entire velocity space between the multiple components, but at low densities, high temperatures, or both, and is unobservable.

Direct measures of stellar diameters by different techniques (lunar occultation, interferometry, speckle, etc.) will be discussed elsewhere.(See the section *Geometrical Shell Expansion*.)

Summary: Structure of Expanding Gaseous Envelope

Discrete velocity components in the circumstellar material are commonly observed in M giants, supergiants, and Miras. Table 2-3 summarizes such velocity structures from infrared CO observations in some typical stars.

A component at 200 K is common both to the supergiant, α Ori, and to the Mira stars and even to the dust enshrouded carbon star, IRC + 10216. This component characterizes the classical expanding shell detected in the optical range of the unobscured stars (e.g., in the K I line of α Ori). Assuming that decreasing temperature corresponds to increasing distance from the photosphere, a more extreme outer shell ($T \sim 70$ K) is clearly resolved at high spectral resolution (i.e., at 0.6 km/s, Hall, 1980). The Mira stars (not only χ Cygni and R Leo, but 10 other Miras observed by Hinkle et al., 1982) show another component around 800 K which is stationary at the center-of-mass velocity. (See the section *Changes in Absorption-Line Radial Velocities with Phase*.) At present, such a CO component is not observed in giants and supergiants. Is it unique to Miras? As noted by Hall (1980), such circumstellar features are difficult to separate from their photospheric counterparts because the photospheric motions are far too small in the late-type supergiants. Nevertheless, this author states that, in supergiants, some fundamental CO lines of low rotational number have a line strength corresponding to a radiation (brightness) temperature of $\leq$1000 K. However, in the case of the CO fundamental lines, there can be marked departures from local thermodynamic equilibrium (LTE) in the vibrational levels though not in the rotational levels (Carbon et al., 1976; Heasley et al., 1978), which leaves open to question the relation between the radiation and the electron temperature. Bernat (1981) notes that such a component may be present at too high a temperature, too low a density, or too large a turbulent velocity to be observable. As Clegg (1980) points out, if such a layer exists around the M supergiants, "this observation will be of extreme importance for mass-loss theories, because a cool, almost stationary layer of gas outside the star but interior to the CS flow would be incompatible with any theory predicting a flow sonic point in the stellar chromosphere (e.g., Mullan, 1978)."

In the Mira, χ Cyg, it is interesting to mention that the 800 K stationary layer was rapidly built up late in 1975, as described by Hinkle et al. (1982). Bearing in mind that the shock-wave model works well in the Mira stars (see part *Atmospheric Kinematics* in the section *Emission Lines*), it is quite feasible that the 800 K layer represents gas ejected from the star, either by a particularly violent oscillation or by the pulsation degenerating into a relaxation oscillation during which mass loss occurs (for example, see discussions by Wood, 1981; and Willson and Hill, 1979). Thus, it could provide a reservoir for any outflowing material driven possibly by radiation pressure on dust grains formed there (Tielens, 1983). Hinkle et al. (1982) find support for this point of view in the temperature of 800 K suitable for dust condensation and in the total mass they estimate for the layer ($>10^{-5} M_\odot$), which is large enough to explain the classical $10^{-6} M_\odot$/yr mass-loss rate in these stars. Moreover, in χ Cyg, the stationary layer is observed to weaken steadily over the three cycles following its creation. It appears to provide a source for material infalling to the photosphere, particularly the source of the visible spectrum, as previously discussed in the section *Photospheric Absorption Lines*. The authors add that the 800 K shell

might be the source of SiO maser emission observed in χ Cygni, a hypothesis which could be confirmed by correlating long-term variations in SiO maser characteristics with the formation and dissipation of the 800 K shell.

In the outermost CS shells, the multiple layers in many semiregular M variables present no correlation between expansion velocity, hydrogen column density, CO column density, or dust column density (Bernat, 1981). The absence of correlations favors multiple episodic ejections, according to Bernat, giving rise to individual shells formed under different physical conditions at various times. However, such a component structure does not necessarily imply the ejection of discrete shells. A continuous distribution of matter may produce it; the condition is that the flow velocity changes relatively slowly with distance (Mihalas, 1979). This condition is fulfilled if several distinct dust condensation events occur in the envelope, producing regimes of rapid acceleration by radiation pressure on grains, separated by regions of quasi-constant velocity in the gas flow, as emphasized by Keady et al. (1984). These authors apply such a distribution to the dusty C star, IRC + 10216 (Table 2-3). Because the observations indicate the presence of gas and dust, they assume that various grain species (described in the section *Circumstellar Dust*) may condense at different places in the envelope due to different physical characteristics, and they present the following scenario. First, SiC condenses close to the photosphere, and it results in the gas being accelerated to ~ 2 km/s; then carbon soot condensation meets favorable conditions to begin at 3 R_*, resulting in a gas acceleration to ~ 11 km/s; finally another condensation event, possibly from Mg S, occurs at 11 R_* and accelerates the gas to ~ 14 km/s.

Jura (1984) also comes to the conclusion of a hybrid model for the mass loss, in connection with the spectral appearance of the CS lines; although very dusty stars (such as IRC + 10216) with multiple CS components as broad troughs experience continuous outflow of matter, stars (such as α Ori and o Cet) with distinct sharp CS components experience impulsive discontinuous mass loss. In fact, for α Ori, multiple episodic ejections seem best adapted to the presence of companion objects. (See the section *Geometrical Shell Expansion*.)

Finally, it is worth noting that shells of cool stars have characteristics similar to planetary nebula envelopes (Table 1 in Ridgway, 1981a), suggesting the possibility of a common mechanism of origin.

CIRCUMSTELLAR DUST

Detection of Circumstellar Dust

In some infrared wavelength intervals, late-type stars radiate an excess above the blackbody radiation expected for the assumed effective temperature or measured color temperature of the star. Such infrared excesses can be attributed to circumstellar dust: grains absorbing starlight are heated and then reradiate in the infrared, causing the excess. For example, the excess observed between 8 and 14 μm in the M stars was found to be identical to the energy distribution expected from an optically thin cloud of silicate grains. Additional evidence comes from these color temperatures, which are less than 1000 K in stars in which most of the energy longward of 3 μm is due to infrared excess (e.g., Forrest et al., 1975). Because this temperature is less than the effective temperature of the star, longward radiation has to come from a cooler additional source. Moreover, these stars show that, shortward of 3 μm, the radiation is consistent with radiation weakened by dust absorption. In fact, a weakening of photospheric absorption bands due to a veiling by thermal emission from a circumstellar dust shell is currently observed. In carbon stars, the strength of the CO band at 2.2 μm is seen to vary with the infrared color; the thicker the shell, the redder the colors and the weaker the bands. Note that the systematic weakening of the CO band in Mira variables is normal at maximum light where the photospheric temperature is higher. (See the section *Survey of Changes in Absorption-Line Strengths with Phase*.) Another example of thermal emission

acting to fill in the absorption bands and giving an increasingly featureless spectrum as the shell's thickness grows concerns the carbon star, V Cyg, with its smooth spectrum longward of the 4.6-μm CO band (Puetter et al., 1977). The circumstellar nature of the excess emission longward of 8 μm has been confirmed by spatially resolving the shells from the stars. (See the section *Geometrical Shell Expansion.*)

Finally, the reality of dust shells is proved through linear polarization due partly to the scattering and absorption of the stellar radiation by small grains. These grains need not be the same grains responsible for the infrared excesses; nevertheless, this may be the case in favorable envelope geometry and optical depth.

Infrared Excesses

The shape of the infrared excess depends on whether the cool star is oxygen-rich (M star) or carbon-rich (C star). Silicates are expected in the first case (e.g., bands at 9.7 and 18 μm); silicon carbide, which exhibits a distinctive resonance at 11.2 μm, and graphite, which presents a featureless spectrum and is thought to be responsible for the extinction encountered from the optical to the far-infrared, are expected in the C stars. Infrared excesses are recognized from infrared spectrophotometry or infrared photometry.

Let us remark that the quoted observations do not include the data from 8 to 22 μm collected by the Infrared Astronomical Satellite (IRAS), launched in January 1983, and not yet available at this time. Preliminary results should be found in the Proceedings of the Meeting on "Mass Loss from Red Giants" held in June 1984 at California State University, Los Angeles.

Spectral Energy Distribution of Excess Emission. Reviews of the infrared excesses shown through moderate spectral resolution infrared spectrophotometry for M and C giants and supergiants have been given by Merrill (1977).

Some examples of energy distributions from 2 to 14 μm are reproduced in Figure 2-24. The signature of silicate grains in the M stars is clearly visible through the emission feature at 9.7 μm. It is stronger in supergiants in class Ia than in class Ib. In the M giants with very thick dust shells, the feature is seen in absorption. In several M-type Mira stars, the spectral energy distribution over the 8- to 14-μm wavelength range observed by Forrest et al. (1975) is clearly seen to be different: "Some appear to show a somewhat more sharply increasing distribution in the 8–9.5 μm range and a more slowly decreasing distribution at wavelengths larger than 11 μm (e.g. R. Leo)." In carbon stars, SiC emission at 11.2 μm appears in all the stars shown in Figure 2-24, being strong in the semiregular late C star, UU Aur, and in the Mira, R Lep. Forrest et al. (1975) note that the amount of blackbody excess is much stronger from carbon Miras than from semiregular variables. Among a sample of 25 irregular carbon stars, none appear to have infrared excess at wavelengths shorter than 3.4 μm (Walker, 1980).

Forrest et al. (1979) observe the 16- to 39-μm spectra of many M stars (supergiants and Miras) known to have a 10-μm excess; they confirm the presence of an excess emission due to a silicate material in this region (first detected around 20 μm by Treffers and Cohen (1974) in α Ori) "in the form of a broad hump peaking near 18 μm and falling smoothly to longer wavelength" as a blackbody continuum. That no sharp structure is observed in the spectra is indicative of a silicate in an amorphous disordered form. Hagen et al. (1975) report on a possible silicate emission band at 33 μm in some M stars, although this is not confirmed by Forrest et al. (1979) in μ Cep. However, Hagen (1982), by broadband photometry, concludes that there are infrared excesses not only at 33 μm, but also at 20 and 25 μm for stars that show a 10-μm silicate emission feature; such excesses are explained by radiation from silicate dust. Epchtein et al. (1980) also detect 30-μm emission in Mira M stars. Incidentally, they show that the 35-μm emission is strong enough to pump the OH circumstellar masers in the thin envelope of Mira variables. Hagen (1982) also

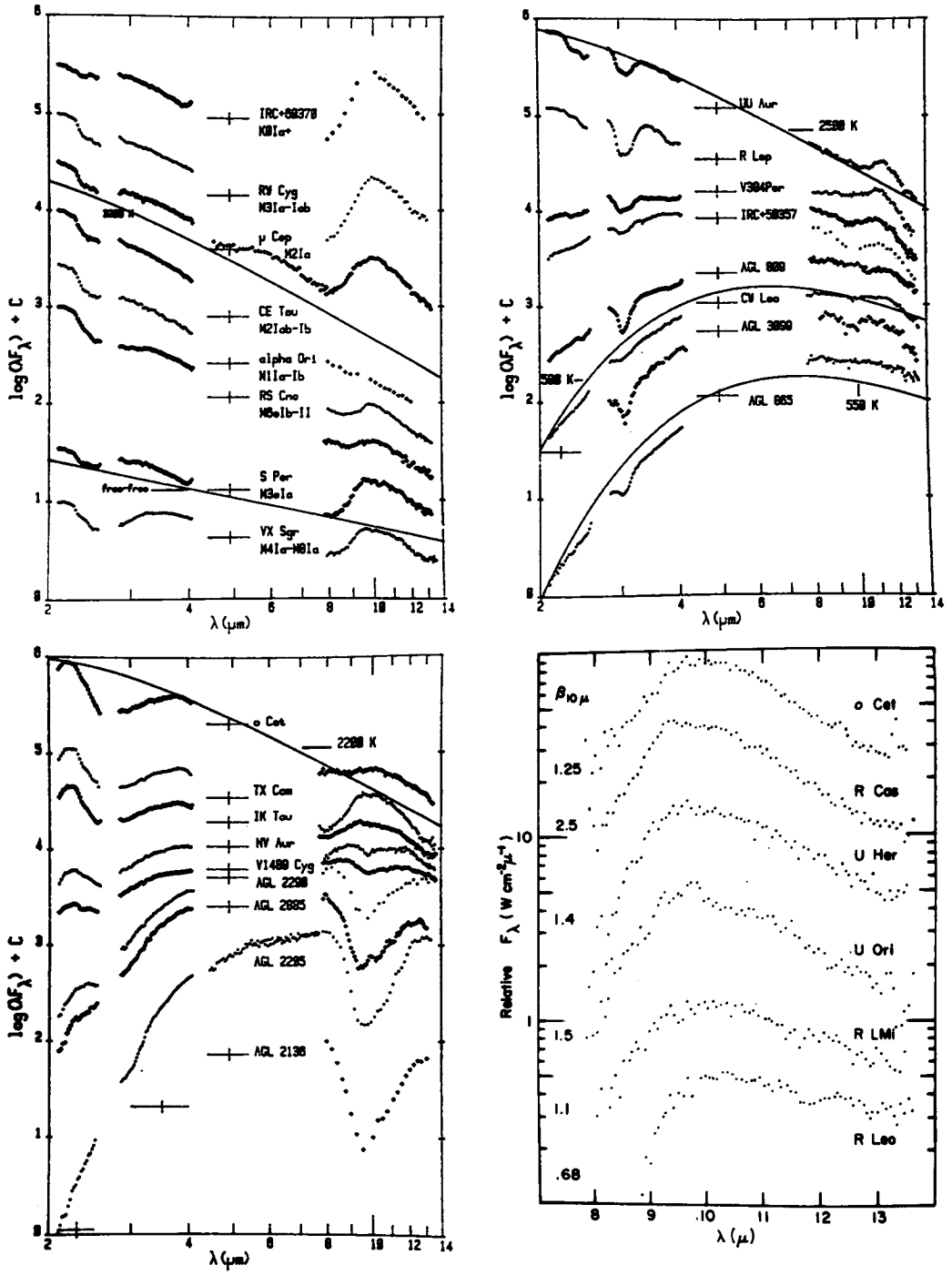

Figure 2-24. Spectral energy distribution of IR excess emission. Top left: in representative luminous M supergiants as examples of optically thin shell emission (a 3300 K blackbody and a free-free slope are included for comparison). Bottom left: in M stars and top right, in C stars, to illustrate the observed range in total optical depth in dusty CS shells (from Merrill, 1977). Bottom right: in several M-type Miras (the "relative flux" represents the actual flux normalized by an arbitrary constant for convenient display); $\beta_\lambda \equiv \{ F_\lambda \text{ (total)} - F_\lambda \text{ (continuum)} \} F_\lambda^{-1}$ (continuum), calculated with appropriate blackbody temperatures (from Forrest et al., 1975).

shows that there is sufficient 35-μm flux to pump the 1612-MHz OH masers for all the stars she observes—Miras, giants, and supergiants—except for the Mira, R Aql. An emission feature beginning at 24 μm and extending to at least 37 μm is identified in dusty carbon-star spectra, including IRC + 10216 (Forrest et al., 1981; Herter et al., 1982). It is interpreted as resulting from a solid-state resonance in the dust grains which have condensed around this star. The grain material causing this feature is MgS (Goebel and Mosely, 1985; Nuth et al., 1985).

The N-type carbon star, Y CVn, deserves special attention. It has been observed over a complete IR wavelength coverage from 1.2 to 30 μm by spectrophotometry at high resolution by Goebel et al. (1980). The particulate emission band of SiC at 11.2 μm, well known in several carbon stars, is also present in Y CVn. By superposing the emission of an optically thin shell with the dust temperature, $T = 1600$ K, on a blackbody spectrum of $T = 2750$ K, the authors show that a mixture of SiC crystalline forms fits the 11.5-μm band better than amorphous SiC, in agreement with the conclusion by Friedemann et al. (1981). The latter estimate that the column density of SiC grains is 7.0×10^{-5} g cm^{-2} and the total mass of SiC grains in the shell is 10^{24} g (if the star's photospheric radius and the radius of the envelope are evaluated according to Cohen, 1979).

As for graphite, its lack of distinct spectral features in the infrared makes its identification difficult. However, the photospheric C_3 molecule, the main vaporization product of graphite, is observed and is particularly strong at 5.2 μm. Its strength constrains the degree of veiling present (i.e., the amount of graphite in the circumstellar shell). It appears that there is little or no graphite in the CS shell about Y CVn.

Generally speaking, apart from the 11.5-μm SiC band, the photosphere in Y CVn is dominant over circumstellar emission to 30 μm. The conclusion is also valid for the violet range, in which the cause of the opacity in carbon stars has been debated at length for years (e.g., Gilra, 1973; Hartmann and Dolan, 1974; Bregman and Bregman, 1978; Walker, 1980). For Y CVn, Goebel et al. (1978) show that reradiation by circumstellar SiC is inadequate and that the violet opacity is primarily due to photospheric C_3, as was also concluded by Bregman and Bregman (1978). The dominance of the photospheric light might imply a limit to the amount of graphite ejected through the mass-loss process by such early N-type stars as Y CVn.

In contrast with Y CVn, the bright infrared object, IRC + 10216, a late-type carbon star, shows a substantial infrared excess emission. The overall flux distribution is similar to a blackbody, indicative of gray grains. This star is one of those extreme carbon stars, embedded in thick dusty CS shells that efficiently convert starlight into thermal emission. The overall featureless infrared excess is assumed to be predominantly due to graphite grains (soot) by Cohen (1979), who also discusses 16 other carbon stars (AFGL infrared sources from 10-μm sky surveys, Price and Walker, 1976). Mitchell and Robinson (1980) ascribe the infrared excess mainly to an optically thick extended graphite shell that contains 1 to 2 percent per number of SiC particles. Nevertheless, due to the inverse greenhouse effect, SiC is expected to condense close to the star, while graphite condenses much farther out, as developed by McCabe (1982; see also Lefèvre, this volume).

A feature similar to the MgS emission feature at about 30 μm appears in the spectra of the planetary nebulae, NGC 6572 and IC 418 (Forrest et al., 1981); the presence of the same type of dust indicates a possible evolutionary link between carbon stars and some planetary nebulae. Remember that gaseous shells of cool stars and planetary nebulae also have common properties (Ridgway, 1981a). Zuckerman et al. (1976) have previously described a sequence leading from extreme carbon stars to planetary nebulae. However, about the 11.2-μm SiC feature observed in NGC 6572 and IC 418, Kwok (1981) asks if the SiC grains are left over from the preceding red-giant phase or not. In

fact, it appears that some properties of planetary nebulae may be explained if their progenitors are red giants with extensive circumstellar envelopes, but the transition from red giants to planetary nebulae is not yet completely resolved.

It is worth noting the observation of an unexpected high peak in the flux energy distribution at 1.5 mm in the Mira carbon star, V Cyg (Querci et al., 1979). This star is known to be so dusty that emission in the dust shell provides more than 90 percent of the total flux for $\lambda > 5.5$ μm (Puetter et al., 1977). The flux at 1.5 mm is about four times larger than the flux measured at 1 mm by Campbell et al. (1976) from IRC + 10216. A flare-like event is suggested. Let us note that a radio flare at 2.8 cm has also been observed on the M Mira, R Aql (Woodsworth and Hughes, 1973, 1977). For the M supergiant, α Ori, Oster (1971) reports a flux variation at 10 μm from night to night supporting a flare-type origin.

An interesting point in carbon stars concerns the relationship between SiC dust and the SiC_2 molecules that are a vaporization product of solid SiC: the strength of the SiC_2 molecular bands investigated from the Merrill-Sanford bands observed in the visible part of carbon-star spectra should be correlated with the strength of the ultraviolet absorption feature (Walker, 1976) and the infrared SiC emission feature (e.g., Mitchell and Robinson, 1980).

An additional contribution to the infrared excess might arise from chromospheric free-free emission. A modeling of the observed infrared flux in some cool stars, including free-free emission, has been attempted by Gilman (1974) and Lambert and Snell (1975). Nevertheless, further observations by Fawley (1977) and Hagen (1982) of stars common with Gilman favor an additional grain species rather than free-free emission.

Time Variability of Infrared Excesses. Forrest et al. (1975) investigate the possibility of a temporal variation of the excess infrared radiation by observing M stars with broadband photometry at effective wavelengths of 3.5, 4.9, 8.4, and 11 μm. As stressed by Gehrz and Woolf (1971), at 3.5 μm the optical depth of the silicate envelope is minimal for both its absorption and emission effects; at 11 μm, silicates have their peak emissivity, but are often optically thick, whereas at 8.4 μm, the emission has a low optical depth but is rarely saturated. Therefore, designating $[\lambda_n]$ as the observed magnitude of the wavelength λ_n, the color [8.4 μm]–[3.5 μm] measures silicate emission, and the color [11 μm]–[8.4 μm] is indicative of the optical depth of the envelope of the excess dust emission. An example of such a color-color diagram as a function of phase is given for R Cas (Figure 2-25). Although visual light and light at 3.5 μm vary by a large amount, the infrared colors appear to show no significant changes throughout the cycle. This conclusion applies to the 25 program stars of all kinds of variability types (including Miras), except for R Gem (S Mira star), in which the [11 μm]–[3.5 μm] color changes significantly. Considering the large number of stars observed, the authors conclude that the total abundance of grains surrounding these stars does not change by a large amount with time.

The same authors also show spectra of *o* Cet, R Cas, and μ Cep obtained at several times (Figure 2-26). Very little change is seen in the spectral energy distribution from 8 to 14 μm over 4 years for the Mira, R Cas, and over 6 years for the supergiant, μ Cep. In *o* Cet, a large change is observed in the excess emission strength at 9.7 μm between 1967 and 1973, with a slow decrease from 1971 to 1973. For the authors, this would represent a secular decrease by about a factor 1.5 to 2 in the amount of dust around *o* Cet from 1967 to 1971. Infrared observations are also reported for *o* Cet by McCarthy et al. (1978) at various wavelengths around the December 18, 1977, maximum light. Between phases 0.76 and 0.92, the 10.2-μm flux density increased by a factor of 1.7. At the same time, both the [10.5 μm]–[3.5 μm] and [8.4 μm]–[3.5 μm] color indices increase by 0.50 mag relative to those observed between $\varphi = 0.25$ and $\varphi = 0.8$ by Forrest et al. (1975). During the light cycle (from $\varphi = 0.76$ to $\varphi = 0.28$),

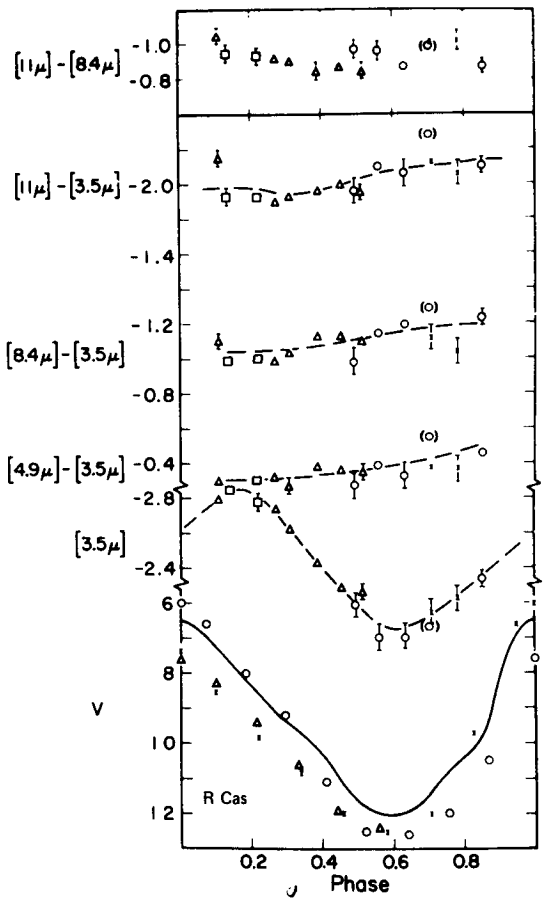

Figure 2-25. Color-color diagram as a function of phase for the M Mira, R Cas (from Forrest et al., 1975).

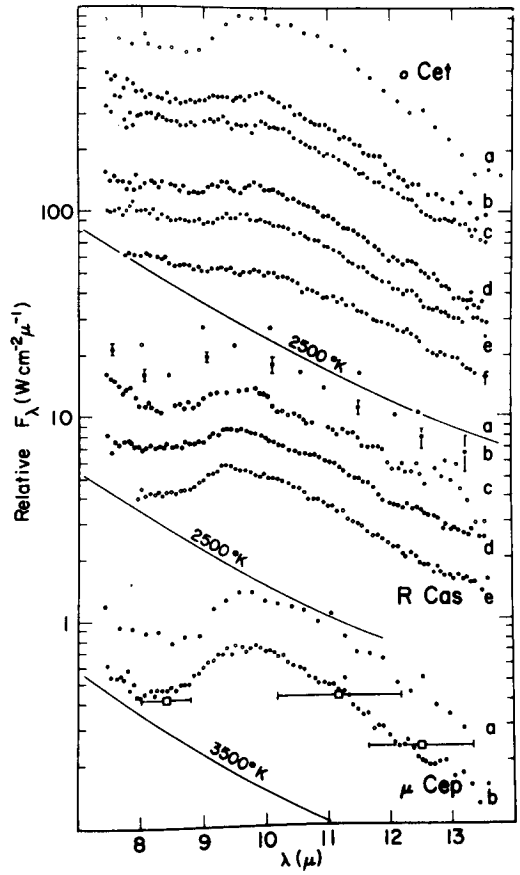

Figure 2-26. Spectral energy distribution as a function of time from o Cet, R Cas, and μ Cep. The blackbody curves are typical assumed stellar continua referring to the spectrum just above. For o Cet: (a) October 17, 1967 (UT), φ = 0.96; (b) December 13, 1971, φ = 0.45; (c) January 10, 1972, φ = 0.54; (d) November 4, 1972, φ = 0.42; (e) December 4, 1972, φ = 0.50; (f) December 18, 1973, φ = 0.64. For R Cas: (a) November 22, 1969 (UT), φ = 0.86; (b) November 13, 1970, φ = 0.71; (c) December 17, 1971, φ = 0.64; (d) November 4, 1972, φ = 0.39; (e) September 21, 1973, φ = 0.14. For μ Cep: October 17, 1967, and June 17, 1973 (UT) (from Forrest et al., 1975).

the 10.2-μm flux varies by a factor ≥3.5 (~1.4 times more than the bolometric flux), the change in 20-μm flux is 2.5 times (like the change in bolometric flux), and the 3.5-μm flux varies by less than a factor of 2. The excess emission at 10 μm is strongly phase-dependent: from $\varphi = 0.6$ to $\varphi = 1.0$, the ratio of photospheric to excess emission at 10 μm changes from 0.50 to 0.26. The authors suspect that existing circumstellar dust must be cyclically heated by periodic changes in stellar luminosity; changes in stellar temperature may produce changes in the contrast of silicate dust emission relative to the stellar continuum, as previously suggested by Forrest et al. (1975). Large contrast changes do occur at 10 μm, as proved by the observations. These probably begin at $\varphi =$ 0.8 in conjunction with increases in the bolometric and visual energy. The possible origin of these temperature changes might be flare-like events as developed in the section *Interpretations of the Polarization Observations.*

Relationships Between Gas and Dust in Circumstellar Envelopes. The amount of CS material from observations of CS dust has been estimated by Gehrz and Woolf (1971), by Dyck and Simon (1975), by Hagen (1978), by Hagen et al. (1983), and by Knapp (1985), who studies not only M stars but also S and C stars. Because the last three authors combine a study on CS gas and dust shells in a sample of stars, the bulk of the results given below is from these sources. (See also Goldberg and Glassgold and Huggins, this volume.)

Hagen et al. (1983) estimate the quantity of dust from the contrast in the 10-μm silicate emission feature through a dust-shell model described in Hagen (1978, 1982). This model calculates the emergent radiation from an optically thin circumstellar dust shell following the code of Dyck and Simon (1975), modified to include the effects of self-absorption by dust. It is shown that the shell parameters that have a strong effect on the appearance of the 10-μm feature (specifically, its height) are: (1) the dust temperature determined by assuming that the grains emit thermally at the same rate at which they absorb starlight (i.e., by the absorption efficiency of the grains shortward of 5 μm where the photosphere emits strongly); (2) the inner radius of the dust shell; and (3) the optical depth of the dust. In Hagen et al. (1983), the inner radius is (somewhat arbitrarily) set to 10 R_*, the grain mixture is "dirty" silicates, and the power-law density distribution, $N(r)$, is proportional to radius $r^{-\alpha}$ with $\alpha = 1.5$. (See Lefèvre, this volume, for a discussion of such a model.) An equal fractional condensation of the elements is assumed (crudely justified by a roughly constant relative abundance of the elements from star to star); therefore, the ratio of the amount of metal in the gaseous state to that condensed on grains is the ratio of the total column density determined from gas to that determined by dust. (See the section *Quantitative Analysis of CS Lines* for the method for determining the column density.)

Knapp (1985) also finds the dust content of the envelopes from the 10-μm feature, but uses the models of Rowan-Robinson and Harris (1982, 1983a, 1983b; see also Lefèvre, this volume). Although the amount of circumstellar gas is estimated through the optical CS line, Sr II λ4077, in Hagen et al. (1983), Knapp uses the CO (1–0) line. The main difference between the two works is that the observations by Hagen et al. cover a small range in mass-loss rate (10^{-6} to 10^{-8} $M_\odot$/yr) and thus any relationship between gas and dust abundances may be altered by uncertainties in the data, as Knapp remarks. In fact, uncertainties are numerous in such approaches (see Goldberg, this volume), and the suggestion by Hagen et al. that the dust-to-gas ratio in the circumstellar envelopes is not constant is dismissed by the results of Knapp, who observes stars over a very wide range in mass-loss rate (10^{-7} to a few $\times$ 10^{-4} $M_\odot$/yr). Clearly, the gas-loss rate is proportional to the dust-loss rate for M, S, and C variables (giants and OH/IR supergiants; Mira or not Mira variables). Consequently, the dust-to-gas ratio is roughly constant over almost 4.5 decades in mass-loss rate, with mean values of $\sim$160 by mass for M and S stars and $\sim$400 by mass for carbon-rich stars. This constancy is expected when the mass-loss mechanism is radiation pressure on grains (Deguchi, 1980). Knapp notes that the value found for the oxygen stars is very close to the value found for the interstellar medium ($\sim$150), suggesting that, in all the studied envelopes with silicate grains, all the available heavy elements condense out as grains.

Hagen et al. (1983) argue that the CS envelopes have clumpy regions of greater density in which the grain formation may be essentially complete, whereas there is little or no grain formation in less dense regions. The possibility of high-density condensations present in the envelope and moving in the line of sight had been raised by Reimers (1978), for example, to explain the weak multiple velocity components present in the CS Ca II H and K lines of early M giants. (See the section *Evidence of Multiple Absorption Components in CS Lines.*)

Intrinsic Polarization of Starlight

As noted in the section *Detection of Circumstellar Dust*, the presence of dust has also been detected from optical polarization observations. The linear intrinsic polarization in red variables is distinguished from the interstellar polarization by its variability with time, by its wavelength dependence, which differs from that of the interstellar polarization, and/or by the rotation of the position angle of polarization with wavelength. At the origin, these properties have been measured over broad spectral ranges; the reviews by Serkowski (1971) and by Shawl (1974) report on these results. On the other hand, the relatively recent review given by Coyne and McLean (1979) emphasizes the results from high spectral resolution. Let us also note King's (1983) didactic article on polarized light in astronomy, intended for the general reader.

First, we shall summarize general results; then we shall study details from high spectral resolution, particularly from well-documented specific stars—Miras and giant and supergiant semiregulars. Finally, we shall resume the interpretations suggested at the present moment for these observations.

Overall Results on Polarization. All the supergiants studied by Dyck and Jennings (1971), as well as the giants later than M2, show intrinsic linear polarization. These authors remark that, among the giants, "the frequency of the phenomenon increases rather abruptly at M4 and remains high in later spectral type." The percentage of polarization may be high, with $P \geq 2$ percent, especially higher than 2 percent in the blue spectral region, as high as 10 percent for extreme red objects (Figure 2-27), and up to 20 percent at 1 μm in IRC + 10216 (Shawl and Zellner, 1970; Cohen and Schmidt, 1982).

In short, quoting Magalhaes (1981) about polarization in red late-type stars: "its amount, position angle and spectral behavior generally vary with time for a given object, as does the polarization wavelength dependence from one star to another." In the Mira variables, these changes are not necessarily in phase with light variations. Temporal variability on short time scales (months) has been detected in the majority of stars and indicates that considerable anisotropy exists near the star.

Although the wavelength dependence of polarization changes its shape with time, there is a general trend toward an increase in the amount of polarization with decreasing wavelength. The increase toward the ultraviolet often follows the Rayleigh λ^{-4} law; an exception is the supergiant, μ Cep, which departs completely from this rule (Figure 2-27). Furthermore, a maximum toward 1 μm is not so rare, such as that for L_2 Pup, showing a peak around 1.6 μm (Shawl, 1975). Secondary ups and downs in the wavelength dependence of polarization appear at times, with their strengths also varying with time (for example, R CrB, Figure 3 in Coyne and Shawl, 1973).

Correlations between the polarization and other parameters have been sought because they should be useful in interpreting the observations.

It appears that there is no general relationship between changes in the polarization and light changes with time. In Mira stars, a decreasing polarization in the yellow, blue, and ultraviolet spectral regions is seen as the visual light increases, with the largest polarization observed halfway between the minimum and maximum light (as we shall detail for o Cet below), whereas for the semiregular, V CVn, the largest polarization in the yellow and blue spectral regions is observed at minimum light (Serkowski, 1971). In the case of this latter star, the polarization in the B filter suddenly increases by more than a factor of 1.5 between phases 0.6 and 0.8 (Shawl, 1974).

Shawl (1974) notes that the presence of intrinsic polarization is always associated with emission lines in the stellar spectrum. He quotes that a spectrogram of V CVn at phase 0.68 shows no emission and a low polarization, while another one at phase 0.84 shows strong emission and a high polarization. In fact, Hβ emission increases as the polarization increases.

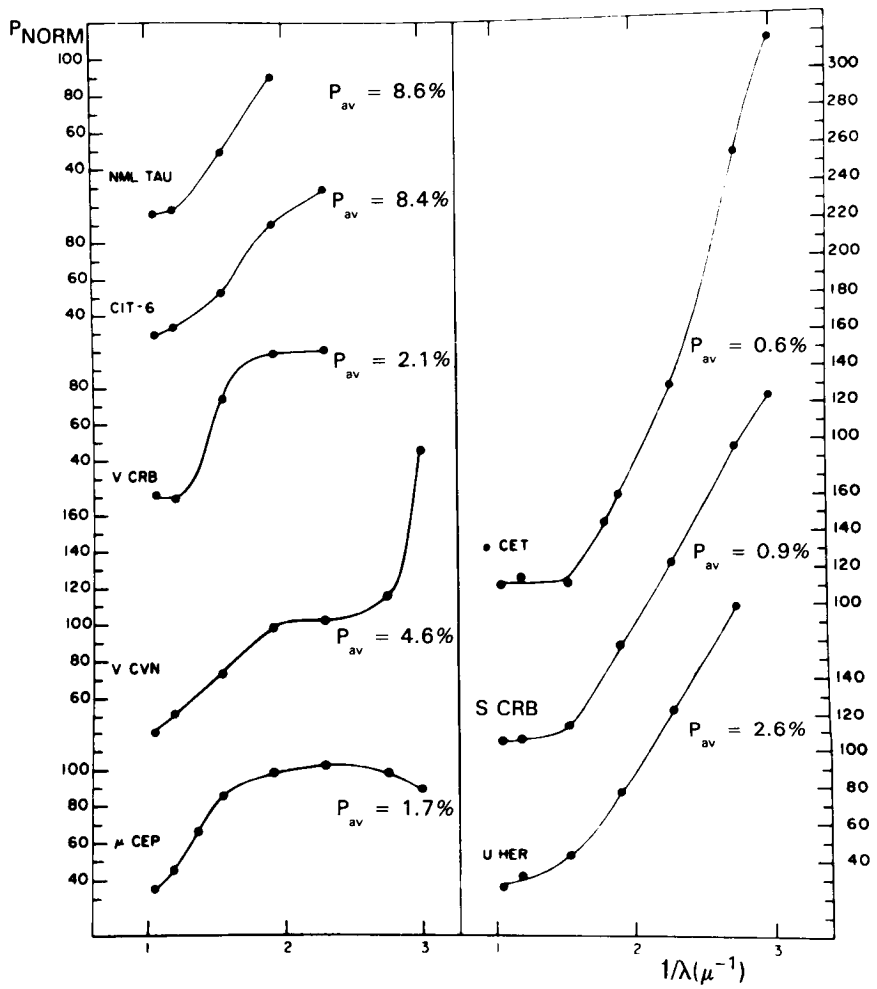

Figure 2-27. Wavelength dependence of polarization for a representative sample of red variables. The observed values were normalized by setting the average polarization through the green and blue filters equal to 100 percent. The actual value of this average is marked to the right side of each curve (from Kruszewski et al., 1969).

In *o* Cet, the polarization begins to increase as soon as the hydrogen lines appear. However, Shawl (1975) reports on L_2 Pup, which presented a very high polarization when the hydrogen emission was barely visible. This is in agreement with Dyck and Jennings (1971), who noted that the existence of intrinsic polarization does not necessarily imply concurrent Balmer emission lines, although it is likely to be found in stars having shown Balmer emission lines.

Dyck et al. (1971) demonstrate a linear relationship between the observed average degree of polarization in the blue and yellow spectral ranges and the amount of excess infrared emission—the latter attributed to reradiation from circumstellar grains (see the section *Infrared Excesses*)—also verified in the near infrared at 1.21 μm (McCall and Hough, 1980). They find that, if the presence of intrinsic polarization is always linked to an infrared excess, the reverse is not necessarily verified, particularly for Miras. In the data of Dyck et al. (1971), some of the Miras show a low mean polarization and

a large infrared excess simultaneously (Landstreet and Angel, 1977). Shawl (1974) discusses that details in the geometrical aspects in the envelope (e.g., clumpy regions of dust) might be the cause of high and low polarization for a given infrared excess in various stars. This is also the opinion of Landstreet and Angel (1977).

The correlation between the intrinsic polarization and the infrared excess (Dyck et al., 1971) is similar for M stars and carbon stars, implying that the polarization mechanism is independent of the chemical composition of grains (Reimers, 1975).

Kruszweski and Coyne (1976) and McCall and Hough (1980) show a clear correlation between the level of polarization and the separation of the 18-cm emission lines in the OH maser stars (i.e., between the expansion velocity and the scattering optical depth of the shell).

Forrest et al. (1975) conclude that there is no evidence that the variations in polarization are caused by a change in the total amount of circumstellar dust. No time variation of infrared flux is observed in stars in which the polarization varies greatly, suggesting a local rather than a global polarization effect (McCall and Hough, 1980). In fact, the infrared excess is interpreted in terms of large-scale emission of grains far around the star, and the variable polarization in terms of more localized scattering and absorption effects in transient regions of gas and dust. However, circumstellar dust at large distances from the star has been brilliantly detected by the discovery of linearly polarized blue continuum light from 15 to 90″ around the supergiant, α Ori (that is, from 550 to 3300 R_* in the frame of reference of Table 2-3), by McMillan and Tapia (1978). Indeed, these authors attribute the polarization to starlight scattered by the dust shell around the central star. The polarization structure is centrosymmetric—except that the polarization map is rather asymmetrical at 15 and 30″ from the star—and is detectable as far as 90″ in the north-east direction. The apparent polarization decreases slowly with angular distance; its directions are generally perpendicular to the radius vectors of the star. Similar, preliminary observations around o Cet reported by Coyne and McLean (1979) show that polarized light extends to at least 30″ (i.e., 1650 R_*) from the central star.

The possibility of observing the circular polarization produced by the scattering of linearly polarized light by circumstellar grains in red supergiants is discussed by Shafter and Jura (1980).

Specific Stars

The Mira, o Ceti. Broadband observations showed that the polarization in the ultraviolet increases abruptly at phase 0.8—coinciding with the first appearance of the hydrogen emission lines (see the section *Emission Lines*)—and then reaches a maximum value at phase 0.9 (Shawl, 1974).

Narrowband observations were obtained around maximum light, from about 3600 to 6200 Å, with additional wavelength regions in the near infrared. They showed small-scale polarimetric structure, detailing a complex dependence of the polarization with wavelength.

McLean and Coyne (1978) studied the phases from 0.94 to 0.97 near the 1977 maximum, with a resolution of about 50 Å. We quote the summary of the most notable features in the polarization spectrum from Coyne and McLean (1979): "(i) virtually no wavelength dependence of θ [less than 10°, but at an unusually high value of 107°]; (ii) increases in the degree of polarization across the Balmer lines, Hα to Hδ [indicating the presence of polarized Balmer-line flux]; (iii) decreases in P across TiO bands, e.g. 4955 Å, 5847 Å, and 7054 Å; and (iv) a general λ^{-4} increase in P into the blue as far as 4500 Å; (v) a wide polarization minimum in the UV at 3775 Å [also called the UV dip] having a sharp rise on the violet side [with no obvious relationship to absorption features in the flux spectrum]" (Figure 2-28, upper panel). Figure 2-29 illustrates the polarization profile at Hβ measured at a spectral resolution of about 0.5 Å; the increase in

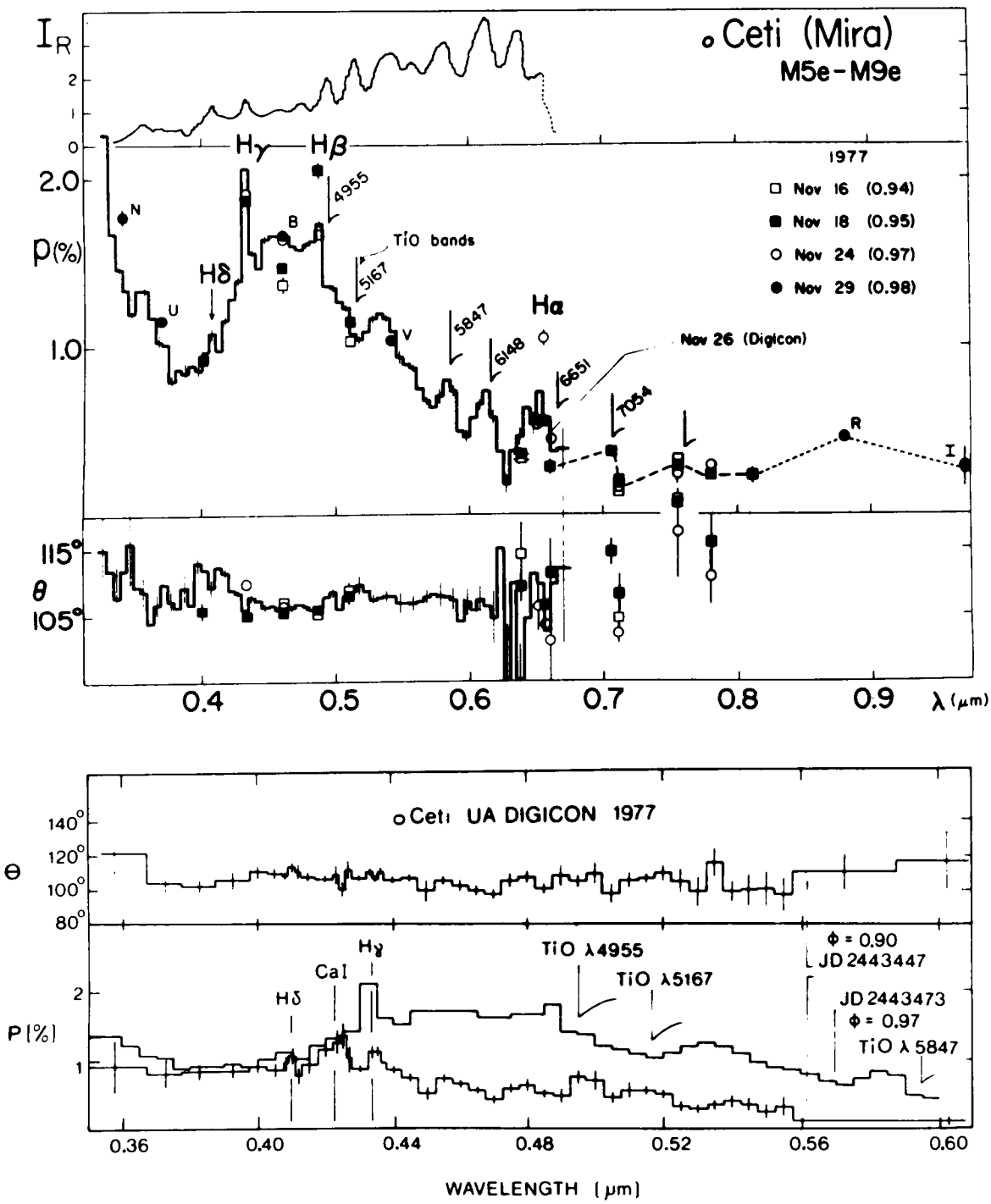

Figure 2-28. Wavelength-dependence of the degree of linear polarization P (in percent) and of the position angle θ for the M Mira, o Ceti, in 1977. Upper panel: around phase 0.95 from data obtained with various technologies (the flux profile I_R is also marked) (from McLean and Coyne, 1978). Lower panel: at phase 0.90 (the polarization data from the upper panel on November 26, 1977, at phase ~0.97 have also been plotted) (from Tomaszewski et al., 1980).

P is up to 6.8 percent, four times the continuum value, although there is no significant change in the position angle across the emission. Figure 2-29 also reports measurements using the 2.3 Å filter that obviously demonstrate the need for very high resolution. With respect to the flux profile, the polarization profile at Hβ is wider and more asymmetric, with its maximum displaced about 0.5 Å to the blue.

At φ = 0.90, 1 month before the 1977 maximum, Tomaszewski et al. (1980) note that they observe a polarization peak at Ca I λ4226 (Figure 2-28, lower panel). No evidence of this peak is seen about 1 month later at φ = 0.97 on McLean and Coyne's (1978) scan, also drawn on Figure 2-29. An earlier phase (around 0.85) reported by Coyne and McLean (1979) showed that the polarization was generally

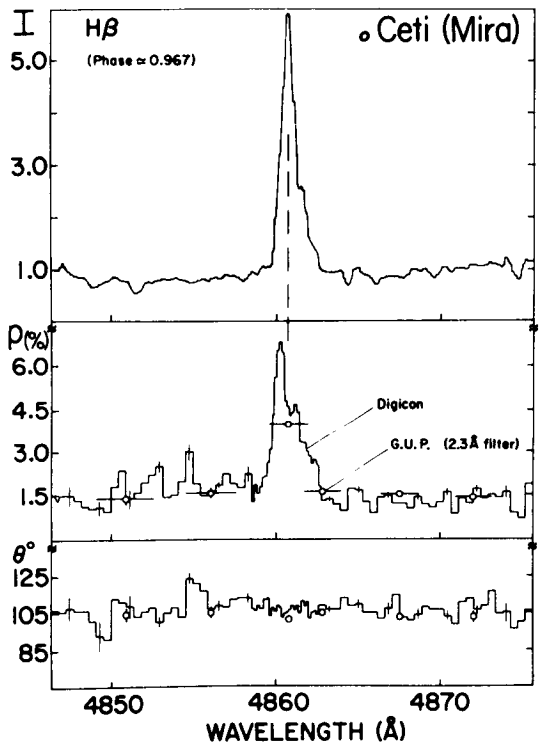

Figure 2-29. Relative flux (I), percentage of linear polarization P, and position angle θ across the Hβ region in the M Mira, o Ceti, on November 24, 1977 (from McLean and Coyne, 1978).

much weaker and that changes across Hβ were not significant. The location of the UV dip varied with respect to its location at phase around 0.95, indicating that the UV dip changes its location with time in the same star.

Around the 1978 maximum (a faint one with $m_v \sim 5.0$), observations at 20 Å resolution are reported by Tomaszewski et al. (1980; Figure 2-30). The conspicuous result is a striking change in the wavelength dependence of the polarization during the rise to maximum. At φ = 0.92, in addition to the general polarization features described by McLean and Coyne (1978) at the 1977 maximum, Tomaszewski et al. again find a peak in the degree of polarization corresponding to the Ca I 4226 Å resonance line, but they do not detect Hβ in either the flux or the polarization spectra. At φ = 1.09 (nearly 1 month after maximum), the sharp polarization peak at Ca I 4226 Å is no longer visible. The peak at Hδ is still visible but reduced. The position angle of polarization is about 45° smaller during the 1978 maximum than during the 1977 one. Shawl (1974) noted from Serkowski's observations that the position angle for o Cet, as well as for R Hya and R Lep, may show alternate high and low values in each cycle, recalling the behavior of the position angle with the light phase in the RV Tauri star, U Mon. However, Landstreet and Angel (1977) comment that most Mira variables show long-term stability of mean position angle, as would be expected if the asymmetries (see the section *Interpretations of the Polarization Observations*) were coupled to a rotation axis.

Around the 1979 maximum, Magalhaes (1980) observes a polarization peak at the Ca I wavelength approximately at phase 0.93 and also at phases 0.08 to 0.09. The striking feature is that the position angle at this wavelength changes dramatically, varying from near 5° at $\varphi \sim 0.93$ to about 170° at φ = 0.08 to 0.09, while staying around 25° in the other wavelengths.

As concerns other Mira variables observed around maximum light, we cite the observations of Landstreet and Angel (1977) about R Boo, RU Her, U Her, and R And; they detect

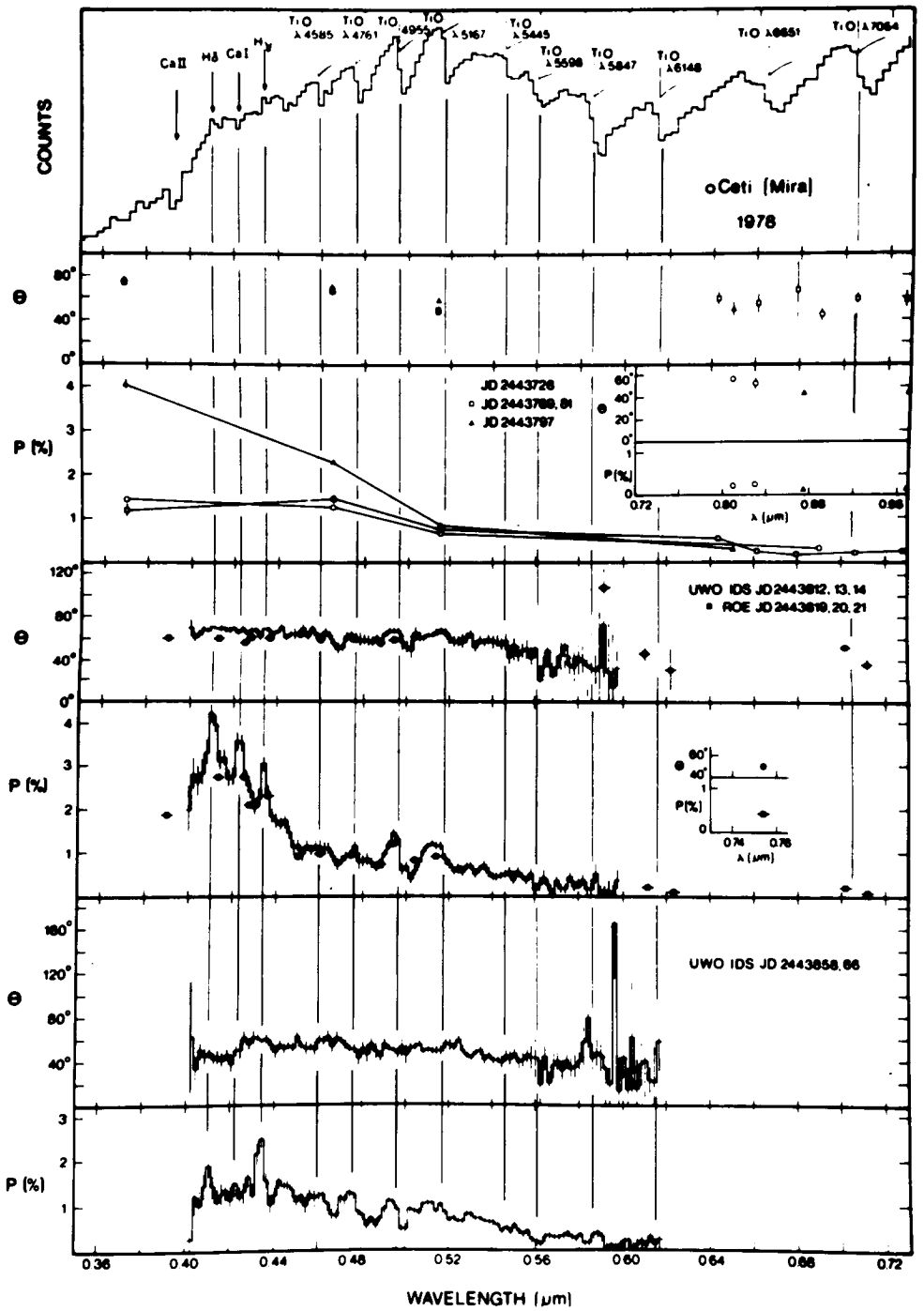

Figure 2-30. Wavelength dependence of the degree of linear polarization P and of the position angle θ for the M Mira, o Ceti, around the 1978 faint maximum. The first section is a flux spectrum in which the positions of the strongest spectral features are indicated by vertical lines. The remaining sections are divided into three panels according to phase—Panel 1: φ = 0.70, 0.80, 0.88; Panel 2: φ = 0.92 (IDS data) and 0.94 (ROE data); Panel 3: φ = 1.09 (from Tomaszewski et al., 1980).

a significant variation in the percentage of polarization peaks coinciding with molecular and atomic absorption features. This behavior has also been studied in the other Mira variables, R Car and R Cen, by Codina-Landaberry and Magalhaes (1980); they see changes across the TiO λ6159 band in R Car and R Cen that are decreases in percentage of polarization *not* accompanied by significant position angle changes. In contrast, in R Boo and U Her, Landstreet and Angel (1977) observe clear variations of about 20 to 30° in position angle across the strongest absorption features longward of 5500 Å. Coyne and McLean (1979) notice that the location of the UV dip varies from star to star.

Because the carbon stars have rarely been subject to polarization measurements, the observation of R Lep, a carbon Mira, is of special interest. This star was observed by Landstreet and Angel (1977) at minimum light (φ = 0.49). The polarization spectrum is nearly featureless, but a sharp change of position angle is observed at the Na I D lines.

The Semiregular Variable, V CVn. Important clues for the interpretation of the observed polarization have been extracted from V CVn, especially through two sets of observations by Coyne and Magalhaes (1977, 1979). In this star, the wavelength dependence of the polarization, $P(\lambda)$, in the blue-violet range strongly varies with time from 2 to 8 percent. The last remarkably large percentage often, but not always, coincides with minimum light. Relevant features of the $P(\lambda)$ curve are: (1) an increase of the polarization near Hβ with a shift of the polarization peak to shorter wavelengths as the polarization in the visual increases from about 2 to 8 percent; (2) a rising of the continuum polarization in the UV at the high-polarization phases, following a wide minimum at about 3800 Å or UV dip (also noted in *o* Cet, see above; Figure 2-31); (3) a change with time of

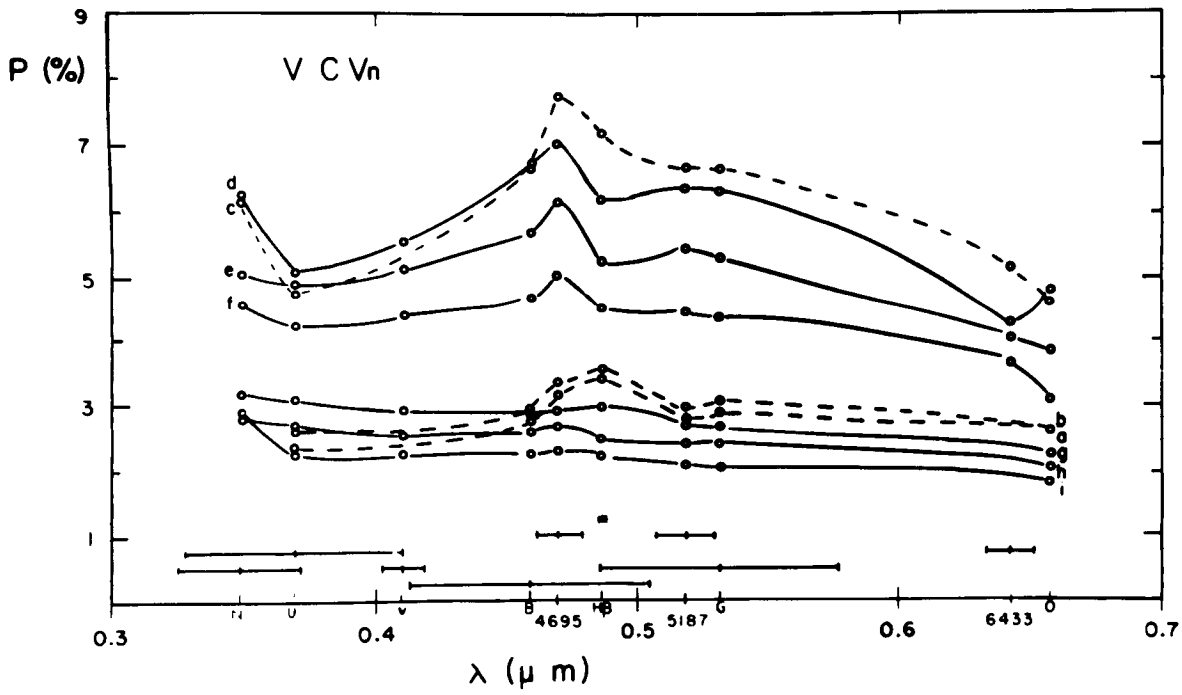

Figure 2-31. Temporal changes in the wavelength dependence of the polarization in the semiregular M star, V CVn, in 1976: (a) February 19–23, (b) February 25–26, (c) April 8–11, (d) April 22–28, (e) May 7–8, (f) May 14–18, (g) June 5, (h) June 13–14, (i) June 23 (from Coyne and Magalhaes, 1977).

the ratio of the polarization in the Hβ region to that in the adjoining continuum; it is less than one at the high-polarization phases and about one at the lower polarization phases; and (4) across the TiO bands, a clear dependence of the change in polarization across the 4955 Å band for which *increases* at times occur (see Figure 1 in Coyne and Magalhaes, 1979) and are seen with smaller amplitude across the 5167 Å band; otherwise, there is no observed change in the polarization greater than ±0.1 percent across any of the other TiO bands. There is virtually *no* change in the polarization angle with time.

Other semiregulars, such as S Lep and L_2 Pup observed by Codina-Landaberry and Magalhaes (1980), are also known to show changes at the time of observation (i.e., decreases) across at least one of the two TiO bands studied. S Lep shows changes across the TiO band at 4761 Å; L_2 Pup shows changes across the TiO bands at 4761 and 6159 Å and across the Ca I 4227 Å line for which the position angle at this wavelength also strongly differs from the one expected from the small gradual rotation position angle with wavelength. On the other hand, there is *no* significant position angle rotation at the TiO bands.

The Supergiant Semiregular Variables, μ Cep and α Ori. For μ Cep, unlike the previous stars, the wavelength dependence of polarization shows variations in *both* degree and position angle across *each* of the observed TiO bands (McLean, 1979; Coyne and Magalhaes, 1979). This makes us expect a different origin of polarization from that found in V CVn, all the more since a λ^{-4} curve never occurs for μ Cep, as already noted in the section *Overall Results on Polarization*. A UV dip is also present in this star (Coyne and McLean, 1979).

Time variation of the change in polarization has proved to be remarkably large in recent years. Prior to 1980, this star was not known to present large-scale polarization. The measurements in wide bands by Coyne and Kruszewski (1968) showed a polarization varying from about 0.2 to 2.5 percent. Narrowband observations in October 1976 (McLean, 1979) also reported an increase in percentage from red to blue of about 0.7 to 1 percent. Furthermore, in June 1979, the polarization measured by Coyne and Magalhaes (1979) belonged to this range of variation. However, from August to December 1980, wideband polarization measurements showed a surprisingly high percentage—around 4 percent (Arsenijevic et al., 1980; Hayes, 1981a). Then, measurements from August (P ~ 2.47 percent) to December (P ~ 1.85 percent) 1981 indicate that a remarkable decrease occurred in the course of about 1 year (Hayes, 1982). The polarization angle did not change significantly in 1980 and in 1981. We are not aware of spectroscopic observations during that time; however, if such observations exist, it would be interesting for the interpretation of such an event to determine whether the hydrogen emission (Balmer alpha is observed near maximum light in μ Cep; see the section *Hydrogen Emission Lines*) was barely visible when the polarization was high at 4 percent, as is the case in L_2 Pup.

For α Ori, we choose to present two sets of data, each being quasi-continuous over several years: (1) multicolor observations from 4250 to 8250 Å during seven observing periods from December 1973 to February 1975 (Tinbergen et al., 1981); (2) wideband (B filter) measurements over four consecutive observing seasons during 1979–1983 (Hayes, 1980, 1981b, 1984); as an example, the 1979–1980 and 1980–1981 observations are reported in Figure 2-32 (upper panel) as plots of the degree and angle polarization against time (Schwarz and Clarke, 1984). Figure 2-32 (lower panel) reports the polarization data as a function of wavelength from 4500 to 8000 Å, by Tinbergen et al. (1981), at various dates, in a presentation again due to Schwarz and Clarke: the degree of polarization shows a monotonous increase with decreasing wavelength from 6600 to 5000 Å, corresponding well to a λ^{-4} law. Furthermore, for a given observing time, when the polarization in the various filters from 6600 to 5000 Å is plotted in the Stokes vector diagram, it falls on a straight line. All these facts suggest that a

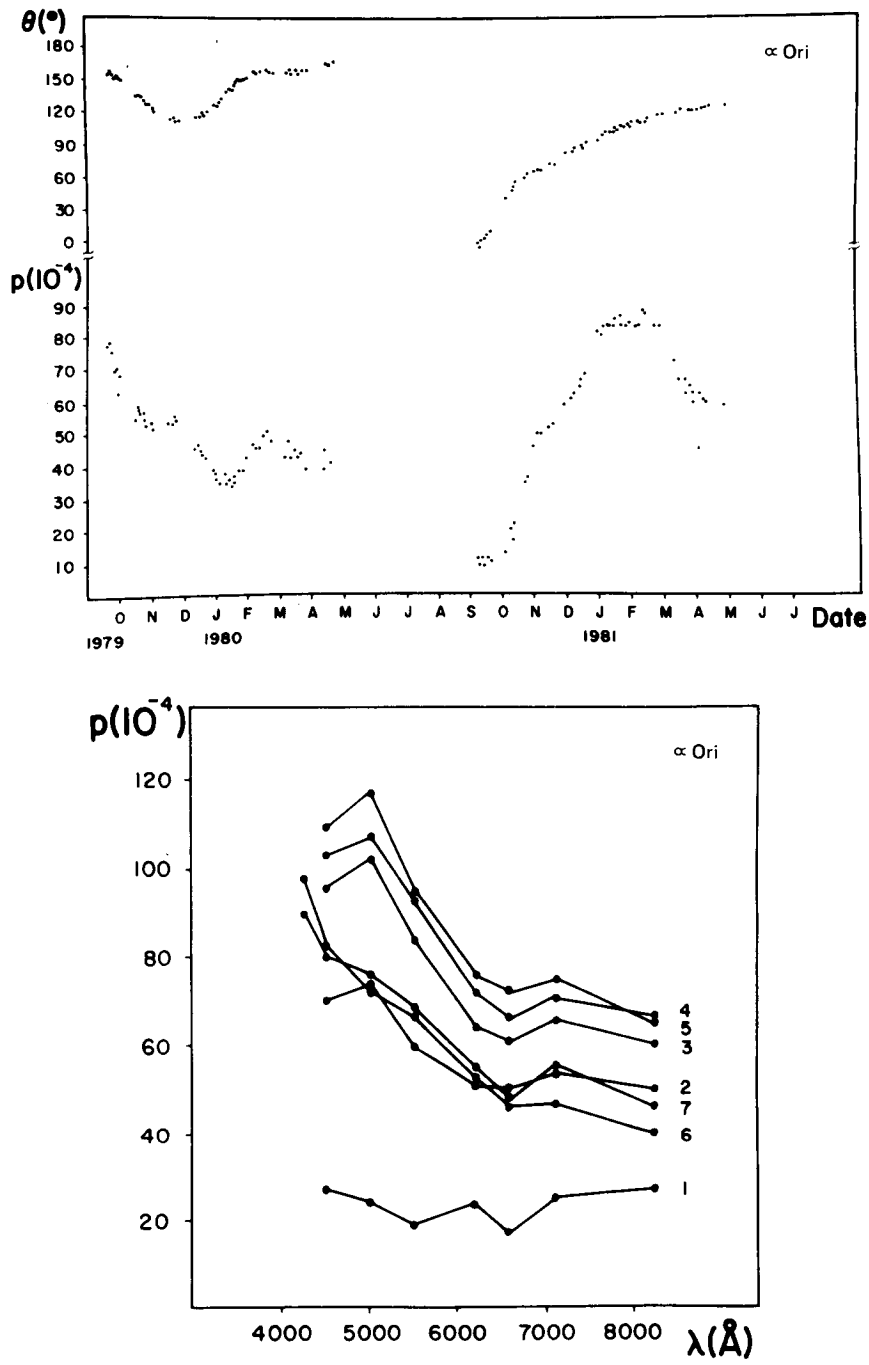

Figure 2-32. The polarization in the M supergiant, α Ori. Upper panel: Hayes's polarimetric data as plots of P and θ_P against time from 1979 to 1981 (the units for P are 10^{-4} (i.e., 0.01 percent) while θ_P is in degrees in the equatorial frame). Lower panel: Tinbergen et al.'s data plotted as P(λ) curves for different dates of observation: (1) 01.12.73; (2) 01.02.74 to 06.02.74; (3) 19.02.74 to 24.02.74; (4) 27.02.74 to 06.03.74; (5) 07.03.74 to 14.03.74; (6) 23.08.74 to 26.08.74; (7) 04.02.75 to 08.02.75 (from Schwarz and Clarke, 1984).

single physical process is responsible for the polarization in the quoted wavelength range.

The observations displayed in Figure 2-32 emphasize time variations. From the upper panel, the important points noted by Hayes (1980, 1981b) are: (1) changes in the position angle; (2) an almost complete reversal of the direction of polarization that happened between October and December 1979; and (3) the occurrence of two distinct events suggested by differences in the morphology of the 1979–1980 and 1980–1981 observations. Significant changes take place on time scales of about one to several months. Also, changes in the stellar brightness distribution over time scales correlated with changes in the Hayes polarization measurements are reported by Goldberg et al. (1981).

Finally, it is worth noting that Coyne and McLean (1979) do not find clear evidence of polarization structure in high-resolution Hβ data and 50 Å scans of the yellow TiO bands in α Ori. In fact, Clarke and Schwarz (1984) obtain a variation of the degree of polarization in the TiO absorption features on 50 Å resolution spectra; the polarization is less than 1 percent.

In addition, we recall that polarization up to 90″ from the central star has been observed by McMillan and Tapia (1978). (See the section *Overall Results on Polarization*.)

Interpretations of the Polarization Observations. The wavelength dependence, as well as the time variations of the position angle and of the percentage, are characteristics of the intrinsic polarization. It is now admitted that their interpretation may require the combination of several mechanisms in the same star; for example, the fact that the observed variations in polarization across absorption features sometimes occur primarily in P and sometimes in θ suggests that in some cases two different polarization mechanisms (having different principal axes) are competing to produce the observed polarization (Landstreet and Angel, 1977). Also, besides the mechanisms of the polarization, intrinsic polarization can be expected only if there is a concomitant asymmetric atmosphere. In brief, even if the physical processes underlying the observations are not yet understood in detail, theoretical models put forward to explain the origin of polarization are linked to "the scattering properties of either asymmetrically distributed circumstellar grains and/or the photospheric gas," as concisely formulated by Magalhaes (1981). The merit of the higher wavelength resolution observations with regard to the large-band data was to show that dust alone is not accountable for the intrinsic polarization, but that a contribution from the photospheric gas may be required.

The various sources of asymmetries for a nonuniform brightness distribution over the photosphere may be: (1) geometrical effects of nonradial pulsation; (2) pole-to-equator temperature gradients or small variations of temperature over the stellar surface; for example, coming from cooler regions of grain formation or from hotter spots at the surface (the excess brightness near the limb breaks the azimuthal symmetry and results in net residual linear polarization); (3) giant convective cells according to the Schwarzschild (1975) hypothesis; and (4) active regions on the stellar surface. As for the envelope, its likely clumpiness would make it appear asymmetric when viewed from any angle. Finally, asymmetries produced by the dynamical effects of a binary system may exist (as is probable for α Ori as discussed below). McCall and Hough (1980) point out that such nonuniformities not only provide highly asymmetric scattering geometries, but also cause anisotropic illumination of the dust envelope.

Details on the origin of the continuum polarization, as well as on the UV dip—probably due to absorption by the numerous lines around 4000 Å—have been thoroughly developed in the Coyne and McLean (1979) review. In the following, we discuss the up-to-date theoretical models favored for explaining some specific observations described above. (It would thus be most interesting to have polarization measurements in the corresponding region in N-type carbon stars which exhibit a more drastic decrease in flux shortward of 4000 Å.)

Causes of Polarization Variations Across Molecular Absorption Bands or Atomic Lines. On the basis of the observations in V CVn, Coyne and Magalhaes (1979) suggested that the time variations in the polarization across TiO absorption bands (with no change in the polarization angle) support the model of Harrington (1969). In this model, the radiation emitted into the line of sight from near the stellar limb of the pulsating atmosphere is polarized by Rayleigh scattering. (The polarization is largest near the maximum expansion.) According to Magalhaes (1981), who combines Tsuji's (1978a) model atmosphere computations for M stars with Harrington's model, it is indeed relatively small changes in the ratio of absorption to scattering due to variations with time in the photospheric optical depth that produce the observed polarization changes, particularly verified across the 4955 Å band in V CVn. Thus, as emphasized by Coyne and Magalhaes (1979): "the time dependence of the polarization in V CVn is fundamentally connected to the pulsation cycle and to photospheric parameters which vary with the pulsation cycle...namely: temperature, extent, ratio of absorption to scattering, variation of source function, molecular constituents and their energy states etc." Increase (such as in V CVn) or decrease (such as in S Lep, L_2 Pup, or *o* Cet) in the bands is related to the optical depths at which the Rayleigh scattering (mainly by atomic and molecular hydrogen) dominates over the absorption (mainly by TiO and H^-). Magalhaes (1981) writes: "In certain cases, this region is situated too deep in the atmosphere [as when later spectral types are considered], in which situation only decreases should be expected. In others, the relevant region may be found nearer to the surface so that either decreases or increases may be expected." Incidentally, Codina-Landaberry and Magalhaes (1980) remark that small solid particles could well exist in the very outer atmospheric layers and partly contribute to scattering in the visible region.

For Coyne and Magalhaes (1979), the more likely source of the asymmetry required to give a net polarization integrated over the disk necessitates the consideration of the star as a rotating one: the asymmetry is produced by systematic pole-to-equator temperature differences due to pole-to-equator gravity differences. An equatorial rotational velocity of about 11 km/s (rotational period ~7 years), which is a reasonable value for red giants (Allen, 1973), is implied.

The high polarization across the Ca I absorption line at 4227 Å in L_2 Pup or *o* Cet would also come in support of the photospheric mechanism as suggested by Codina-Landaberry and Magalhaes (1980). Furthermore, remember that the position angle at this wavelength is very different from the value for the continuum polarization and even from that in the TiO bands. The authors just quoted imagine that the necessary remarkable asymmetry at this wavelength might be caused by an unevenly distributed Ca I across the stellar surface.

An alternative application of Harrington's (1969) model is made to *o* Cet by Tomaszewski et al. (1980). These authors interpret the observed polarization as effects of Rayleigh scattering in an atmosphere which is not uniformly bright, owing to one large-spot region near the limb which is hotter and brighter than the rest of the photosphere. They explain local decreases through the strongest TiO absorption bands and polarization increases in the weakest bands as follows: "At wavelengths where absorption is strong, photons are likely to have last interacted with photospheric material by absorption and reemission (which usually results in no polarization) rather than by scattering. Thus, since local emission is largely unpolarized, the integrated radiation will be as well."

In the supergiant, μ Cep, the polarization varies in both degree and position angle across each of the TiO bands. McLean (1979) suggests two competing polarization mechanisms: a photospheric Rayleigh scattering and Mie scattering from circumstellar grains, the former being suppressed at wavelengths at which strong molecular absorption dominates. However, Coyne and Magalhaes (1979) attribute the polarization only to Mie scattering from grains in

an extended asymmetric envelope; the smaller polarization observed in the continuum with respect to the TiO bands might be due to a depolarization of the light undergoing a larger path length. The authors propose the following model: in the TiO bands are mainly seen the outer regions of an extended asymmetric dust-scattering envelope in which dust and gas are well mixed and which is characterized by given mean grain size and scattering geometry; in the continuum are seen deeper regions of the envelope characterized by different grain sizes and another scattering geometry. In fact, if there is a systematic increase of mean grain size with distance to the star, Mie scattering calculations show that the plane of polarization rotates by 90° beyond a certain grain size for a given wavelength. Moreover, the systematic change in scattering geometry of the envelope with distance might be caused by changes in the alignment of elongated grains.

The drastic rapid change in continuum polarization observed in 1980 in μ Cep helps to specify the source of the polarization. According to Hayes (1982), the observed time scales of variability give evidence that the polarization changes were not linked to a mass-loss event as it traversed the extended circumstellar envelope (1.8 years might be necessary for matter to traverse one stellar radius in μ Cep). Rather, they are consistent with a continuum polarization originating in the lower atmosphere where the survival of grains might be probable (Draine, 1981; Schmid-Burgk and Scholz, 1981). In addition, the polarization variations might be indirectly produced through photospheric processes that control time changes in the anisotropic illumination of the polarizing circumstellar material (e.g., the waxing and waning of one or, at most, a few large-scale convective cells on the stellar surface).

The case of α Ori will be discussed in the following section.

In o Cet, as well as in other Mira variables, the flux is polarized in the Balmer emission lines. These lines originate in the ionization front of the shock wave traveling through the stellar atmosphere. (See the section *Atmospheric Kinematics*.) According to Feofilov (1961), this ionization zone also produces Lyman photons which are the polarizing agents of the Balmer line flux (McLean and Coyne, 1979; Svatos and Solc, 1981). However, the emitting region must not be spherically symmetric about the star. To circumvent this difficulty, Svatos and Solc argue for a magnetic field transverse to the line of sight as a more probable agent of the high polarization degree in the Balmer lines.

The α Ori Case: Is a Binary Nature Accountable for Its Polarization Changes? Ordered (as opposed to stochastic) polarization changes appear over the course of each of four consecutive observing seasons in α Ori (Hayes, 1984). As Hayes already proposed for μ Cep, the time scales of the changes suggest that the latter are a manifestation of the waxing and waning of large-scale convective cells at or near the photospheric surface. Tinbergen et al. (1981) also adopt such an explanation. Schwarz and Clarke (1984) and Clarke and Schwarz (1984) model photospheric Schwarzschild's convection cells (hotspots) to give account for the observations of Hayes and Tinbergen et al. Goldberg et al. (1981), reconstructing the image of α Ori observed by speckle interferometry in 6500 Å continuum radiation on February 3, 1981, find an asymmetry due to an unresolved bright feature near the southwest limb at position angle 208°; they lend support to the Hayes model, assuming the bright feature to be a convective photospheric cell. Since the polarization resumed its variation in October 1980 (see Figure 2-32, upper panel), these authors conjecture that a bright feature developed in September–October 1980 on or near the stellar limb at position angle 208° and grew in luminosity until around the end of December 1980 when the integrated visual light curve begins a steady decline. They support their conjecture that the asymmetry needed for a net polarization is due to a convective cell by the fact that on February 1, 1981, the angle of the plane of polarization was within 5° of being at right angles to the direction of the bright spot. They interpret the

evolution of the cell in relation to the observed polarization degree in the following manner: "The progressive increase in the angle of the plane of polarization before and after February 3 implies either that the bright feature was moving around the limb, which seems unlikely, or that light from the surface feature was being scattered by material in motion above the limb and changing its orientation with respect to the active region." However, Karovska (1984) contests these two interpretations. She remarks that, due to the increase observed in the polarization angle from, say, November 17, 1980, to April 28, 1981 (i.e., $\Delta\theta = 52°$), the bright feature ought to have a proper motion on the stellar disk characterized by a too high velocity. Karovska also applies the remark to an eventual scattering matter in motion above the stationary cell. She suggests that the unresolved bright feature observed by Goldberg et al. (1981) is a companion star near α Ori (see the section *Geometrical Shell Expansion*) that might account for the observed changes in polarization. The Hayes data show that the polarization degree strongly increases from the end of 1980 to the beginning of 1981. During this period, the companion might be embedded in the dusty patch observed by Roddier and Roddier (1983; see the section *Geometrical Shell Expansion*). The scattering dust, together with the companion position, might favor the increase in polarization. We suggest that phase-locked polarization variations in the Stokes parameters (Q, U) frame should help to decide on the α Ori binarity. However, the problem might be confused by the presence of another, farther companion.

The Magnetic Field Hypothesis Applied to Mira Stars. Svatos and Solc (1981) recognize that grains—dirty silicates—exposed to short-wavelength radiation might be responsible for the polarization in o Cet. These authors conclude that Mie scattering in an asymmetric envelope cannot explain the observed high degree of continuum polarization because, in particular, only low departures from spherical symmetry (less than 15 percent) have been found by Speckle interferometry by Labeyrie et al. (1977). Thus, just as for explaining the polarized Balmer flux, they call on a magnetic field. Its global value (about 150 gauss) is chosen to be sufficient for obtaining the particle orientation. The transfer of the signal that triggers the polarization is by radiation because it seems more reasonable to the authors that "the location of dust is far from the place where storming processes due to stellar pulsation occur." The source of the grain irradiation energy is surface magnetic flares (or magnetohydrodynamic (MHD) shock waves). The grains irradiated continuously due to flares are responsible for the polarization observed over the entire cycle.

The cyclic variability of the degree of polarization is due to changes in irradiation of the amorphous silicate grains due to changes in their optical properties, linked to chaotic flare-like events (Svatos, 1980). Particularly, enhanced polarization degree is caused by the increase of the imaginary part of the refractive index.

On the other hand, UV emission in the continuum and in lines in o Cet is observed from the IUE satellite before the maximum visual light, showing that UV radiation also lies in the ionization front of the shock wave, according to the model of Hinkle and Barnes (1979a). So, this further irradiation acts at phase 0.8 where the shock wave rises in the photosphere, explaining the observed UV sudden enhanced continuum polarization at that time. Incidentally, the temperature of irradiated grains increases, causing the enhanced 10-μm flux at this phase. (See the section *Time Variability of Infrared Excesses*.)

Finally, Svatos and Solc (1981) distinguish three types of polarizing silicate grains by looking to Shawl's (1975) observations in various filters; some particles scatter in N and U colors, others in B, G, and O, and the last ones in R and I colors. Consequently, they propose the model envelope for Miras, shown in Figure 2-33, that completes the model by Hinkle and coworkers from the molecular gas. (See the section *Photospheric Kinematics*.) Three regions

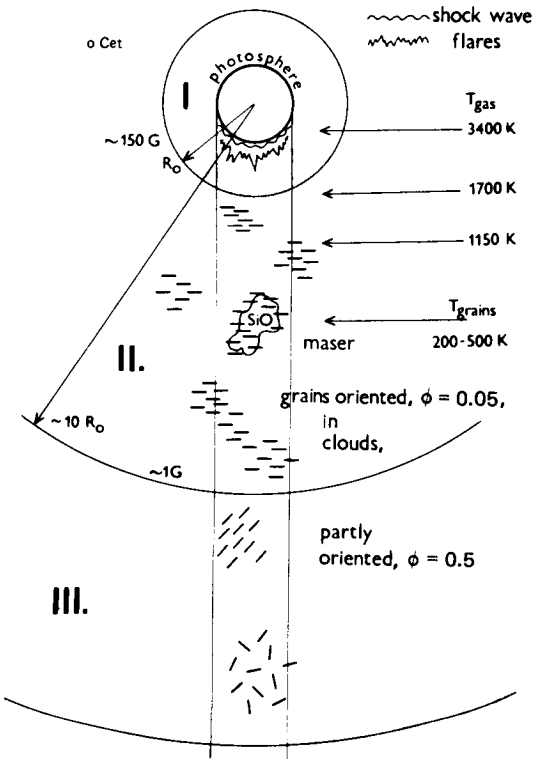

Figure 2-33. Schematic representation of dust in the extended atmosphere of Mira variables submitted to a magnetic dipole field assumed to be perpendicular to the plane of drawing. The various T_{gas} reported on the figure represent the CO, OH, and H_2O gaseous regions described in Hinkle and Barnes's (1979a) shock-wave model applied to R Leo (also see the section, Further Probes of the Pulsating Photosphere). R_o is the measured diameter in the blue color and the TiO bands by Labeyrie et al. (1977); φ is the grain radius in μm (from Svatos and Solc, 1981).

are defined. Region I is the region of gas; regions II and III (which have a cloudy structure, lowering the value of the global magnetic field by enhancing it locally in the dust clouds) mainly contain the silicate grains which become bigger and bigger—by impurities sticking on them as they move away from the star (Draine, 1981)—i.e., more and more efficient from UV to near IR to reproduce the P(λ) behavior. In region II, where the 800 K quasi-stationary gas layer (which is at the origin of grain formation with a resulting outward acceleration) is located (see the section *Summary: Structure of Expanding Gaseous Envelope*), there are "perfectly" oriented elongated grains due to paramagnetic relaxation (Dolginov and Mitrofanov, 1977); these grains are responsible for the relatively large continuum polarization (1 to 4 percent) in the visible. (They polarize at B, G, and O wavelengths mainly with a λ^{-4} law.) In region III, which is far from the star, the grains are partly oriented as they suffer both field and radial orientation and produce less polarization. (They polarize in R and I wavelengths with a nearly λ^{-1} law.)

The systematic change in alignment of elongated grains with distance from the star (i.e., change in scattering geometry) has already been evoked by Coyne and Magalhaes (1979) as a likely cause of the interaction of stellar winds on magnetic fields. Dolginov and Mitrofanov (1977) study the influence of magnetic fields of various strengths on the orientation mechanism of the particles lying in the outflow of gas and dust (either paramagnetic relaxation or the relative motion of the dust and the gas) and, consequently, the percentage of polarization to expect.

Although dust might be the main polarization mechanism in Miras, the polarization structure (decrease) in the TiO bands (without any significant change in θ) shows that at least a part of the polarization originates in the stellar atmosphere, possibly following the photospheric scattering mechanism developed above for V CVn. However, if the grains are outside the region of TiO formation, decreases in polarization across TiO bands might be caused by the great optical depth of these bands (Coyne and McLean, 1979).

Conclusion: The Magnetic Field Frame

To conclude, we comment on the influence of magnetic fields on the outer layers of Miras presented by Svatos and Solc (1981). They propose what likely happens to the dust above the

800 K stationary layer. Let us remember that, concerning o Cet, dust has been detected up to at least 30'' (i.e., 1650 R_*) through polarization measurements (Coyne and McLean, 1979).

Svatos and Solc (1981) superpose flares on the photospheric shock waves. These flares are necessary to produce irradiation of the dust grains and to account for the variable degree of polarization. However, flare-like activity supposes erratic strong intensification of Balmer lines, Ca II lines, and UV continuum (see Rodonò, this volume). Rather, we favor magnetic waves (more precisely, acoustic slow-magnetic shock waves) that travel along magnetic flux tubes (Leibacher and Stein, 1981) and are able to heat magnetic regions, particularly the dust clouds assumed by Svatos and Solc. These waves dissipate higher up in the atmosphere than the photospheric shock waves because they have a longer period. Moreover, it might be that, in the higher layers of the atmosphere, the variability in emergence and decay of the magnetic field dominates (i.e., temporal changes in magnetic field strength are expected there). Such magnetic waves also appear to be very attractive for explaining the erratic behavior of chromospheric emission lines in some carbon stars (Querci and Querci, 1985a; see also the section *Atmospheric Kinematics*).

In support of the magnetic presence, besides the first attempt by Donn et al. (1966, 1968) to explain a few percent visual polarization by a magnetic field of 100 gauss acting on submicron graphite disks, Marcondes-Machado (1979) shows that magnetic grains (Fe_3O_4), which are probably condensing in the envelope of M stars, can be aligned by a minimum magnetic field as low as 1×10^{-5} gauss. (As a purely theoretical example, this author adds that a 10-gauss dipole magnetic field at a stellar surface would give a 0.03-gauss field at 7 R_*.) The produced polarization has a wavelength dependence qualitatively similar to the observed intrinsic continuum polarization; for example, the agreement between the theoretical polarization curve and the g Her observations is striking.

Further support to the presence of a magnetic field might be given by linearly polarized SiO maser emission from R Leo (Clark et al., 1980), where the position angle of polarized emission varies systematically with respect to the spectral-line center. Magnetorotation might be the cause of this change in position angle, with a magnetic field of $9 \times 10^{-3}/\cos\theta$ gauss (where θ is the angle between the magnetic field and the line of sight). Also, magnetic fields are proved by radio flares as observed, for example, on the M supergiant, α Ori (Oster, 1971), on the C giant, V Cyg (Querci et al., 1979), or on the M giants, R Aql (Woodsworth and Hughes, 1973) and α Cet (Boice et al., 1981). Finally, as emphasized by Coyne (1979), polarization might be the best probe of stellar magnetic fields.

Strengths of magnetic fields are poorly known among late-type stars. Direct observations of the Zeeman effect are rare (Babcock, 1958). Nevertheless, there is evidence for time variability in the magnetic fields; this variability may be partially responsible for the difficulty some authors have had in confirming Babcock's work (see comments by Stencel and Ionson, 1979, and Slovak, 1982). In addition, magnetic fields could have very low strength. We mentioned previously that a few gauss should be sufficient to act on the polarization mechanism. It is encouraging that a stellar magnetometer able to measure longitudinal magnetic fields as small as a few gauss has been assembled by Borra et al. (1984).

As for the mechanism-generating fields in red giants and supergiants, it is still debated. Though these stars have deep convective zones, their angular velocity is much lower than a main-sequence star and the radius to pressure scale-height ratio is of the order of unity (Wdowiak, 1977), making a hydrodynamical dynamo unlikely. First proposed by Levy and Rose (1974) and then reviewed by Wdowiak (1977), magnetic fields could be generated in a rapidly rotating core during helium-shell flash instability, with subsequent rise to the surface because of the buoyancy of the magnetic flux tubes.

GEOMETRICAL SHELL EXTENSION—THE DIRECT APPROACH

We discuss here the "direct" approach to measuring the angular diameter of stars and/or to mapping the distribution of dust and gas in their circumstellar shells. In fact, the approach is not really direct because the definitive results must be extracted from geometrical optics through physical optics (Ridgway, 1981b; Wing, 1979).

Generally speaking, the derived apparent angular diameters assume a stellar disk with uniform brightness distribution and/or a linearly fully darkened disk. Information about limb darkening is required to obtain a "true" angular diameter from the apparent one. The correction factor for limb darkening as a function of wavelength can be calculated from model atmospheres (for example, Manduca, 1979); in consequence, it is limited by the inherent assumptions in the models. A possible observational determination of limb darkening might be reached by multiwavelength measurements through the techniques that yield angular diameters.

The spatial scales of dust distribution and, more generally, stellar angular diameters are provided by lunar occultation techniques or by the numerous interferometry techniques—Michelson or heterodyne spatial or speckle or rotation-shearing interferometry. The use of lunar occultations has led to a rapid expansion in the acquisition of angular diameters for numerous giants (e.g., Ridgway et al., 1979, 1980a; White, 1980). Measurements in visible and near-IR wavelengths (say, up to filter K) are suited for stellar photospheric diameters. Longer wavelengths measure circumstellar shells. Let us mention the importance of stellar angular diameters for the interpretation of stellar spectrophotometry, in particular for the calibration of cool-star effective temperatures (Ridgway et al., 1980b).

Reviews about the techniques and/or their results may be found, for example, in Davis and Tango (1979) and in Johnson and Allen (1981). Here, we choose to present two stars that have been observed at length and that display the state of the art in the "direct" knowledge of their size and structure: (1) one of the most frequently studied stars in high angular resolution astronomy, the M supergiant, α Ori, that teaches the most on a spatial stellar structure, and (2) the prototype of very dusty stars, the carbon star, IRC + 10216. We do not intend to discuss the data in terms of radial density and temperature distributions or mass loss (see Goldberg and Lefèvre, this volume).

The M Supergiant, α Ori

Multimeasurements at various optical wavelengths (for example, from the pioneer interferometric observations by Michelson and Pease in 1920, listed in Tsuji, 1976; in Wilkerson and Worden, 1977; and in Welter and Worden, 1980) evaluate *the photospheric* apparent angular diameter and show its *variability*. A mean value is about 0.″050, with a minimum of 0.″034 and a maximum of 0.″069. From the diameter estimates by Bonneau and Labeyrie (1973) and Welter and Worden (1980), the angular diameter appeared to decrease with increasing wavelength, possibly due to decreasing scattering by dust or molecules with wavelength in the stellar atmosphere (also see Tsuji, 1978b). However, the observations by Balega et al. (1982) and Roddier and Roddier (1983) do not really confirm this trend (within the error bars). Also, the diameter measured in the TiO strong absorption bands and their nearby continuum shows a slight excess of about 0.″004 in the TiO band as an effect of their opacity (Lynds et al., 1976; Balega et al., 1982; Roddier and Roddier, 1983). Finally, we have to bear in mind that α Ori is a variable star. Time variability in the diameter is expected, with minimum radius occurring near maximum light when the photospheric layers are at their maximum compression, and vice versa. This statement was called into question by White (1980), who plots angular diameters of α Ori, directly measured at wavelengths between 0.51 and 0.65 μm, against phase. The trend indicates a rapid increase in the diameter to maximum, followed

by a more gradual decrease to minimum. However, Balega et al. (1982) show that such a variation of diameter with time is not meaningful within the range of errors; errors in standard deviations of the fitting at the 1σ confidence level largely overlap when the fit to the data is done through a sine or a serrated curve, as well as a horizontal straight line. Also, arguments of Guinan (1984) that the star attains its maximum radius near the time it is brightest remain speculative, waiting for improvements in the determination of effective temperatures for supergiants and particularly for α Ori (for example, Tsuji, 1976; Scargle and Strecker, 1979; Balega et al., 1982).

Observing by heterodyne spatial interferometry at infrared wavelengths suited for determining the extension of *the dust circumstellar shell*, Sutton et al. (1977) find that the dust exists outside 12 R_* from α Ori, while the density of grains is rather low out to there. Bloemhof et al. (1984), observing at 10 μm in February 1983 with a new spatial array instrument, give an effective outer diameter of the dust radiation of about 2.″5 (i.e., 125 R_*) and detect a shell of dust emission at 0.″9 (i.e., 45 R_*) from the photosphere. We recall that circumstellar dust around α Ori has been detected from 550 to 3300 R_* by polarization measurements (McMillan and Tapia, 1978). *Departure from spherical symmetry* of the circumstellar envelope was apparent in the last-mentioned observations and in the dust distribution found by Bloemhof et al., as well as from line profiles off the stellar disk. (See the section *Physical Conditions in Gaseous Shells.*) Such shell asymmetry is also found by Ricort et al. (1981) observing α Ori by speckle interferometry in October 1979, by Roddier and Roddier (1983, 1985) observing by rotation-shearing interferometry in the visible at 5350 Å in November 1980 (see Figure 3 in Lefèvre, this volume), and by Karovska (1984), also by the same technique, in February 1982 in the continuum at 5350 and 6400 Å and on a TiO band at 6207 Å. This set of observations constituted an enormous advance in knowledge of the morphology and the dynamics of the α Ori atmosphere. The main results of the direct mapping are as follows:

1. The curves representing the azimuthal average of the observed fringe visibilities as a function of spatial frequency indicate an important temporal evolution of the radial distribution of the visibility in the envelope, over 28 months and 15 months with respect to Karovska's observations. (Let us recall that the fringe visibility is a measure of the spatial distribution of the radiation from a given source; generally, this radiation consists partly of stellar photospheric emission and partly of CS dust emission.)

2. None of these curves account for a stellar disk with any limb-darkening coefficient, but rather the curves are consistent with a stellar disk surrounded with an envelope of dust scattering the visible light. The stellar disk diameter is estimated to 0.″035 ± 0.″010 by Ricort et al. and to 0.″037 by Roddier and Roddier (1983; uniform brightness distribution), with 85 and 40 percent of total irradiance coming from the stellar disk, respectively. The light scattered by the envelope therefore increased from 15 to 60 percent, respectively, while Karovska finds a decrease to 30 percent 15 months after Roddier and Roddier's observations (also in agreement with measurements made 9 months later in November 1982 by Petrov, as quoted by Karovska, 1984).

3. The reconstructed image of α Ori from a map of fringe visibilities produced by the star in November 1980 shows a stellar disk surrounded with a bright half-moon asymmetric cloud located at about 2.5 R_* (i.e., 0.″05) from the stellar center and about 1 R_* large (Figure 2-34).

4. The modulation of the fringe visibility produced by α Ori on February 1982 reveals the presence of a companion

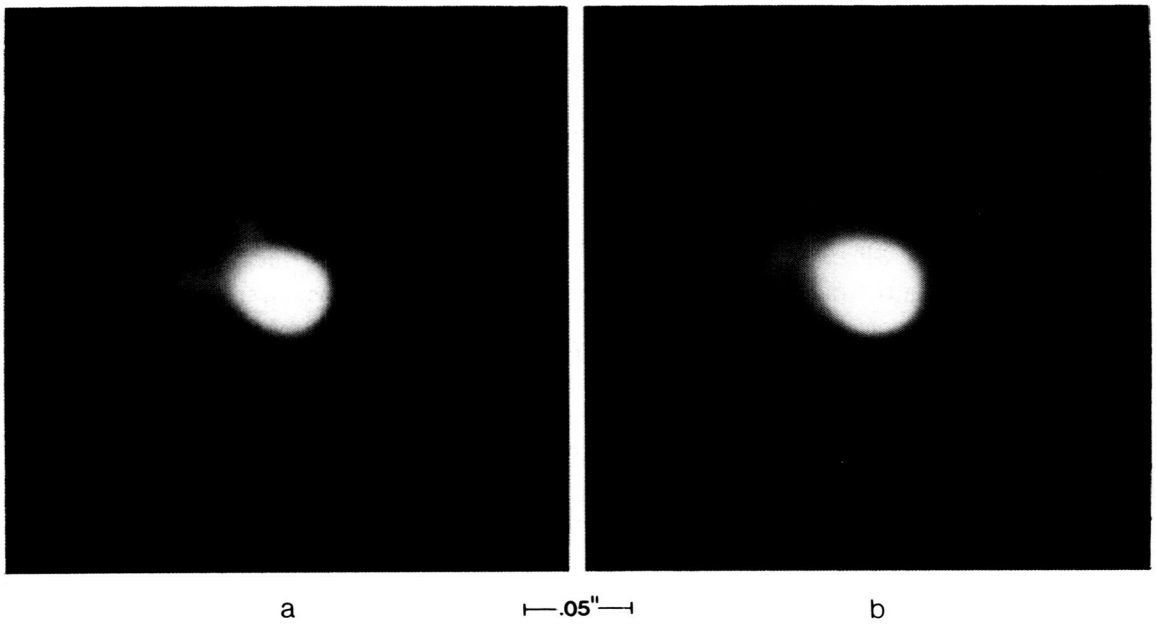

Figure 2-34. Reconstructed images of α Ori from a map of fringe visibilities obtained on November 30, 1980: (a) using the maximum entropy algorithm, (b) with the data extrapolated half-way up to the first zero of the Bessel function (from Roddier and Roddier, 1985).

located at about 0.″4 to 0.″5 (i.e., ~20 to 25 R_*) at 80° (mod 180°) with respect to north in the east direction. The visual magnitude difference is 3.5. The presence of such a companion has also been confirmed by Karovska (1984) on observations by speckle interferometry obtained in November 1982 by another group (C. Aime).

5. A bright feature (much brighter than the envelope) is mentioned by Karovska (1984) to be present in the November 1980 reconstructed image: it is located at 2 R_* from the stellar center (i.e., ~0.″04), at 330° with respect to north (mod 180°). As suspected by Karovska, an identical feature might be present in the reconstructed image observed in January 1976 by Welter and Worden (1980), but at 2.5 R_* and toward the direction 312°5 with respect to north. It may be admitted that this feature is a close companion to the star. In fact, recent analysis of polarization data (Karovska et al., 1985a, 1985b) sustains the existence of such a close companion to α Ori (Figure 2-35). It is also striking that the position angles calculated by Karovska (1984) at the dates of observation by Goldberg et al. (1981; see discussion in the section *Interpretations of the Polarization Observations*) agree with the position angles derived by these authors.

Again, as when interpreting the variability in the chromospheric emission lines (see the section *Atmospheric Kinematics*), we raise the influence of the close companion for explaining the patchy dust shell observed by Roddier and Roddier (1985). Should grains survive at the Lagrangian point L_1? The last is inside the chromosphere, more likely in the low chromosphere where the temperature might allow the Draine (1981) scenario to work to form the dust grains. If the grains are ejected at L_1 at a sufficiently low velocity, a streak of dust might form behind the moving companion during the

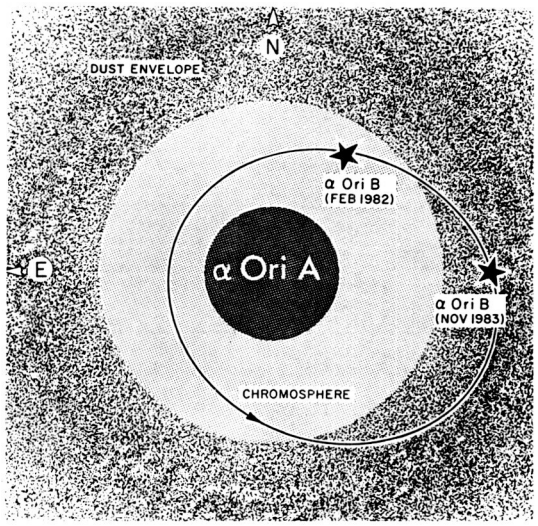

Figure 2-35. Schematic geometry for α Ori system showing the close companion orbiting α Ori. The possible eccentric orbit for the companion is characterized by: P = 2.08 ± 0.05 years, T = 1980.4 ± 0.1; e ~0.35 ± 0.05; i = 30° ± 10°; Ω + ω = 66° ± 10° (from Karovska et al., 1985b).

observed part of its orbit around α Ori and give the half-moon cloud observed by Roddier and Roddier near the stellar surface. The cloud then expands by radiation pressure on the grains such that IR emission is observed at several tens of stellar radii in direct IR mapping by Bloemhof et al. (1984).

The α Ori binary nature is also very attractive for explaining the asymmetries in the shells observed in directions variable with time (see the sections *Physical Conditions in Gaseous Shells* and *Overall Results on Polarization*); it should be the clue to understanding the dust distribution that suggests the involvement of localized and temporary instabilities in the ejection of material from α Ori (Bloemhof et al., 1984). Indeed, more progress in the comprehension of the α Ori dynamic structure is expected, as soon as more information on the companion star(s) is available and more coordinated observations (by spectroscopy, photometry, and polarization) are obtained.

The Dusty Star, IRC + 10216

It is now established that IRC + 10216 is a carbon Mira variable (from 1-μm spectra; e.g., Herbig and Zappala, 1970), nearby (d ~ 200 to 300 pc), luminous (one of the brightest 5- to 10-μm source), heavily enshrouded in an extensive dust envelope of its own making (see Table 1 in Lafont et al., 1982, for the assumed parameters of IRC + 10216). The degree of obscuration is such that all the photospheric stellar radiation is absorbed and reemitted by the dust. Various multiwavelength infrared measurements give indications on the size and shape of the dust envelope and the molecular clouds.

Table 2-5 summarizes data from the literature on the angular extent of the emitting regions. The dust cloud has been mapped up to a radius of 27″ (~1200 R_*), and the CO cloud up to a radius of at least 3′ (8000 R_*). The star is quite asymmetric in its dust shells, with the amount of asymmetry varying with wavelength and radius. *Elliptical contours* are obvious when sufficient position angle coverage is available. At 4.6 μm, the axis ratio b/a is 0.77, while at 0.8 μm, it is equal to 0.4 (Mariotti et al., 1983), with the major axis lying nearly north-south. As for the gaseous emitting regions near the star, we discussed a modeling by Keady et al. (1984) in the section *Summary: Structure of Expanding Gaseous Envelope* (also see Table 2-3). It would be interesting to determine if the scattered light from the gas is as asymmetric as the dust emission by mapping observations in several directions through the center of the star (Beckwith, 1985). Such an available observation, the only one to our knowledge, is from the CO (2–1) emission profile that is circularly symmetric about the center of the star at 6′ (Wannier et al., 1980; Knapp et al., 1982).

It has been suggested that the nonspherical 2.2- to 5.0-μm circumstellar dust geometry could represent a flattened disk viewed at low inclination or be caused by the binary nature

Table 2-5
Multispectral Spatial Mapping of IRC + 10216

λ	Diameter	R/R_* [a]	R_{cm}	References*
	Dust Emitting Regions			
0.8 μm	φ_{E-W} = 1″	22	1.5×10^{15}	1
	φ_{N-S} = 2″5	55	4×10^{15}	1
2.2 μm	φ_{E-W} = 0″14	3	2×10^{14}	1,2
5 μm	φ_{E-W} = 0″36	8	55×10^{14}	1
2.2 to 5 μm	φ_{N-S} = 0″48	11	7×10^{14}	1,3,4
11 μm	φ[b] = 0″9	20	1.3×10^{15}	1,5
20 μm	φ[b] = <2″5	55	4×10^{15}	1
40 to 250 μm	φ[c] = 0′9	1200	8×10^{16}	6
	Gaseous Emitting Regions			
CO (4.6^{abs}μm)	φ_{N-S} ~1″3	30	2×10^{15}	3
CO (4.6^{em}μm)[d]	φ ~ 4″	90	6×10^{15}	7
HCN (mm)	φ < 40″	<980	$<6 \times 10^{16}$	8
CN (mm)	φ ~ 1′80	2400	1.6×10^{17}	9
CO (1–0)	φ ~ 2′3	3040	2×10^{17}	8,10,11
CO (2–1)	φ_{sph} ~ 6′	8000	5.5×10^{17}	12,13

*References: 1. McCarthy et al., 1980; 2. Selby et al., 1979; 3. Dyck et al., 1983; 4. Mariotti et al., 1983; 5. Sutton et al., 1979; 6. Fazio et al., 1980; 7. Sahai and Wannier, 1984; 8. Wilson et al., 1973; 9. Wootten et al., 1982; 10. Ulich and Haas, 1976; 11. Kuiper et al., 1976; 12. Wannier et al., 1980; 13. Knapp et al., 1982.

Notes:

[a]With d = 200 pc (see comment in Lafont et al., 1982)
(1″ ≡ 3×10^{15} cm ≡ 44 R_* with 1 R_* ~ 970 $R_\odot$ from Keady et al., 1984, and
1 $R_\odot$ = 6.96×10^{10} cm).

[b]Lack of sufficient position angle coverage at high spatial frequencies to investigate an asymmetry.

[c]At a position angle of 151° measured east from north (along the minor axis of the elliptical optical image).

[d]By isolating radiation being scattered resonantly from the gas in the expanding envelope.

of the star (e.g., McCarthy et al., 1980). A close binary system may explain the evidence for a mixed morphology (sphere plus disk) according to Bowers et al. (1983), as well as the large mass-loss rate ($\sim 1.5 \times 10^{-4}$ $M_\odot$ yr^{-1} from Knapp et al., 1982). Also, an ellipsoidal or disk-shaped envelope would generate the larger polarization observed in IRC + 10216 (e.g., Fazio et al., 1980). Such large degrees of polarization have been detected in other dust-enshrouded carbon stars by Cohen and Schmidt (1982). Particularly interesting is the extreme C star, GL 1403, for which these authors find two orthogonally polarized spectral components, implying a dusty equatorial torus and polar scattering lobes. Such a structure favors an evolutionary link between those objects and bipolar nebulae. On the other hand, Bowers et al. (1983) suggest that evolved stars with non-spherical envelopes, which are spatially rare, are influenced by close binary companions, while evolved stars with spherical envelopes (most OH Miras) may be responsible for the optical halos associated with some planetary nebulae.

REFERENCES

Abt, H.A., and Biggs, E.S. 1972, *Bibliography of Stellar Radial Velocities* (Tucson: Kitt Peak National Observatory).

Adams, W.S., and McCormack, E. 1935, *Astrophys. J.*, **81**, 119.

Adams, W.S. 1956, *Astrophys. J.*, **123**, 189.

Allen, C.W. 1973, *Astrophysical Quantities*, 3rd Edition (London: The Athlone Press).

Antia, H.M., Chitre, S.M., and Narasimha, D. 1984, *Astrophys. J.*, **282**, 574.

Arsenijevic, J., Kubicela, A., and Vince, I. 1980, *Inf. Bull. Variable Stars*, IAU Comm. 27, No. 1859.

Avrett, E.H., and Johnson, H.R. 1984, in *Proc. Third Cambridge Workshop on Cool Stars, Stellar Systems, and the Sun*, ed. S.L. Baliunas and L. Hartmann (Berlin, Heidelberg: Springer-Verlag), p. 330.

Ayres, T.R. 1979, *Astrophys. J.*, **228**, 509.

Babcock, H.W. 1958, *Astrophys. J. Supplement*, **3**, 141.

Balega, Y., Blazit, A., Bonneau, D., Koechlin, L., Foy, R., and Labeyrie, A. 1982, *Astron. Astrophys.*, **115**, 253.

Basri, G.B., and Linsky, J.L. 1979, *Astrophys. J.*, **234**, 1023.

Basri, G.B., Linsky, J.L., and Eriksson, K. 1981, *Astrophys. J.*, **251**, 162.

Beckwith, S. 1985, in *Proc. Conf. on Mass Loss from Red Giants*, ed. M. Morris and B. Zuckerman (Dordrecht: Reidel).

Bernat, A.P. 1977, *Astrophys. J.*, **213**, 756.

Bernat, A.P. 1981, *Astrophys. J.*, **246**, 184.

Bernat, A.P., Hall, D.N.B., Hinkle, K.H., and Ridgway, S.T. 1979, *Astrophys. J. (Letters)*, **233**, L135.

Bernat, A.P., Honeycutt, R.K., Kephart, J.E., Gow, C.E., Sandford, M.T., and Lambert, D.L. 1978, *Astrophys. J.*, **219**, 532.

Bernat, A.P., and Lambert, D.L. 1975, *Astrophys. J. (Letters)*, **201**, L153.

Bernat, A.P., and Lambert, D.L. 1976a, *Astrophys. J.*, **204**, 830.

Bernat, A.P., and Lambert, D.L. 1976b, *Astrophys. J.*, **210**, 395.

Bidelman, W.P. 1950, *Astrophys. J.*, **112**, 219.

Bidelman, W.P. 1954, *Astrophys. J. Supplement*, **1**, 225.

Bidelman, W.P., and Pyper, D.M. 1963, *Pub. Astron. Soc. Pacific*, **75**, 389.

Bloemhof, E.E., Townes, C.H., and Vanderwyck, A.H.B. 1984, *Astrophys. J. (Letters)*, **276**, L21.

Boesgaard, A.M. 1973, in *Proc. IAU Colloq. 19, Stellar Atmospheres*, ed. S.D. Jordan and E.H. Avrett, NASA SP-317, p. 158.

Boesgaard, A.M. 1979, *Astrophys. J.*, **232**, 485.

Boesgaard, A.M. 1981, *Astrophys. J.*, **251**, 564.

Boesgaard, A.M., and Boesgaard, H. 1976, *Astrophys. J.*, **205**, 448.

Boesgaard, A.M., and Hagen, W. 1979, *Astrophys. J.*, **231**, 128.

Boesgaard, A.M., and Magnan, C. 1975, *Astrophys. J.*, **198**, 369.

Bohn, H.U. 1984, *Astron. Astrophys.*, **136**, 338.

Boice, D.C., Kuhn, J.R., Robinson, R.D., and Worden, S.P. 1981, *Astrophys. J. (Letters)*, **245**, L71.

Bonneau, D., and Labeyrie, A. 1973, *Astrophys. J. (Letters)*, **181**, L1.

Borra, E.F., Edwards, G., and Mayor, M. 1984, *Astrophys. J*, **284**, 211.

Bouchet, P., Querci, M., and Querci, F. 1983, *The Messenger*, ed. P. Véron, ESO, No. 31, p. 7.

Bowers, P.F., Johnston, K.J., and Spencer, J.H. 1983, *Astrophys. J.*, **274**, 733.

Bregman, J.D., and Bregman, J.N. 1978, *Astrophys. J. (Letters)*, **222**, L41.

Bretz, M.C. 1966, in *Proc. Trieste Colloq. on Astrophysics, Late-Type Stars*, ed. M. Hack, June 1966 (Osservatorio Astronomico di Trieste), p. 166.

Brooke, A.L., Lambert, D.L., and Barnes, T.G. 1974, *Pub. Astron. Soc. Pacific*, **86**, 419.

Brown, A., and Carpenter, K.G. 1984, *Astrophys. J. (Letters)*, **287**, L43.

Buhl, D., Snyder, L.E., Lovas, F.J., and Johnson, D.R. 1975, *Astrophys. J. (Letters)*, **201**, L29.

Buscombe, W., and Merrill, P.W. 1952, *Astrophys. J.*, **116**, 525.

Campbell, M.F., Elias, J.H., Gezari, D.Y., Harvey, P.M., Hoffmann, W.F., Hudson, H.S., Neugebauer, G., Soifer, B.T., Werner, M.W., and Westbrook, W.E. 1976, *Astrophys. J.*, **208**, 396.

Carbon, D.F., Milkey, R.W., and Heasley, J.N. 1976, *Astrophys. J.*, **207**, 253.

Carpenter, K.G. 1984, *Astrophys. J.*, **285**, 181.

Carpenter, K.G., Brown, A., and Stencel, R.E. 1985, *Astrophys. J.*, **289**, 676.

Carpenter, K.G., and Wing, R.F. 1979, *Bull. Amer. Astron. Soc. (Abstract)*, **11**, 419, and private communication.

Cassatella, A., Heck, A., Querci, F., Querci, M., and Stickland, D.J. 1980, in *Proc. Second European IUE Conference*, ESA SP-157, p. 243.

Catchpole, R.M., Robertson, B.S.C., Lloyd Evans, T.H.H., Feast, M.W., Glass, I.S., and Carter, B.S. 1979, *South Africa Astron. Obs. Circ.*, **1**, 61.

Clark, F.O., Johnson, D.R., Troland, T.H., and Heiles, C.E. 1980, in *Proc. IAU Symp. 87, Interstellar Molecules*, ed. B.H. Andrew (Dordrecht: Reidel) p. 543.

Clarke, D., and Schwarz, H.E. 1984, *Astron. Astrophys.*, **132**, 375.

Clegg, R.E.S. 1980, in *Proc. 5th European Regional Astronomy Meeting*, ed. P. Ledoux (Liège, Belgium).

Codina-Landaberry, S.J., and Magalhaes, A.M. 1980, *Astron. J.*, **85**, 875.

Cohen, M. 1979, *Mon. Not. Roy. Astr. Soc.*, **186**, 837.

Cohen, M., and Schmidt, G.D. 1982, *Astrophys. J.*, **259**, 693.

Contadakis, M.E., and Solf, J. 1981, *Astron. Astrophys.*, **101**, 241.

Coyne, G.V. 1979, in *Proc. IAU Colloq. 47, Spectral Classification of the Future*, ed. M.F. McCarthy, A.G.D. Philip, and G.V. Coyne (Citta del Vaticano: Specola Vaticana).

Coyne, G.V., and Kruszewski, A. 1968, *Astron. J.*, **73**, 20.

Coyne G.V., and Magalhaes, A.M. 1977, *Astron. J.*, **82**, 908.

Coyne, G.V., and Magalhaes, A.M. 1979, *Astron. J.*, **84**, 1200.

Coyne, G.V., and McLean, I.S. 1979, in *Proc. IAU Colloq. 46, Changing Trends in Variable Star Research*, ed. F.M. Bateson, J. Smak, and I.H. Urch (Hamilton, New Zealand: Univ. Waikato Press), p. 386.

Coyne, G.V., and Shawl, S.J. 1973, *Astrophys. J.*, **186**, 961.

Davis, J., and Tango, W.J., ed. 1979, *Proc. IAU Colloq. 50, High Angular Resolution Stellar Interferometry* (College Park, Maryland) published by Chatterton Astron. Dept., School of Physics, Univ. Sydney, N.S.W. 2006 Australia.

Deguchi, S. 1980, *Astrophys. J.*, **236**, 567.

de Jager, C., Kondo, Y., Hockstra, R., Van der Hucht, K.A., Kamperman, T.M., Lamers, H.J.G.L.M., Modisette, J.L., and Morgan, T.H. 1979, *Astrophys. J.*, **230**, 534.

Deutsch, A.J. 1956, *Astrophys. J.*, **123**, 210.

Deutsch, A.J. 1960, in *Stars and Stellar Systems, Vol. VI: Stellar Atmospheres*, ed. J.L. Greenstein (Chicago: Univ. Chicago Press), p. 543.

Deutsch, A.J., and Merrill, P.W. 1959, *Astrophys. J.*, **130**, 570.

Dickinson, D.F., Reid, M.J., Morris, M., and Redman, R. 1978, *Astrophys. J. (Letters)*, **220**, L113.

Doherty, L.R. 1972, *Astrophys. J.*, **178**, 495.

Dolginov, A.Z., and Mitrofanov, I.G. 1977, *Sov. Astron.*, **21**(6), 715.

Donn, B., Stecher, T.P., Wickramasinghe, N.C., and Williams, D.A. 1966, *Astrophys. J.*, **145**, 949.

Donn, B., Stecher, T.P., Wickramasinghe, N.C., and Williams, D.A. 1968, *Astrophys. J. (Letters)*, **153**, L143.

Draine, B.T. 1981, in *Proc. Second Workshop on Physical Processes in Red Giants*, ed. I. Iben and A. Renzini (Dordrecht: Reidel), p. 317.

Drake, S.A., and Linsky, J.L. 1983, *Astrophys. J.*, **273**, 299.

Dupree, A.K., Sonneborn, G., Baliunas, S.L., Guinan, E.F., Hartmann, L., Hayes, D.P. 1984, *Future of UV Astronomy Based on 6 Years of IUE Research*, ed. J. M. Mead, R. D. Chapman, and Y. Kondo, NASA CP-2349.

Dyck, H.M., Beckwith, S., and Zuckerman, B. 1983, *Astrophys. J. (Letters)*, **271**, L79.

Dyck, H.M., Forrest, W.J., Gillett, F.C., Stein, W.A., Gehrz, R.D., Woolf, N.J., and Shawl, S.J. 1971, *Astrophys. J.*, **165**, 57.

Dyck, H.M., and Jennings, M.C. 1971, *Astron. J.*, **76**, 431.

Dyck, H.M., and Simon T. 1975, *Astrophys. J.*, **195**, 689.

Eaton, J.A., Johnson, H.R., O'Brien, G.T., and Baumert, J.H. 1985, *Astrophys. J.*, **290**, 276.

Engels, D. 1979, *Astron. Astrophys. Supplement*, **36**, 337.

Epchtein, N., Guibert, J., Nguyen-Quang Rieu, Turon, P., and Wamsteker, W. 1980, *Astron. Astrophys.*, **85**, L1.

Eriksson, K., Gustafsson, B., Johnson, H.R., Querci, F., Querci, M., Baumert, J.H., Carlsson, M., and Olofsson, H. 1985, *Astron. Astrophys.*, in press.

Fawley, W.M. 1977, *Astrophys. J.*, **218**, 181.

Fazio, G.G., McBreen, B., Stier, M.T., and Wright, E.L. 1980, *Astrophys. J. (Letters)*, **237**, L39.

Feofilov, P.P. 1961, *The Physical Basis of Polarized Emission* (New York: Consultants Bureau).

Ferlet, R., and Gillet, D. 1984, *Astron. Astrophys.*, **133**, L1.

Forrest, W.J., Gillett, F.C., and Stein, W.A. 1975, *Astrophys. J.*, **195**, 423.

Forrest, W.J., Houck, J.R., and McCarthy, J.F. 1981, *Astrophys. J.*, **248**, 195.

Forrest, W.J., McCarthy, J.F., and Houck, J.R. 1979, *Astrophys. J.*, **233**, 611.

Fox, M.W., Wood, P.R., and Dopita, M.A. 1984, *Astrophys. J.*, **286**, 337.

Friedemann, C., Gürtler, J., Schmidt, R., and Dorschner, J. 1981, *Astrophys. Space Sci.*, **79**, 405.

Gahm, G.F., and Hultquist, L. 1971, in *Proc. Third Trieste Colloq. on Astrophysics*, ed. M. Hack (Osservatorio Astronomico di Trieste), p. 148.

Gehrz, R.D., and Woolf, N.J. 1971, *Astrophys. J.*, **165**, 285.

Gilman, R.C. 1974, *Astrophys. J.*, **118**, 87.

Gilra, D.P. 1973, in *IAU Symp. 52, Interstellar Dust and Related Topics*, ed. J.M. Greenberg and H.C. Van de Hulst (Dordrecht: Reidel), p. 517.

Gilra, D.P. 1976, *Mém. Soc. Roy. Sci. Liège*, **IX**, Sér. 6, p. 77.

Goebel, J.H., Bregman, J.D., Goorvitch, D., Strecker, D.W., Puetter, R.C., Russell, R.W., Soifer, B.T., Willner, S.P., Forrest, W.J., Houck, J.R., and McCarthy, J.F. 1980, *Astrophys. J.*, **235**, 104.

Goebel, J.H., Bregman, J.D., Strecker, D.W., Witteborn, F.C., and Ericksson, E.F. 1978, *Astrophys. J. (Letters)*, **222**, L129.

Goebel, J.H., and Mosely, S.H. 1985, *Astrophys. J. (Letters)*, **290**, L35.

Goldberg, L. 1976, *Mém. Soc. Roy. Sci. Liège*, **IX**, Sér. 6, p. 387.

Goldberg, L. 1979, *Quart. J. Roy. Astron. Soc.*, **20**, 361.

Goldberg, L. 1981, in *Proc. Second Workshop on Physical Processes in Red Giants*, ed. I. Iben and A. Renzini (Dordrecht: Reidel), p. 301.

Goldberg, L. 1984, *Pub. Astron. Soc. Pacific*, **96**, 366.

Goldberg, L., Hege, E.K., Hubbard, E.N., Strittmatter, P.A., and Cocke, W.J. 1981, SAO Special Report 392, p. 131.

Goldberg, L., Ramsey, L., Testerman, L., and Carbon, D. 1975, *Astrophys. J.*, **199**, 427.

Goldreich, P. 1980, in *Proc IAU Symp. 87, Interstellar Molecules*, ed. B.H. Andrew (Dordrecht: Reidel), p. 522.

Guinan, E.F. 1984, in *Proc. Third Cambridge Workshop on Cool Stars, Stellar Systems, and the Sun*, ed. S.L. Baliunas and L. Hartmann (Berlin, Heidelberg: Springer-Verlag), p. 336.

Hagen, W. 1978, *Astrophys. J. Supplement*, **38**, 1.

Hagen, W. 1982, *Pub. Astron. Soc. Pacific*, **94**, 835.

Hagen, W., Simon, T., and Dyck, H.M. 1975, *Bull. Amer. Astron. Soc.*, **7**, 434.

Hagen, W., Stencel, R.E., and Dickinson, D.F. 1983, *Astrophys. J.*, **274**, 286.

Hall, D.N.B. 1980, in *Proc. IAU Symp. 87, Interstellar Molecules*, ed. B.H. Andrew (Dordrecht: Reidel), p. 515.

Hall, D.N.B., Hinkle, K.H., and Ridgway, S.T. 1979, in *Proc. IAU Colloq. 46, Changing Trends in Variable Star Research*, ed. F.M. Bateson, J. Smak, and I.H. Urch (Hamilton, New Zealand: Univ. of Waikato Press), p. 264.

Harrington, J.P. 1969, *Astrophys. Letters*, **3**, 165.

Hartmann, L.W., and Avrett, E.H. 1984, *Astrophys. J.*, **284**, 238.

Hartmann, L.W., and Dolan, J.F. 1974, *Astrophys. J.*, **187**, 151.

Hayes, D.P. 1980, *Astrophys. J. (Letters)*, **241**, L165.

Hayes, D.P. 1981a, *Inf. Bull. Variable Stars IAU Comm. 27*, No. 1984.

Hayes, D.P. 1981b, *Pub. Astron. Soc. Pacific*, **93**, 752.

Hayes, D.P. 1982, *Inf. Bull. Variable Stars, IAU Comm. 27*, No. 2064.

Hayes, D.P. 1984, in *Proc. Third Cambridge Workshop on Cool Stars, Stellar Systems, and the Sun*, ed. S.L. Baliunas and L. Hartmann (Berlin, Heidelberg: Springer-Verlag), p. 342.

Heasley, J.N., Ridgway, S.T., Carbon, D.F., Milkey, R.W., and Hall, D.N.B. 1978, *Astrophys. J.*, **219**, 970.

Herbig, G.M. 1956, *Pub. Astron. Soc. Pacific*, **68**, 204.

Herbig, G.H., and Zappala, R.R. 1970, *Astrophys. J. (Letters)*, **162**, L15.

Herter, T., Briotta, D.A., Gull, G.E., and Houck, J.R. 1982, *Astrophys. J. (Letters)*, **259**, L25.

Herzberg, G. 1948, *Astrophys. J.*, **107**, 94.

Hill, S.J., and Willson, L.A. 1979, *Astrophys. J.*, **229**, 1029.

Hinkle, K.H. 1978, *Astrophys. J.*, **220**, 210.

Hinkle, K.H., and Barnes, T.G. 1979a, *Astrophys. J.*, **227**, 923.

Hinkle, K.H., and Barnes, T.G. 1979b, *Astrophys. J.*, **234**, 548.

Hinkle, K.H., Hall, D.N.B., and Ridgway, S.T. 1982, *Astrophys. J.*, **252**, 697.

Hinkle, K.H., Lambert, D.L., and Snell, R.L. 1976, *Astrophys. J.*, **210**, 684.

Hinkle, K.H., Scharlach, W.W.G., and Hall, D.N.B. 1984, *Astrophys. J. Supplement*, **56**, 1.

Honeycutt, R.K., Bernat, A.P., Kephart, J.E., Gow, C.E., Sandford, M.T., and Lambert, D.L. 1980, *Astrophys. J.*, **239**, 565.

Huggins, P.J. 1984, in *Proc. Mass Loss from Red Giants*, meeting held in UCLA Faculty Center on June 20-21, 1984.

Jennings, M.C., and Dyck, H.M. 1972, *Astrophys. J.*, **177**, 427.

Johnson, H.L., and Allen, C., ed. 1981, *Proc. Symp. on Recent Advances in Observational Astronomy*, (Ensenada, Baja California: Universidad Nacional Autónoma de Mexico).

Johnson, H.R., and Ake, T.B. 1984, in *Proc. Third Cambridge Workshop on Cool Stars, Stellar Systems, and the Sun*, ed. S.L. Baliunas and L. Hartmann (Berlin, Heidelberg: Springer-Verlag), p. 362.

Johnson, H.R., Ake, T.B., and Eaton, J.A. 1985a, in *Cool Stars with Excesses of Heavy Elements*, ed. M. Jaschek and P.C. Keenan (Dordrecht: Reidel), p. 53.

Johnson, H.R., Baumert, J.H., Querci, F., and Querci, M. 1985b, *Astrophys. J.*, in press.

Johnson, H., and Mendez, M. 1970, *Astron. J.*, **75**, 785.

Johnson, H.R., and O'Brien, G.T. 1983, *Astrophys. J.*, **265**, 952.

Joy, A.H. 1947, *Astrophys. J.*, **106**, 288.

Joy, A.H. 1954, *Astrophys. J., Supplement*, **1**, 39.

Jura, M. 1984, *Astrophys. J.*, **282**, 200.

Karovska, M. 1984, *Thèse de 3e cycle*, U.E.R. Institut de Mathématiques et Sciences Physiques, et Observatoire de Nice (Sept. 1984).

Karovska, M., Nisenson, P., Noyes, R.W., Stachnik, R.V. 1985b, in *Proc. Fourth Cambridge Workshop on Cool Stars, Stellar Systems, and the Sun*, held in Santa Fe, New Mexico, Oct. 16–18, 1985, in press.

Karovska, M., Noyes, R.W., Roddier, F., Nisenson, P., Stachnik, R.V. 1985a, *Bull. Amer. Astrophys. Soc.*, **17**, 598.

Keady, J.J., Hall, D.N.B., and Ridgway, S.T. 1984, preprint to appear in *Astrophys. J.*

Keenan, P.C. 1966, *Astrophys. J. Supplement*, **13**, 333.

Keenan, P.C., Garrison, R.F., and Deutsch, A.J. 1974, *Astrophys. J. Supplement*, **28**, 271.

King, D.J. 1983, *Mercury*, March–April 1983.

Kipper, T.A., and Kipper, M.A. 1979, *Pub. Astrophys. Obs. Tartu*, **XLVII**, p. 222.

Knapp, G.R., 1985, *Astrophys. J.*, **293**, 273.

Knapp, G.R., Phillips, T.G., and Huggins, P.J. 1980, *Astrophys. J. (Letters)*, **242**, L25.

Knapp, G.R., Phillips, T.G., Leighton, R.B., Lo, K.Y., Wannier, P.G., Wootten, A., and Huggins, P.J. 1982, *Astrophys. J.*, **252**, 616.

Kondo, Y. 1973, in *Proc. IAU Colloq. 19, Stellar Atmospheres*, ed. S.D. Jordan and E.H. Avrett, NASA SP-317, p. 122.

Kondo, Y., Duval, J.E., Modisette, J.L., and Morgan, T.H. 1976, *Astrophys. J.*, **210**, 713.

Kondo, Y., Giuli, R.T., Modisette, J.L., and Rydgren, A.E. 1972, *Astrophys. J.*, **176**, 153.

Kondo, Y., Modisette, J.L., Morgan, T.H., de Jager, C., Lamers, H.J., and Van der Hucht, K.A. 1977, *Bull. Amer. Astron. Soc.*, **9**, 365.

Kondo, Y., Morgan, T.H., and Modisette, J.L. 1975, *Astrophys. J. (Letters)*, **196**, L125.

Kovar, R.P., Potter, A.E., Kovar, N.S., and Trafton, L. 1972, *Pub. Astron. Soc. Pacific*, **84**, 46.

Kruszewski, A., and Coyne, G.V. 1976, *Astron. J.*, **81**, 641.

Kruszewski, A., Coyne, G.V., and Gehrels, T. 1969, in *Proc. Second Trieste Colloq. on Astrophysics, Mass Loss from Stars*, ed. M. Hack (Dordrecht: Reidel), p. 42.

Kuiper, T.B.H., Knapp, G.R., Knapp, S.L. and Brown, R.L. 1976, *Astrophys. J.*, **204**, 408.

Kukarkin, B.V., Kholopov, P.N., Efremov, Yu.N., Kukarkina, N.P., Kurochkin, N.E., Medvedeva, G.I., Perova, N.B., Fedorovich, V.P., and Frolov, M.S. 1969, *General Catalogue of Variable Stars*, Third Ed., Vol. I, and Supplements (Moscow).

Kukarkin, B.V., Kholopov, P.N., Efremov, Yu.N., Kukarkina, N.P., Kurochkin, N.E., Medvedeva, G.I., Perova, N.B., Fedorovich, V.P., and Frolov, M.S. 1970, *General Catalogue of Variable Stars*, Third Ed., Vol. II and Supplements (Moscow).

Kunasz, P.B. 1974, Ph.D. Thesis, Univ. of Colorado.

Kunasz, P.B., and Hummer, D.G. 1974, *Mon. Not. Roy. Astr. Soc.*, **166**, 57.

Kwok, S. 1981, in *Proc. Second Workshop on Physical Processes in Red Giants*, ed. I. Iben and A. Renzini (Dordrecht: Reidel), p. 421.

Labeyrie, A., Koechlin, L., Bonneau, D., Blazit, A., and Foy, R. 1977, *Astrophys. J. (Letters)*, **218**, L75.

Lafont, S., Lucas, R., and Omont, A. 1982, *Astron. Astrophys*, **106**, 201.

Lambert, D.L., and Snell, R.L. 1975, *Mon. Not. Roy. Astr. Soc.*, **172**, 277.

Lambert, D.L., and Vanden Bout, P.A. 1978, *Astrophys. J.*, **221**, 854.

Landstreet, J.D., and Angel, J.R.P. 1977, *Astrophys. J.*, **211**, 825.

Lang, K.R. 1980, *Astrophysical Formulae* (Berlin, Heidelberg: Springer-Verlag), p. 535.

Leibacher, J., and Stein, R.F. 1981, in *Proc. Second Cambridge Workshop on Cool Stars, Stellar Systems, and the Sun, Vol. I*, ed. M.S. Giampapa and L. Golub, Spec. Report 392 (Smithsonian Astrophys. Obs.), p. 23.

Levy, E.H., Rose, W.K. 1974, *Astrophys. J.*, **193**, 419.

Linsky, J.L., Basri, G.S., Chiu, H.Y., Chang, S.W., and Maran, S.P. 1977, *Bull. Amer. Astrophys. Soc.*, **9**, 345.

Linsky, J.L., Worden, S.P., McClintock, W., and Robertson, R.M. 1979, *Astrophys. J. Supplement*, **41**, 47.

Lockwood, G.W. 1969, *Astrophys. J.*, **157**, 275.

Lynds, C.R., Harvey, J., and Goldberg, L. 1977, *Bull. Amer. Astron. Soc.*, **9**, 345.

Lynds, C.R., Worden, S.P., and Harvey, J.W. 1976, *Astrophys. J.*, **207**, 174.

Maehara, H. 1968, *Pub. Astron. Soc. Japan*, **20**, 77.

Maehara, H. 1971, *Pub. Astron. Soc. Japan*, **23**, 503.

Maehara, H., Yamashita, Y. 1979, *Annals Tokyo Astron. Obs.*, **XVII**, Ser. 2, p. 93

Magalhaes, A.M. 1980, in *Proc. Colloq. on Phenomena of Mass Ejection*, Cambuquira (Sociedade Astronomica Brasileira: MG Brazil).

Magalhaes, A.M. 1981, in *Proc. Second Workshop on Physical Processes in Red Giants* ed. I. Iben and A. Renzini (Dordrecht: Reidel), p. 231.

Manduca, A. 1979, *Astron. Astrophys. Supplement,* **36**, 411.

Marcondes-Machado, J.A. 1979, in *Proc. IAU Colloq. 46, Changing Trends in Variable Star Research*, ed. F.M. Bateson, J. Smak, and I.H. Urch (Hamilton, New Zealand: Univ. Waikato Press), p. 273.

Mariotti, J.M., Chelli, A., Foy, R., Léna, P., Sibille, F., and Tchountonov, G. 1983, *Astron. Astrophys.*, **120**, 237.

Mauron, N., Fort, B., Querci, F., Dreux, M., Fauconnier, T., and Lamy, P. 1984, *Astron. Astrophys.*, **130**, 341.

McCabe, E.M. 1982, *Mon. Not. Roy. Astr. Soc.*, **200**, 71.

McCall, A., and Hough, J.H. 1980, *Astron. Astrophys. Supplement,* **42**, 141.

McCarthy, D.W., Howell, R., and Low, F.J. 1978, *Astrophys. J. (Letters),* **223**, L1.

McCarthy, D.W., Howell, R., and Low, F.J. 1980, *Astrophys. J. (Letters),* **235**, L27.

McLaughin, D.B. 1946, *Astrophys. J.*, **103**, 35.

McLean, I.S. 1979, *Mon. Not. Roy. Astr. Soc.*, **186**, 21.

McLean, I.S., and Coyne, G.V. 1978, *Astrophys. J. (Letters),* **226**, L145.

McMillan, R.S., and Tapia, S. 1978, *Astrophys. J. (Letters),* **226**, L87.

Meinel, A.B., Aveni, A.F., and Stockton, M.W. 1969, *Catalog of Emission Lines in Astrophysical Objects.*, 2nd ed. (Tucson, Arizona: Optical Sciences Center and Steward Observatory, Univ. Arizona).

Merchant, A.E. 1967, *Astrophys. J.*, **147**, 587.

Merrill, P.W. 1940, *Spectra of Long-Period Variable Stars* (Chicago: Univ. Chicago Press).

Merrill, P.W. 1945, *Astrophys. J.*, **102**, 347.

Merrill, P.W. 1946, *Astrophys. J.*, **103**, 275.

Merrill, P.W. 1947a, *Astrophys. J.*, **105**, 360.

Merrill, P.W. 1947b, *Astrophys. J.*, **106**, 274.

Merrill, P.W. 1952a, *Astrophys. J.*, **116**, 21.

Merrill, P.W. 1952b, *Astrophys. J.*, **116**, 344.

Merrill, P.W. 1952c, *Astrophys. J.*, **116**, 337.

Merrill, P.W. 1960, in *Stars and Stellar Systems, Vol. VI: Stellar Atmospheres,* ed. J.L. Greenstein (Chicago: Univ. Chicago Press), p. 509.

Merrill, K.M. 1977, in *Proc. IAU Colloq. 42, The Interaction of Variable Stars with their Environment*, ed. R. Kippenhahn, J. Rake, and W. Strohmeier (Erlanger-Nurnberg: Astronomisches Institut der Universitat).

Merrill, P.W., and Greenstein, J.L. 1956, *Astrophys. J. Supplement,* **2**, 225.

Merrill, P.W., and Wilson, O.C. 1956, *Astrophys. J.*, **123**, 392.

Mihalas, D. 1978, in *Stellar Atmospheres*, 2nd ed., ed. G. Burbidge and M. Burbidge (San Francisco: W.H. Freeman and Company).

Mihalas, D. 1979, *Mon. Not. Roy. Astr. Soc.*, **189**, 671.

Mihalas, D., Kunasz, P.B., and Hummer, D.G. 1975, *Astrophys. J.*, **202**, 465.

Mitchell, R.M., and Robinson, G. 1980, *Mon. Not. Roy. Astr. Soc.*, **190**, 669.

Modisette, J.L., Nicholas, R.E., and Kondo, Y. 1973, *Astrophys. J.*, **186**, 219.

Morris, M., and Alcock, C. 1977, *Astrophys. J.*, **218**, 687.

Mullan, D.J. 1984, *Astrophys. J.*, **284**, 769.

Mullan, D.J. 1978, *Astrophys. J.*, **226**, 151.

Munch, G., Roesler, F., and Tranger, J. 1979, in *Proc. 4th Trieste Colloq. Astrophysics, High Resolution Spectroscopy*, ed. M. Hack (Osservatorio Astronomico di Trieste).

Nuth, J.A., Moseley, S.H., Silverberg, R.F., Goebel, J.H., and Moore, W.J. 1985, *Astrophys. J. (Letters)*, **290**, L41.

O'Brien, G., and Johnson, H.R. 1982, in *Advances in Ultraviolet Astronomy: Four Years of IUE Research*, ed. Y. Kondo, J.H. Mead, and R.D. Chapman, NASA CP-2238, p. 255.

O'Brien, G., and Lambert, D.L. 1979, *Astrophys. J. (Letters)*, **229**, L33.

Odell, A.P., Vrba, F.J., Fix, J.D., and Neff, J.S. 1970, *Pub. Astron. Soc. Pacific*, **82**, 883.

Oster, L. 1971, *Astrophys. J.*, **169**, 57.

Peery, B.F. 1979, *Pub. Astron. Soc. Japan*, **31**, 461.

Peery, B.F., and Wojslaw, R.S. 1977, *Bull. Amer. Astron. Soc.*, **9**, 365.

Phillips, J.G., and Freedman, R.S. 1969, *Pub. Astron. Soc. Pacific*, **81**, 521.

Pilachowski, C., Wallerstein, G., and Willson, L.A. 1979, in *Proc. Goddard Conf. on Current Problems in Stellar Pulsation Instabilities*, ed. D. Fischel et al., NASA TM-80625, p. 577.

Price, S.G., and Walker, R.G. 1976, *AFGL Infrared Sky Survey*, Environmental Research Papers, No. 576.

Puetter, R.C., Russell, R.W., Sellgren, K., and Soifer, B.T. 1977, *Pub. Astron. Soc. Pacific*, **89**, 320.

Querci, M., Courtin, R., Querci, F., Coron, N., and Gispert, R. 1979, *Astron. Astrophys.*, **77**, 155.

Querci, M., and Querci, F. 1978, *Astron. Astrophys.*, **70**, L45.

Querci, M., and Querci, F. 1985a, *Astron. Astrophys.*, **147**, 121.

Querci, M., and Querci, F. 1985b, in preparation.

Querci, F., Querci, M., Wing, R.F., Cassatella, A., and Heck, A. 1982, *Astron. Astrophys.*, **111**, 120.

Reid, M.J., and Dickinson, D.F. 1976, *Astrophys. J.*, **209**, 505.

Reimers, D. 1975, in *Problems in Stellar Atmospheres and Envelopes*, ed. B. Baschek, W.H. Kegel, and G. Traving (Berlin, Heidelberg: Springer-Verlag), p. 229.

Reimers, D. 1977, *Astron. Astrophys.*, **57**, 395.

Reimers, D. 1978, in *Proc. IAU Colloq. 42, Interaction of Variable Stars with Their Environment*, ed. R. Kippenhahn, J. Rahe, and W. Strohmeier (Erlangen-Nürnberg: Astronomisches Institut der Universität), p. 559.

Reimers, D. 1981, in *Proc. Second Workshop on Physical Processes in Red Giants*, ed. I. Iben and A. Renzini (Dordrecht: Reidel), p. 269.

Richer, H.B. 1971, *Astrophys. J.*, **167**, 521.

Ricort, G., Aime, A., Vernin, J., and Kadiri, S. 1981, *Astron. Astrophys.*, **99**, 232.

Ridgway, S.T. 1981a, in *Proc. Second Workshop on Physical Processes in Red Giants*, ed. I. Iben and A. Renzini (Dordrecht: Reidel), p. 305.

Ridgway, S.T. 1981b, in *Proc. Symp. on Recent Advances in Observational Astronomy*, ed. H.L. Johnson and C. Allen (Ensenada, Baja California: Universidad Nacional Autónoma de Mexico), p. 81.

Ridgway, S.T., and Hall, D.N.B. 1980, in *Proc. IAU Symp. 87, Interstellar Molecules*, ed. B.H. Andrew (Dordrecht: Reidel), p. 509.

Ridgway, S.T., Jacoby, G.H., Joyce, R.R., and Wells, D.C. 1980a, *Astron.J.*, **85**, 1496.

Ridgway, S.T., Joyce, R.R., White, N.M., and Wing, R.F. 1980b, *Astrophys. J.*, **235**, 126.

Ridgway, S.T., Wells, D.C., Joyce, R.R., and Allen, R.G. 1979, *Astron. J.*, **84**, 247.

Roddier, F., and Roddier, C. 1983, *Astrophys. J. (Letters)*, **270**, L23.

Roddier, F., and Roddier, C. 1985, *Astrophys. J. (Letters)*, **295**, L21.

Rottenberg, J.A. 1952, *Mon. Not. Roy. Astr. Soc.*, **112**, 125.

Rowan-Robinson, M., and Harris, S. 1982, *Mon. Not. Roy. Astr. Soc.*, **200**, 197.

Rowan-Robinson, M., and Harris, S. 1983a, *Mon. Not. Roy. Astr. Soc.*, **202**, 767.

Rowan-Robinson, M., and Harris, S. 1983b, *Mon. Not. Roy. Astr. Soc.*, **202**, 797.

Sahai, R., and Wannier, P.G. 1985, *Astrophys. J.*, **299**, 424.

Sanford, R.F. 1950, *Astrophys. J.*, **111**, 270.

Sanner, F. 1976, *Astrophys. J. Supplement*, **32**, 115.

Sanner, F. 1977, *Astrophys. J. (Letters)*, **221**, L35.

Scargle, J.D., and Strecker, D.W. 1979, *Astrophys. J.*, **228**, 838.

Schmid-Burgk, J., and Scholz, M. 1981, *Mon. Not. Roy. Astr. Soc.*, **194**, 805.

Schmitz, F., and Ulmschneider, P. 1981, *Astron. Astrophys.*, **93**, 178.

Schwarz, H.E., and Clarke, D. 1984, *Astron. Astrophys.*, **132**, 370.

Schwarzschild, M. 1975, *Astrophys. J.*, **195**, 137.

Selby, M.J., Wade, R., and Sanchez Magro, C. 1979, *Mon. Not. Roy. Astr. Soc.*, **187**, 553.

Serkowski, K. 1971, in *Proc. IAU Colloq. 15, New Directions and New Frontiers in Variable Star Research* (Erlangen-Nürnberg: Astronomisches Institut der Universität).

Shafter, A., and Jura, M. 1980, *Astron. J.*, **85**, 1513.

Shawl, S.J. 1974, *Planets, Stars and Nebulae Studied with Photopolarimetry*, ed. T. Gehrels (Tucson: Univ. Arizona Press), p. 821.

Shawl, S.J. 1975, *Astron. J.*, **80**, 602.

Shawl, S.J., and Zellner, B. 1970, *Astrophys. J. (Letters)*, **162**, L19.

Sherbakov, A.G. 1979, *Pisma V Astron. Zh.*, **5**, 542.

Shinkawa, D. 1973, *Astrophys. J. Supplement*, **25**, 253.

Simon, T., Linsky, J.L., and Stencel, R.F. 1982, *Astrophys. J.*, **257**, 225.

Slovak, M.H. 1982, *Astrophys. J.*, **262**, 282.

Slutz, S. 1976, *Astrophys. J.*, **210**, 750.

Spinrad, H., and Wing, R.F. 1969, *Ann. Rev. Astron. Astrophys.*, **7**, 249.

Stein, R.F., and Leibacher, J. 1980 in *Proc. IAU Colloq. 51, Stellar Turbulence*, ed. D.F. Gray and J.L. Linsky (Berlin, Heidelberg: Springer-Verlag), p. 225.

Stencel, R.E. 1977, *Astrophys. J.*, **215**, 176.

Stencel, R.E. 1978, Astrophys. J. (Letters), **223**, L37.

Stencel, R.E., and Carpenter, K.G. 1982, in *Advances in Ultraviolet Astronomy: Four Years of IUE Research*, ed. Y. Kondo, J.M. Mead, and R.D. Chapman, NASA CP-2238.

Stencel, R.E., and Ionson, J.A. 1979, *Pub. Astron. Soc. Pacific*, **91**, 452.

Stencel, R.E., Linsky, J.L., Brown, A., Jordan, C., Carpenter, K.G., Wing, R.F., and Czyzak, S. 1981, *Mon. Not. Roy. Astr. Soc.*, **196**, 470.

Stencel, R.E., Mullan, D.J., Linsky, J.L., Basri, G.S., and Worden, S.P. 1980, *Astrophys. J. Supplement*, **44**, 383.

Stephenson, C.B. 1973, *Pub. Warner and Swasey Obs.*, Vol. 1, No. 4.

Sutton, E.C., Betz. A.L., Storey, J.W.V., and Spears, D.L. 1979, *Astrophys. J. (Letters)*, **230**, L105.

Sutton, E.C., Storey, J.W.V., Betz, A.L., Townes, C.H., and Spears, D.L. 1977, *Astrophys. J. (Letters)*, **217**, L97.

Svatos, J. 1980, *Bull. Astron. Inst. Czech*, **31**, 302.

Svatos, J., and Solc, M. 1981, *Astrophys. Space Science*, **77**, 511.

Tanabé, T., and Kamijo, F. 1981, in *IAU Colloq. 59, Effects of Mass Loss on Stellar Evolution* ed. C. Chiosi and R. Stalio (Dordrecht: Reidel).

Tielens, A.G.G.M. 1983, *Astrophys. J.*, **271**, 702.

Tinbergen, J., Greenberg, J.M., and de Jager, C. 1981, *Astron. Astrophys.*, **95**, 215.

Tomaszewski, L., Landstreet, J.D., McLean, I.S., and Coyne, G.V. 1980, *Astrophys. J.*, **238**, 935.

Treffers, R.R., and Cohen, M. 1974, *Astrophys. J.*, **188**, 545.

Tsuji, T. 1971, *Pub. Astron. Soc. Japan*, **23**, 275.

Tsuji, T. 1976, *Pub. Astron. Soc. Japan*, **28**, 567.

Tsuji, T. 1978a, *Astron. Astrophys.*, **62**, 29.

Tsuji, T. 1978b, *Pub. Astron. Soc. Japan*, **30**, 435.

Tsuji, T. 1979, *Pub. Astron. Soc. Japan*, **31**, 43.

Ulich, B.L. and Haas, R.W. 1976, *Astrophys. J. Supplement*, **30**, 247.

Utsumi, K. 1971, *Pub. Astron. Soc. Japan*, **23**, 437.

Van der Hucht, K.A., Stencel, R.E., Haisch, B.M., and Kondo, Y. 1979, *Astron. Astrophys. Supplement*, **36**, 377.

Vaughan, A.H., and Skumanich, A. 1970, in *Proc. IAU Colloq. 2, Spectrum Formation in Stars with Steady-State Extended Atmospheres,* ed. H.G. Groth and P. Wellman, NBS-SP-332, p. 295.

Vaughan, A.H., and Zirin, H. 1968, *Astrophys. J.,* **152**, 123.

Walker, A.R. 1976, *Mon. Not. Roy. Astr. Soc.,* **174**, 609.

Walker, A.R. 1980, *Mon. Not. Roy. Astr. Soc.,* **190**, 543.

Wallerstein, G. 1959, *Astrophys. J.,* **130**, 560.

Wallerstein, G. 1975, *Astrophys. J. Supplement,* **29**, 375.

Wallerstein, G. 1977, *J. Roy. Astr. Soc. Canada,* **71**, 298.

Wannier, P.G., Redman, R.O., Phillips, T.G., Leighton, R.B., Knapp, G.R., and Huggins, P.J. 1980, in *Proc. IAU Colloq. 87, Interstellar Molecules*, ed. B.H. Andrew (Dordrecht: Reidel), p. 487.

Wdowiak, T.J. 1977, *Pub. Astron. Soc. Pacific,* **89**, 569.

Weiler, E.J., and Oegerle, W.R. 1979, *Astrophys. J. Supplement,* **39**, 537.

Welter, G. L., and Worden, S.P. 1980, *Astrophys. J.,* **242**, 673.

Weymann, R. 1962, *Astrophys. J.,* **136**, 844.

White, N.M. 1980, *Astrophys. J.,* **242**, 646.

Whitney, C.A., and Skalafuris, A.J. 1963, *Astrophys. J.,* **138**, 200.

Wilkerson, S., and Worden, S.P. 1977, *Astron. J.,* **82**, 642.

Willson, L.A. 1976, *Astrophys. J.,* **205**, 172.

Willson, L.A. 1979, in *Proc. IAU Colloq. 46, Changing Trends in Variable Star Research*, ed. F.M. Bateson, J. Smak, and I.H. Urch (Hamilton, New Zealand: Univ. Waikato Press), p. 199.

Willson, L.A., and Bowen, G.H. 1985, in *Proc. Third Trieste Workshop on the Relations Between Chromospheric-Coronal Heating and Mass Loss in Stars*, ed. R. Stalio and J. Zirker (Trieste: Tabographs-TS), pp. 127–176.

Willson, L.A., and Bowen, G.H. 1986, in *Proc. Fourth Cambridge Workshop on Cool Stars, Stellar Systems, and the Sun*, ed. M. Zeilik and D.M. Gibson (Heidelberg: Springer-Verlag), p. 385.

Willson, L.A., and Hill, S.J. 1979, *Astrophys. J.,* **228**, 854.

Willson, L.A., Wallerstein, G., and Pilachowski, C.A. 1982, *Mon. Not. Roy, Astr. Soc.,* **198**, 483.

Wilson, W. J., Schwartz, P.M., and Epstein, R.E. 1973, *Astrophys. J.,* **183**, 871.

Wing, R.F. 1978, in *Proc. 4th International Colloq. on Astrophysics, High Resolution Spectrometry*, ed. M. Hack (Osservatorio Astronomico di Trieste), p. 683.

Wing, R.F. 1979, in *Proc. Goddard Conference on Current Problems in Stellar Pulsation Instabilities*, ed. D. Fischel et al., NASA TM-80625, p. 533.

Wing, R.F., Baumert, J.H., Strom, S.E., and Strom, K.M. 1972, *Pub. Astron. Soc. Pacific,* **84**, 646.

Wood, P.R. 1979, *Astrophys. J.,* **227**, 220.

Wood, P.R. 1981, in *Proc. Second Workshop on Physical Processes in Red Giants*, ed. I. Iben and A. Renzini (Dordrecht: Reidel), p. 205.

Wood, P.R. 1982, in *Proc. Conf. on Pulsations in Classical and Cataclysmic Variable Stars*, ed.

J.P. Cox and C.J. Hansen (Boulder, Colorado: JILA), p.284.

Woodsworth, A.W., and Hughes, V.A. 1973, *Nature Phys. Sci.*, **246**, 111.

Wordsworth, A.W., and Hughes, V.A. 1977, *Astron. Astrophys.*, **58**, 105.

Wootten, A., Lichten, S.M., Sahai, R., and Wannier, P.G. 1982, *Astrophys. J.*, **257**, 151.

Yamashita, Y. 1972, *Annals Tokyo Astron. Obs.*, **XIII**, Ser. 2, p. 169.

Zirin, H. 1976, *Astrophys. J.*, **208**, 414.

Zirin, H. 1982, *Astrophys. J.*, **260**, 655.

Zuckerman, B., Gilra, D.P., Turner, B.E., Morris, M., and Palmer, P. 1976, *Astrophys. J. (Letters)*, **205**, L15.